Design of Protective Structures for Optimal Blast and Impact Mitigation

by

Tanaz Rahimzadeh

A dissertation submitted in partial fulfillment
of the requirements for the degree of
Doctor of Philosophy
(Mechanical Engineering)
in The University of Michigan
2016

Doctoral Committee:

Professor Ellen M. Arruda, Co-Chair
Professor Michael Thouless, Co-Chair
Assistant Professor Steven P. Broglio
Professor Gregory M. Hulbert
Professor Anthony M. Waas

ACKNOWLEDGEMENTS

The completion of this dissertation is accomplished upon the dedicated work of certain people to whom I wish to acknowledge my appreciation.

I would like to express my deepest gratitude to my co-advisors Prof. Ellen M. Arruda and Prof. Michael Thouless for their excellent guidance, caring, patience and support during my PhD studies. I was tremendously fortunate to have them throughout my PhD project providing me with brilliant ideas and inspiration towards research.

Next, I wish to express my sincere thanks to my dissertation committee, Prof. Anthony Waas, Prof. Gregory Hulbert and Prof. Steven Broglio for their advice and participation in my dissertation committee. I am also thankful to Prof. James Ashton Miller and Prof. James T. Eckner for providing me with access to their laboratories equipments.

During this work, I have collaborated with many colleagues and friends for whom I have great regard, and I wish to extend my warmest thanks to all those who have helped me with my work. I would like to thank Cameron McBride, Haolu Zhang, Kaitlyn Mallett and Benjamin Marchi for their help with collecting experiment data.

I wish to express my love and gratitude to my husband, Rasul, without his patience

and support, the successful completion of this work would not have been possible. I also wish to thank my daughter, Tina, and my son, Aiden, for their inspiration. I am also extremely grateful to my father, Khosro, and my mother, Lili, who taught me to give priority in my life to the quest for knowledge. Finally, I owe special thanks to my family back home for their encouragement through the duration of my studies.

This work was financially supported by the Office of Naval Research, the Natural Sciences and Engineering Research Council of Canada (NSERC), Rackham Graduate School and the College of Engineering.

TABLE OF CONTENTS

LIST OF FIGURES

Figure

LIST OF TABLES

Table

LIST OF APPENDICES

Appendix

ABSTRACT

Design of Protective Structures for Optimal Blast and Impact Mitigation

by

Tanaz Rahimzadeh

Chairs: Ellen M. Arruda, Michael Thouless

Design of blast-resistant and impact-resistant armor requires an understanding of how blast/impact load on structures look, how structures are damaged by blast/impact, and how the effects of blast/impact can be dissipated by the armor in an optimal manner. The focus of this dissertation is on these challenges to propose a systematic design approach for armor with optimal blast/impact mitigation capabilities. The objective is to study concurrently the mechanics of blast/impact, the mechanics of damage to structures due to blast/impact, and the mechanics of mitigating effectively the damaging features of blast/impact through the design of armor. The systematic design approach proposed in this research is missing in the solid mechanics literature in which the design of armor has used observation and experience rather than theory and optimization.

In this dissertation, the contact/impact behavior of spherical shells with varying shell thickness to shell outer radius ratios has been investigated analytically and computationally to identify the major features of an impact pulse exerted on a structure. A simple dynamic model of the protected structure has also been developed to iden-

tify the features of a blast/impact responsible for the stress (damage) on the delicate target within the protected structure. These damaging features include both the peak pressure and the impulse delivered to the structure. This study examines how layers of elastic, plastic, and visco-elastic materials may be assembled to mitigate these features. The impedance mismatch between two elastic layers is known to reduce the pressure, but dissipation is required to mitigate the transmitted impulse in lightweight armor. A novel design concept called impact or blast tuning is introduced in which a multi-layered armor is used to tune the stress waves resulting from an impact or blast to specific frequencies that match the damping frequencies of visco-elastic layers. Moreover, the dimensionless material and geometrical parameters controlling the viscous dissipation of the energy within the armor are identified for a simplified one-dimensional system, to provide insight into how the optimal design of multi-use armor might be based on this concept.

CHAPTER I

Project Motivation and Outline

In the US military, the Advanced Combat Helmet (ACH) is one of the main pieces of equipment used for head protection against blast and ballistic loading. Wearing the current ACH design near an explosion (blast) can still produce a range of injuries called blast-born Traumatic Brain Injury (TBI). Blast-born TBI is generally considered as a signature injury of current military conflicts, with costly and life-altering long-term effects. Soldiers with blast-born TBI mostly suffer from headaches, sleep disturbances, delayed reaction time during problem solving as well as disturbances in attention, memory, or language. Often, the most troubling symptoms of TBI are behavioral ones such as mood changes, depression, anxiety, impulsiveness, and emotional outbursts [14, 115]. Similarly, mild Traumatic Brain Injury (mTBI), also known as concussion, is a serious injury resulting from impact in most contact sports including professional football. Concussion manifests several physical, psychological, and cognitive symptoms as well. The symptoms associated with concussions are mostly transient. However, there are cases with lasting symptoms such as memory impairment which can last for months or Post-Concussion Syndrome (PCS) which can take months or even years to be resolved. PCS occurs in situations in which an athlete is not properly treated after a concussion [94, 112, 133]. Beside blast-born TBI in military battles and concussion in professional football, there are several other

impact-born threats causing brain injuries regardless of whether one is wearing protective equipment. These threats include motorcycle crashes, typical falls/collisions in hockey, baseball, soccer, biking, skateboarding, skiing, and lacrosse and finally accidents for fire fighters and construction workers. For all of these threats, wearing a helmet can reduce the risk of a severe head injury. However, no helmet design has been proven to effectively prevent brain injuries. Therefore, there is an urgent need to battle TBI and concussion by redesigning head protection systems with superior blast/impact mitigation capabilities.

Traditionally, the design of blast-resistant and impact-resistant protective structures has used observation and experience rather than theory and optimization. This limitation is addressed in this thesis by proposing a systematic rather than empirical design approach in which the focus is on the features of a blast/impact that sensitive targets need to be protected against, and on how protective structures might be optimized to achieve this. A novel design concept of blast/impact tuning and mitigation is proposed which drastically improves the performance of blast-resistant and impact-resistant protective structures, in particular, helmets. This original design idea is a simple, applicable, and creative solution to TBI in military conflicts and concussion in professional football and other aforementioned impact-born threats.

The challenges in proposing effective design strategies for protective structures are to understand and consider concurrently: 1) the mechanics of blast/impact in these threats; 2) the mechanics of damage to the behind-armor target due to blast/impact; and 3) the mechanics of how to mitigate effectively the damaging features of blast/impact through the design of protective structures. The objective of this thesis is to focus on these challenges. Specifically, Chapter 2 first reviews the literature on the studies and research already done to describe these three mechanics issues: 1) the contact/impact

behavior of full rigid spheres and thin (plane stress) spherical shells; 2) the head response to mechanical impact, hypothesized injury mechanisms including hypothesized brain injury criteria; and finally 3) blast mitigation strategies and impact mitigation. The current state of understanding along with the gaps and limitations in each topic are discussed in detail.

Chapter 3 focuses on identifying and understanding the major features of a blast pulse or an impact pulse exerted on a structure. First, the existing mechanics of blast is reviewed to identify the profile and parameters of the blast wave and most importantly, the profile and significant features of the pressure wave exerted on a surface as the blast wave impinges on the structure. Moreover, the contact behavior of spherical shells with intermediate shell thickness to shell outer radius ratios is investigated. A computational analysis is performed to assess the load-deflection behavior of spherical shells with intermediate shell thickness to shell outer radius ratios subjected to axial compression from a rigid flat plate under quasi-static loading. To verify the validity of the numerical simulations, the results are validated against the existing contact laws. Then, using the derived contact load-deflection relationships and incorporating Newton's second law of motion, the parametric formulations for the major features of the impact of spherical shells are extracted.

Chapter 4 investigates the dynamic response of a typical protected system to a transmitted blast load or impact load to pinpoint the damaging features of the blast/impact. The protected system considered in this study involves a supporting structure and a delicate target, modelled by two point masses and coupled by either an elastic spring or a combination of an elastic spring and a dissipative dashpot. The motivation for this assumption is a simple model of a head that can be envisaged as a brain coupled to a skull through cerebrospinal fluid. In the former approach, the

brain and the celebrospinal fluid are assumed to be elastic while in the latter, the viscoelastic behavior of the brain is taken into account. In this chapter, the damaging features of the transmitted blast load or impact load responsible for stress (or acceleration) on the delicate target (i.e. brain) are identified.

In Chapter 5, the detailed mitigation approaches of the identified damaging features of a transmitted blast load or impact load are discussed. The alternative strategies to dissipate the transmitted pressure and the transmitted impulse are explored. Available strategies to mitigate the transmitted pressure include impedance mismatch, visco-elasticity and plasticity. Available solutions to mitigate the transmitted impulse involve energy dissipation in visco-elastic polymers and plastic foams.

Chapter 6 introduces a novel design concept called "blast/impact tuning and mitigation" involving a multi-layered structure in which the outer layers tune the transmitted blast/impact stress wave to match the critical damping frequency of the inner visco-elastic layer. As the high frequency stress wave travels through this visco-elastic layer, it undergoes multiple loading-unloading cycles which can result in significant energy dissipation over a short duration and distance. The dimensionless material and geometrical parameters controlling viscous energy dissipation are identified to provide insight into how one might undertake the optimal design of a protective structure based on this novel concept. The dominant performance of the proposed design in mitigating both the transmitted pressure and the transmitted impulse is compared to the elastic design and plastic design.

In Chapter 7, two impact-born threats are reviewed in terms of impact characteristics. This investigation provides a useful tool for design optimization and clarifies the sensitivity of each impact characteristic with respect to material and geometrical

parameters of protective structures. Moreover, it makes costly (in terms of memory and time) computational analysis and costly (in terms of time and price) experimental analysis of impact events in these impact-born threats unnecessary. Finally, it may suggest the proper design strategies/regimes.

Finally, Chapter 8 briefly summarizes the work presented in this thesis, highlighting the significance of the results obtained and suggesting future efforts in developing blast-resistant and impact-resistant protective structures.

CHAPTER II

Introduction

2.1 Literature Review

2.1.1 Contact/Impact Mechanics in Solids

In contact mechanics, the contact behavior of a deformable spherical shell loaded by a rigid flat plate has received considerable attention among researchers. The first analytical solution for the deflection (displacement, δ) of a thin elastic spherical shell under a load (F) was given by Reissner [100] in which a system of equations for the direct stress resultants, transverse shear stress resultants, stress couples, and small strains of the spherical shell was derived by solving the equations of equilibrium, compatibility, and Hooke's Law in plane stress. Reissner also provided a load-deflection relationship which depends on the shell thickness to outer radius ratio (h_1/R_1) and its material properties - Young's modulus (E_1) and Poisson's ratio (ν_1). Later, Updike [125, 126, 127, 124] studied the load-deflection behavior of an elastic, thin, hemispherical shell being compressed by a flat, rigid surface based on large deflection shell theory and concluded that when the load increases, and the shell deflection to thickness ratio, δ/h_1, reaches ≈ 2, there is a change in deformation configuration. For low applied forces, the contact region lies flat against the rigid plate (configuration I) and for higher compression forces, the flattened region buckles forming

a circular fold (configuration II). The discontinuous transition between configurations I and II generates a dissipative hysteresis [93]. Other researchers attempted theoretically [29, 107, 136, 73, 69], experimentally [107, 64, 93, 42], and computationally [64, 41, 42, 72] to improve and validate the contact theory of thin-walled spherical shells initiated by Reissner [100]. Some of these investigations have focused on the nature of the interior stress state (direct stress resultant, bending stress couple, and transverse shear stress) and load-deflection relationship of thin elastic shells up to the onset of buckling [125, 29, 107, 136]. Others paid particular attention to the collapse behaviour of thin structural elements after buckling takes place to review the modes of collapse and their associated energy absorbing capacities [73, 127, 124, 64, 41, 42, 72].

Contact behavior of thin (plane stress) elastic spherical shells studied originally by Reissner [100] is considered one limiting case with the shell thickness to outer radius ratio of ≈ 0. The other limiting case belongs to the Hertzian contact theory in which the contact behavior of a solid elastic full sphere loaded by an elastic half space has been considered [55, 51]. In the Hertzian contact theory, the shell thickness to outer radius ratio is unity. These limiting cases have been studied extensively in the contact mechanics literature and their associated load-deflection relationships are of the form $F = Cf(\delta^n)$ where C is a coefficient and n, a constant exponent. More detail on these load-deflection relationships are presented in Section 3.2.1. Studies of the contact behavior of spherical shells with intermediate shell thickness to outer radius ratios, $0 < h_1/R_1 < 1$, loaded by a rigid flat plate have been limited to a single computational analysis [72], in which a numerical study has shown how the onset of plastic yielding in spherical shells with $0.00125 < h_1/R_1 < 1$, loaded by a rigid flat plate, is affected by the spherical shell geometry and material properties. Beyond this study, there has been little focus in the mechanics literature on the load-deflection relationships for spherical shells with intermediate shell thickness to outer radius ratios

in Updike's configuration I and the sensitivity of the features (e.g. C, and n) of these load-deflection relationships to the spherical shell geometry and material properties. These questions are addressed in this thesis. Here I am only interested in the elastic contact deformation in spherical shells in configuration I before buckling takes place.

The other interesting aspect of spherical shells with intermediate shell thickness to outer radius ratios centers around their impact response. There are several applications in bioengineering in which the impact behavior of spherical shells has a particular importance. One such application would be in contact sports including professional football in which a direct helmet-to-helmet impact in head-down tackles induces concussion in football players [131, 134]. A football helmet may be approximated as a spherical half shell with a shell thickness ($\approx$ 4 mm) to outer radius ($\approx$ 140 mm) ratio of $\approx$ 0.03, thus the impact response of two football helmets is of great interest in investigations aimed at preventing concussion in professional football. Specifically, the impact response of spherical shells provides us with three major characteristics of impact including the overpressure, P_o, duration, t_o, and impulse, I_o, transmitted to a helmet, with which we can study the stress transmitted through the helmet to the skull and thus to the brain.

The contact behavior of two deformable elastic bodies becomes more complicated when these bodies are impacted upon each other, due to the transient and non-linear essence of the problem [77]. Under impact, the rate of loading is high and dynamic effects become important. Many attempts have been made to derive analytically [28, 92, 65, 93, 144, 77, 119] linear and non-linear differential equations for the impact process of thin spherical shells and to validate experimentally [62, 67] the derived analytical solutions. Engin [28] investigated the dynamic response of a fluid-filled thin spherical shell subjected to a local radial impulsive load and obtained

the governing differential equations of the impact (by means of Hamilton's principle and Laplace transforms). Koller [65] studied the elastic impact of solid spheres on thin spherical shells and developed non-linear differential equations of the impact on the basis of Reissner shell theory and Hertzian contact theory. Young [144] proposed an approximate analytical model to predict the response of a fluid-filled thin spherical shell impacted by a solid elastic sphere based on combining the Hertzian contact stiffness and Reissner shell stiffness in series (and applying the principles of conservation of momentum and conservation of energy). Mansoorbaghaei [77] studied the impact of a thin-walled elastic spherical shell with an elastic barrier based on combining Hertzian and Reissner deformation equations, proposing a linearization technique (and applying Newton's second law of motion) to obtain the impact force and the duration. The above investigations have focused on the impact response of thin spherical shells. On the other hand, Johnson [55] examined the impact response of solid spheres using the load-deflection relationship in Hertzian contact theory (and applying Newton's second law of motion) to derive impact characteristics. What is missing in the mechanics literature is the impact response of spherical shells with intermediate shell thickness to outer radius ratios loaded by a rigid flat plate. This gap has been addressed in this thesis.

2.1.2 Head Response to Mechanical Impact

Head injuries result from various sources such as vehicle/motorcycle crashes, military activities, and typical falls/collisions in sports. The physiological origin of the damage in such head injuries is not well understood, although there are some hypothesized brain injury mechanisms available in the literature including negative pressure, positive pressure, pressure gradient, translational acceleration, rotational acceleration and deviatoric stress [47]. The primary component of the negative pressure mech-

anism is cavitation [76] which can occur either at coup (the area under the site of impact) or contrecoup (the area on the opposite side of impact) sites. Negative pressures at contrecoup sites initiate upon impact while negative pressures at coup sites form when the skull rapidly returns to its original geometry after being deformed. One of the most popular proposed head injury mechanisms is pressure gradient. A study on the dynamic stresses on the skulls of impacted dogs was carried out experimentally by employing strain gauges, pressure plugs, and accelerameters [44, 45]. This study suggested that there exists compression at the impact site, and tension at the opposite site and the pressure gradient is the cause for the dynamic stresses. Another finding of this study was that the brain injuries might develop either due to high acceleration and high pressure for a short duration of impact or due to low acceleration and low pressure for a long duration of impact. Pressure gradient can create shear stress which results in local deformations of brain tissue, thus, pressure gradient is a preliminary root to the development of another proposed injury mechanism which is deviatoric stress [114, 88, 56]. Moreover, the idea behind the proposed rotational acceleration injury mechanism is the fact that the brain is unable to rotate freely in the frontal compartments of the skull resulting in the development of shear stresses and thus, brain injuries [47].

Besides hypothesized brain injury mechanisms, biomechanical researches have proposed several brain injury criteria in an effort to identify a threshold for such injuries. These criteria relate brain injury mechanisms to observed injury phenomena and cognitive symptoms. The first criteria is the Wayne State Tolerance Curve (WSTC) based on a pressure-time tolerance curve and an acceleration-time tolerance curve created by Gurdjian [44, 45, 43]. These curves are shown in Fig 2.1. The basic finding was that high translational accelerations and high impact pressures can be withstood for short durations, while low translational accelerations and low impact

pressures can be tolerated for longer intervals.

The Severity Index (SI) and Gadd Severity Index (GSI) [50, 4] are extensions of the WSTC:

$$SI = \int [a_{trans}(t)]^{2.5}\, dt. \tag{2.1}$$

where $a_{trans}(t)$ is the translational acceleration. The weighting factor of 2.5 suggests that the influence of different levels of translational acceleration are not commensurate with each other, meaning that large translational accelerations have a profound effect upon injury while small translational accelerations have a little effect. A value of 1000 for SI index was suggested as an injury threshold and this index is assumed to be valid for a maximum duration of 50 msec [47].

The Head Injury Criterion (HIC) [50] is another injury index:

$$HIC = (t_2 - t_1) \left[\int a_{trans}(t)\, dt t_2 - t_1 \right]^{2.5}_{max}, \tag{2.2}$$

where $a_{trans}(t)$ is the translational acceleration and t_1 and t_2 are the initial and final times of the interval during which HIC attains a maximum value. The maximum time duration of HIC, $t_2 - t_1$, is limited to a specific value of ≈ 15 msec. HIC includes the effects of both head acceleration and the duration of the acceleration. Large accelerations may be tolerated for very short times. Again, a tolerance limit of 1000 has been adopted for the HIC [47].

Several investigators have used instrumented biomechanical analysis of impact in an effort to identify a threshold for concussion in professional football. To date, however, no variable has been identified to accurately predict injury risk [17]. Several attempts have been made to describe injury roots and to establish a meaningful in-

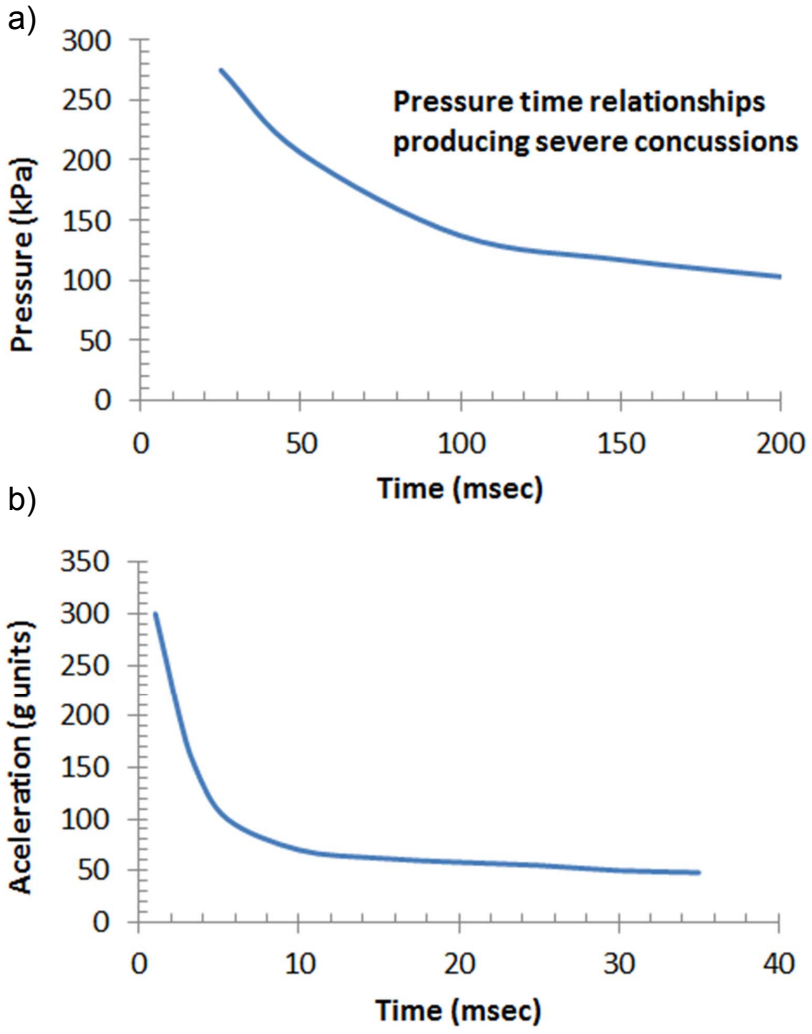

Figure 2.1: Wayne State Tolerance Curve (WSTC) [45], a) pressure-time tolerance curve, b) acceleration-time tolerance curve.

jury criterion through the use of injury data from football field- [17, 18, 38, 46, 103] or laboratory-based impact reconstructions [94, 145]. Linear acceleration and rotational acceleration are the two common kinetic measures of impact severity in these studies. Whereas some researchers have shown that linear acceleration is the fundamental mechanism for MTBI [94, 103] and the injury tolerance criteria such as WSTC, SI, and HIC are acceptable, others presume that rotational acceleration of the head is most likely correlated with strain on the brain tissue [91, 75, 78]. For sustaining MTBI, the head rotational acceleration threshold has been estimated over a wide range of 1,800 - 6,000 rad/sec^2 [145, 91, 75, 78]. Finally, in some instrumented studies, a combination of both linear acceleration and rotational acceleration has been considered as injury roots [38, 17, 46, 21, 63]. Besides these empirical injury criteria, an analytical criterion was introduced using finite element analysis and detailed anatomical modelling of the brain (the Wayne State University Head Injury Model (WSUHIM)) [132]. The WSUHIM is limited by an inability to predict the brain tissue response because this finite element head model is not fully validated and lacks a through treatment of in vivo material properties of brain.

Even though there is disagreement about the underlying mechanisms for brain injuries and consequently the brain injury criteria [47, 97], physics intuition tells us that by minimizing the damaging effects of blast/impact that are transmitted to the brain, injury risk will be minimized. To date the precise description of the harmful effects of blast/impact has been lacking.

2.1.3 Blast Dissipation

The interaction of a blast pressure pulse with structures can cause damage, either of a structural nature, if the blast causes collapse or other loss of structural integrity,

or of a functional nature, if the transmitted stress waves cause delicate components to fail. The two types of failure, loss of structural or functional integrity, lead to two distinct approaches for design against blast. One focus is on designing a system that can accommodate a given intensity of blast without loss of structural integrity. For example, a ship's hull should be designed so that a blast does not cause rupture. The other focus is to design armor to prevent the damaging effects of a blast from reaching a target behind the armor. For example, a helmet should be designed so that a blast does not cause injury to the brain by transmission of a shock wave through the skull and orifices [37].

One requirement for blast mitigation is the design of structures that can absorb all the blast-born energy without structural failure. Clamped monolithic plates [120, 141, 137, 32, 117, 57, 58, 140] provide one such example and they are used as protective structures in military ships and aircrafts. Clamped monolithic plates are made of ductile materials (e.g. steel) and are aimed to capture all the blast-born kinetic energy while experiencing minimum damage. One key damage considered to be minimized in clamped plates is permanent deflection. Clamped steel plates undergo bending and stretching in response to the blast, deform permanently, and dissipate plastic energy [141]. Theoretical formulations for the maximum permanent deflection at the center of rigid-plastic monolithic circular plates with clamped supports are given by Florence [32] for a rectangular impulse, and by Wang and Hopkins [137] for an infinite impulse with a negligible duration. The effect of adding a second source of energy dissipation (creep energy) in addition to plasticity to the response of clamped monolithic steel plates subjected to impulsive loads was also investigated experimentally and numerically [7, 8, 9]. The creep energy was generated through spray casting a layer of polyurea on the back face of the clamped monolithic plates resulting in a reduction in the extent of damage and permanent deformation in the plates.

The structures can also be designed with metallic cores and face-plates [141, 26, 31, 30, 68, 98, 142, 123, 81, 25, 118, 129, 147, 130], composite face-plates and polymeric cores [10, 27, 13, 12, 143, 121, 34], or with metal-polymer hybrids [49]. Clamped metallic-core sandwich plates have drawn a lot of attention in recent years. The dynamic structural response of these plates involves three distinct stages [141]: a) the impulse gets transmitted to the front face sheet making it move with an initial velocity toward the core; b) the front face sheet bends and compresses the core resulting in plastic deformation in the core and the front face sheet; and c) the entire composite plate undergoes bending and then in-plane stretching and energy dissipation continues in this stage mostly associated with the bending phase rather than the stretching phase. Another alternative approach for the design of blast-resistant structures is to incorporate an energy-dissipating core, in the form of foams or trusses, between two face-plates. These sandwich structures dissipate energy when the impulse of the pressure wave transmits momentum to a face-plate, which then deforms the core. The dynamic response of modified clamped sandwich plates consisting of stiff laminated carbon/epoxy composite face sheets and a compliant crushable foam core was also investigated numerically [27]. These plates were intended to have minimum permanent deformation or crushing of the foam core which gives rise to residual stresses and consequent nucleation of local interfacial cracks and fracture. Finally, the effect of introducing polyurethane, polyurea, and elastomeric foam inter-layers under the loaded face sheet in modified clamped sandwich plates was examined [13, 12] concluding that these thin, ductile, inter-layers absorb the face sheet deflection and thus prevent or reduce the extent of damage to the foam core.

Another requirement for blast mitigation focuses on minimizing the transmitted pressure wave and/or the transmitted momentum from the protective armor to the

target structure while the protective armor may or may not fail. One key example is granular systems which have the potential to control the transmitted pressure wave to the target. Granular systems are composed of particles arranged in a tightly packed lattice like configuration in which systematic variations of the mass and stiffness ratios of the particles lead to large variations in the characteristics of the propagating stress wave [70, 86, 22]. Another example belongs to air bladders or fluid chambers [85, 96, 148, 87, 48, 6, 35]. The effect of sandwich samples made from a vinyl-nitrile foam shell filled with either water, glycerin, glass beads, an aerogel, volcanic rock, or expanding foam in minimizing the transmitted pressure wave to the target was investigated experimentally [105]. The possible modes of shock attenuation including inertial effects (based on acoustic impedance) and dispersion (based on porosity) were also observed in this study [105]. An active, rather than a passive, approach to blast mitigation has recently been proposed by Wadley *et al.* [135] to minimize the transmitted compressive stress in a bilayer composite structure made of a buffer plate (exposed to the blast load) and a pre-compressed crushable foam that is relaxed just prior to the arrival of the blast-borne impulse, creating momentum opposing that acquired from the blast.

Studies of the interaction between a blast, armor, and a target have been limited to the specific analysis of a combat helmet [39, 40, 146, 33, 113], among which a numerical study [39] has shown how the replacement of foam by polyurea as a suspension pad may reduce the peak compressive stress in the brain and brain velocity. Beyond this type of empirical study, there has been little focus in the mechanics literature about the features of a blast that sensitive targets need to be protected against, and how armor might be optimized to achieve this. These questions provide the focus for the present work.

2.1.4 Impact Dissipation in Football Helmet

Mild Traumatic Brain Injury (mTBI), also known as concussion, is a serious injury resulting from impact in most contact sports, including professional football. Concussion is induced by mechanical forces such as impact with other objects [79, 80]. It is a brain injury resulting from a force transferred to the head leading to a collision between the brain and skull and deformation of the tissue and vascular system of the brain [112]. Concussion injuries can manifest as physical and psychological symptoms in addition to cognitive symptoms [79, 80].

With increasing evidence supporting a link between playing professional football and cognitive destruction in later life, there is an urgent need to reconsider the design of current football helmets. A football helmet is generally constructed with a tough polymer shell lined with a suspension system. The older American football helmets which included a stiff shell and foams were primarily designed to protect the skull from direct linear impact only with no specific consideration to prevent concussion. The shell is designed to protect the delicate areas of the skull from fracture and to remain undamaged itself, so that the impact forces are distributed over a wider skull area. The suspension pad involves materials that are supposed to dissipate the impact-born energy [106, 71, 20]. However, the suspension pads used in the current football helmet designs may have elastic response to the impact force at the relevant time scales with little to no energy dissipation involved. More recently, football safety equipment manufacturers have focused further on developing advanced padding systems to attempt to reduce concussion risks [133, 95]. The focus has been on reducing skull accelerations, first just linear but more recently rotational, and I will demonstrate that is part of what is required.

According to the National Football League (NFL) MTBI committee [131, 134], a

typical event that induces concussion in football involves a direct helmet-to-helmet impact in head-down tackles. Here, the striking player lines up his head, neck, and torso and delivers his force and momentum to the struck player whose body is aligned more or less perpendicularly to that of the striking player, such that his head or neck recieves the full force of the impact. There have been several approaches suggested by the NFL MTBI committee to potentially lower the risk of concussion [131]. These approaches include enforcing of head-up tackling techniques, reducing the mass of the helmet, and reducing the stiffness of the outer shell of the football helmet. These approaches are beneficial in terms of lowering the inertia of the striking player and limiting the impact force. However, they focus only on the mechanics of impact itself and how to reduce the impact force by altering the mass and stiffness of the helmet. What is missing is the mechanics of how to mitigate effectively the damaging effects of such impacts using dissipative materials in the design of a football helmet.

Very few researchers have attempted to develop a theoretical basis for helmet analysis and design [84, 36, 108]. These studies have included a lumped mass and spring approach [84, 36] and the experimental cushioning curve principle [108] to investigate the effects of various shell materials and foam densities on the deformation of motorcycle helmets. Cushioning curve principle is primarily used for packaging design. It demonstrates varying peak accelerations of a mass, falling a distance, on to a block of foam with different thicknesses. Beyond this type of theoretical study, there has been little focus in the mechanics literature on the mechanics of helmet-to-helmet impact, the features of such an impact that the brain needs to be protected against, and how football helmets might be optimized to achieve this.

2.2 Purpose and Research Overview

In this work, I focus on the problem of material design for protective structures for optimal blast/impact mitigation to reduce the risk of damage to delicate targets. The objective of this research is to follow a systematic approach rather than empirical approach to tailor material architectures for structures to be used as external protection of delicate targets.

In the design of blast-resistant armors (e.g. advanced combat helmet), there is often an associated goal of minimizing mass. Therefore, the design process eventually involves an optimization of blast-tolerance and mass minimization. This requires an understanding of 1) the major features of the blast pulse upon impinging the target structure, 2) how target structures are damaged by blast, and 3) how the damaging effects of a blast can either be accommodated or dissipated by the armor. Similarly, the design process for an impact-resistant structure (e.g. football helmet), demands an optimization of impact-tolerance and mass minimization. This necessitates a concurrent consideration of 1) the mechanics of contact/impact to identify the impact characteristics, 2) the mechanics of damage to the target as a result of impact, and 3) the mechanics of impact dissipation through the design of protective structures.

The focus of this research is first to investigate the mechanics of both a blast pressure wave (as impinged to a structure) and an impact pressure wave (of two colliding objects) to identify the profiles and the major characteristics of such pressure waves. Second, using a simple dynamic model of the target structure subjected to a blast or impact pressure wave, the damaging features of the transmitted pressure wave causing acceleration to the delicate target are identified. Third, a comprehensive investigation of the mechanics of blast/impact mitigation is carried out to propose proper design strategies for the protective structures such that they can effectively dissipate the

damaging features of blast/impact. In this research, linear visco-elasticity is used to introduce a novel design concept of impact/blast tuning and mitigation. The dimensionless material and geometrical parameters controlling viscous energy-dissipation are identified for a simplified one-dimensional system to provide insight into how one might design protective structures based on this concept.

CHAPTER III

Mechanics of Blast/Impact

3.1 Mechanics of Blast

An explosion can occur as a result of either a detonation of a condensed high explosive or an intense rise in local temperature. An explosion is associated with a rapid rise in the local pressure of the surrounding fluid. A blast is the transmission of this pressure pulse through the fluid by the propagation of a shock wave at approximately sonic velocity [110]. Considering the surrounding fluid as air, the blast-born shock wave traveling through the air is correlated with a pressure change from the ambient pressure, ahead of the shock-wave front, to the pressure behind it. This pressure jump is known as blast peak overpressure, P_{peak}. A fixed location in space first experiences P_{peak} as the shock-wave front passes over it and then, the pressure decays over time exponentially as the shock-wave front moves away. Typically, the duration of a shock-wave pressure pulse at a fixed point, t_{blast}, is quite short, a few tens or hundreds of microseconds. The simplest form of a blast wave has been described by the Friedlander waveform [110] as

$$P_{blast}(t) = P_{peak} e^{\frac{t}{t_{blast}}} (1 - \frac{t}{t_{blast}}), \tag{3.1}$$

while the momentum per unit area, I_{blast}, corresponding to the pressure pulse is

$$I_{blast} = \int_0^\infty P_{blast}(t)\, dt. \tag{3.2}$$

P_{peak} and t_{blast} depend upon the type and mass of explosive material and the distance from the source of the explosion [110, 116, 11]. Scaling laws have been developed to estimate blast wave parameters, e.g. P_{peak} and t_{blast}, for conventional high explosives [83, 16]. The important quantity in scaling laws is the dimensional distance parameter (scaled distance), Z, which is defined as

$$Z = \frac{R}{W^{\frac{1}{3}}}, \tag{3.3}$$

where Z is in m/kg$^{1/3}$, R is the distance from the explosion in meter and W is the basic explosive input or charge weight as an equivalent mass of TNT in kg. A detailed representation of significant blast wave parameters including P_{peak} and t_{blast} as a function of scaled distance, Z, is available in a number of references [110, 116].

When the blast wave, $P_{blast}(t)$, impinges on a structure, it is partly transmitted. The pressure transmitted on the impacted surface, $P(t)$, rises almost instantaneously to a peak value P_o, and then decays over time, t_o, such that

$$P(t) = P_o f(t/t_o). \tag{3.4}$$

The profile of $P(t)$ and the values for P_o and t_o depend on the details of the fluid-solid interaction (FSI) [120, 61, 59, 60]. The peak pressure, P_o, is one of the important characteristics of the stress wave arising in a solid as a result of a blast that can cause damage. The other important characteristic is the impulse imparted by the blast to

the structure, shown as, I_o:

$$I_0 = \int_0^\infty P(t)\, dt. \tag{3.5}$$

This impulse is responsible for the transfer of kinetic energy to the structure which can cause damage to the structure or to the components within it. Early work on FSI by Taylor [120] used the solution for a 1D wave pulse impinging on a free standing solid plate to compute I_o:

$$\frac{I_o}{I_{blast}} = 2q^{\frac{q}{1-q}}, \tag{3.6}$$

where q is the time scale ratio:

$$q = t_o/t^*. \tag{3.7}$$

t^* is the time scale characterizing fluid-plate interaction, defined as

$$t^* = \rho h/\rho_f C_f, \tag{3.8}$$

and ρ_f is the density of the fluid (air or water), C_f is the sonic speed of the blast wave in the fluid, ρ is the density of the plate, and h is the thickness of the plate. As seen by Eqns. 3.6 - 3.8, if $q << 1$, the plate is relatively massive and hardly moving, therefore, the reflected momentum is almost $-I_{blast}$ and the plate acquires momentum approaching $2I_{blast}$. On the other hand, if $q >> 1$, the plate is thin having little effect on the fluid motion and the transmitted impulse to the plate is negligible.

3.2 Mechanics of Impact

To investigate the mechanics of impact of two colliding objects, one requires an understanding of the contact mechanics of the objects. There are two contact laws available in the literature: The Hertzian contact theory [55, 51] for a solid sphere

loaded by an elastic half space and the Reissner contact theory [100] for a very thin spherical shell loaded by a rigid flat plate. In the following, I will describe these existing laws. Then I will go on to derive contact laws for more general shells. Finally, I will apply these derived contact laws to impact.

3.2.1 Existing Contact Laws

Consider an elastic full sphere with a Young's modulus of E_1, a Poisson's ratio of ν_1 and an outer radius of R_1 which is loaded by an elastic flat plate (half space) having a Young's modulus of E_2 and a Poisson's ratio of ν_2. According to the Hertzian contact theory, the relationship between the transmitted load, F_{Hertz}, and the deflection of two elastic bodies, δ_{Hertz}, during the contact [55] is

$$F_{Hertz} = \left[1.33\sqrt{R_1}E^*\right]\delta_{Hertz}^{1.50}, \tag{3.9}$$

where E^* is the effective Young's modulus given by

$$\frac{1}{E^*} = \frac{1-\nu_1^2}{E_1} + \frac{1-\nu_2^2}{E_2}. \tag{3.10}$$

In this theory, the surfaces are continuous, non-conforming, and frictionless. Tangential forces that may develop in applications where the surfaces slide or carry traction are not accounted for, the ratio of the maximum radius of the contact area to the outer radius of the sphere is quite small, and the elastic deformation remains small in comparison with the geometry of each contacting object [55].

Now, I consider a thin hollow spherical shell with a Young's modulus of E_1, a Poisson's ratio of ν_1, an outer radius of R_1, and a thickness of h_1 which is loaded by a rigid flat plate. According to Reissner contact theory, the load, $F_{Reissner}$, versus

deflection, $\delta_{Reissner}$, relationship during the contact [100] is

$$F_{Reissner} = \left[\frac{2.3 E_1 h_1^2}{R_1 \sqrt{1-\nu_1^2}} \right] \delta_{Reissner}. \tag{3.11}$$

In this theory, the ratio of the radius of the loading area to the outer radius of the shell is again quite small and the deflection of the spherical shell is small compared to its outer radius. Moreover, in this theory, the applied load to the spherical shell is assumed to be uniform normal load, parabolic normal load, or inertia load of a relating shell.

3.2.2 Proposed Contact Behavior for Intermediate Spherical Shells

The Hertz contact law and the Reissner contact law are two limiting shell/plate contact cases with shell thickness to shell outer radius ratios of 1 and ≈ 0, respectively. What is missing in the literature is the contact behavior of spherical shells with intermediate shell thickness to shell outer radius ratios (i.e. in the range of 0 - 1) loaded by a rigid flat plate.

In this section, I present results from finite-element analyses conducted to examine the load-deflection behavior of spherical shells with varying thickness to outer radius ratios subjected to axial compression from a rigid flat plate under quasi-static loading. In these results, I am interested in identifying the effect of the thickness to outer radius ratio of spherical shells on the load-deflection relationship. The validity of the results is then compared to the established Hertzian and Reissner contact theories in the limits.

In this analysis, only the elastic contact deformation prior to the onset of buckling or inelastic response was considered and the collapse behaviour at larger deformations

was not addressed. The finite-element calculations were performed using the commercial code ABAQUS Implicit [1]. The spherical shell and the flat plate were modeled using two-dimensional axisymmetric, four-node and three-node continuum elements with reduced integration (CAX4R and CAX3). The geometry is shown in Fig. 3.1. The displacements along the axis of symmetry z- of the flat plate and spherical shell were restricted in the x- direction and the displacements along the base of the spherical shell were restricted in the z- direction. The interface between the flat plate and spherical shell was frictionless. The mesh density in the radial direction at the contact region of the shell was set to be very fine such that the ratio of the thickness of the shell to the the element size becomes > 100.

A displacement of the flat plate was prescribed for loading the shell. A time-varying displacement $\delta(t)$ was applied to the upper surface of the flat plate, along the z- direction (Fig. 3.1). This displacement increased linearly from zero to a peak value such that the displacement to thickness ratio of the spherical shell always remained below unity to insure no buckling [93]. Therefore, the displacement of the spherical shell, $\delta(t)$, was an input to the numerical simulations and the normal contact force, $F(t)$, was obtained as an output for any given displacement. As shown in Fig. 3.2, the normal contact load in the flat plate, $F(t)$, was computed by integrating the stress for axisymmetric plates:

$$F(t) = \int_0^{2\pi} \int_0^{l_{flat}} \sigma_z x dx d\theta, \tag{3.12}$$

where l_{flat} is the radius of the flat plate (Fig. 3.1) and σ_z is the normal nodal stress in the z- direction as calculated from the finite-element simulations.

As with Hertzian theory, the isotropic, elastic spherical shell has a Young's modulus of E_1, a Poisson's ratio of ν_1, an outer radius of R_1, and a thickness of h_1, and

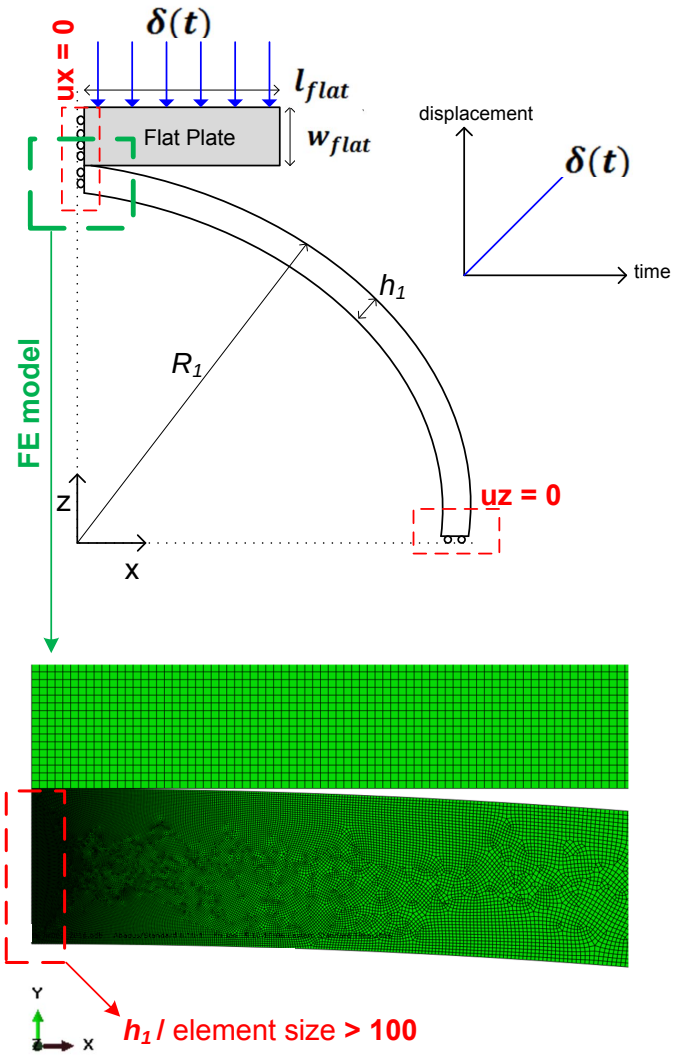

Figure 3.1: Geometry of the spherical shell and the flat plate analyzed in the finite-element model.

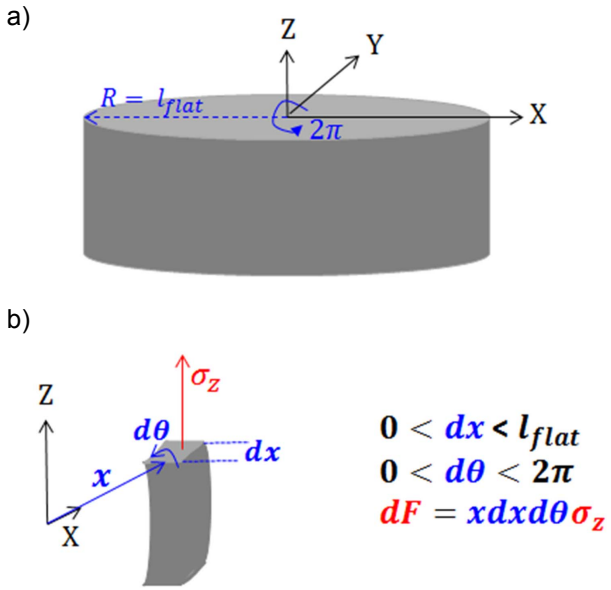

Figure 3.2: a) 3D geometry of the flat plate, b) illustration of calculating the normal contact load, $F(t)$, by integrating the stress, σ_z.

the flat plate is rigid. These dimensions and properties, plus the deflection of the spherical shell, δ, results in a total of five variables (E_1, ν_1, R_1, h_1 and δ) and two different units (meter, and N) to describe the normal contact force, F. Therefore, according to the Buckingham-II theory [111, 128, 19], the normal contact force must be a function of three dimensionless groups. Finite element calculations showed that the normal contact load, F, in a dimensionless form of $FR_1/E^*h_1^3$, can be expressed by the following three dimensionless groups:

$$\frac{FR_1}{E^*h_1^3} = f(\frac{\delta}{h_1}, \frac{h_1}{R_1}, \nu_1), \tag{3.13}$$

where E^* is defined as $E_1/(1-\nu_1^2)$.

Fig. 3.3 and Table 3.1 report the results of calculations over the following ranges

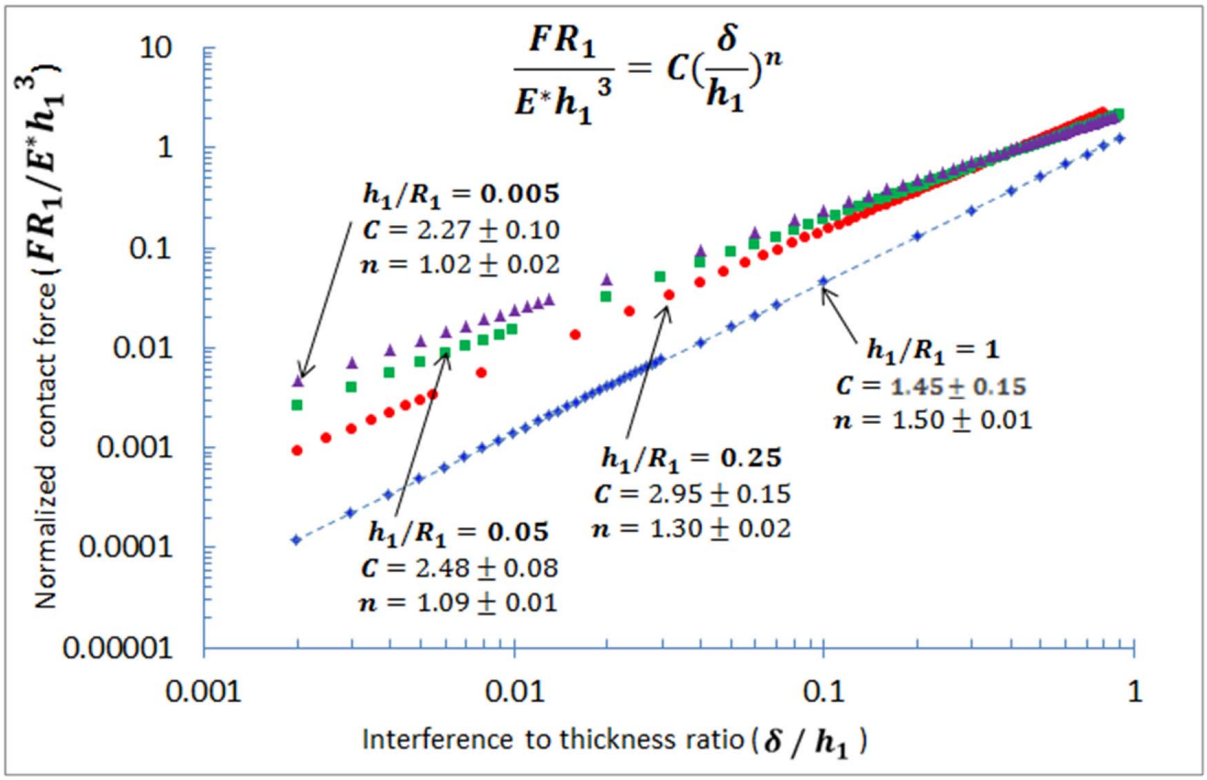

Figure 3.3: The contact load-deflection relationship in dimensionless form: $FR_1/E^*h_1^3$ versus δ/h_1 for four different values of h_1/R_1 $(0.005, 0.05, 0.25$ and $1)$ and $\nu_1 = 0.3$.

of values for ν_1, δ/h_1 and h_1/R_1:

$$\begin{aligned} \nu_1 &= 0.3 \\ 0.001 \leq \frac{\delta}{h_1} &\leq 1 \\ 0.005 \leq \frac{h_1}{R_1} &\leq 1. \end{aligned} \tag{3.14}$$

Fig. 3.3 is indeed the contact load-deflection relationship in a dimensionless form:

$$\frac{FR_1}{E^*h_1^3} = C(\frac{\delta}{h_1})^n, \tag{3.15}$$

for four different values of h_1/R_1 (0.005, 0.05, 0.25, and 1) whereas the resulting contact load-deflection relationship for eight different values of δ/h_1 can be found in Table 3.1. Fig. 3.3 and Table 3.1 illustrate the sensitivity of the contact load-

Table 3.1: The coefficient, C, and the exponent, n, for various h_1/R_1 in the dimensionless contact load-interference relationship $FR_1/E^*h_1^3 = C\ (\delta/h_1)^n$ considering $\nu_1 = 0.3$.

h_1/R_1	Coefficient (C)	Exponent (n)
1	1.45±0.15	1.50±0.01
0.75	2.18±0.13	1.50±0.01
0.5	3.05±0.05	1.46±0.02
0.25	2.95±0.15	1.30±0.02
0.1	2.90±0.20	1.17±0.01
0.05	2.48±0.08	1.09±0.01
0.02	2.39±0.12	1.05±0.01
0.005	2.27±0.10	1.02±0.02

deflection relationship to varying h_1/R_1. These are manifest in the coefficient, C, and the exponent, n. The exponent, n, increases as the thickness to outer radius ratio, h_1/R_1, is increased. The reason why the lower bound for h_1/R_1 has been selected as 0.005 is that any further reduction has insignificant effect on the measured coefficient, C, and exponent, n, values. To verify the validity of the finite element model, the results for $h_1/R_1 = 1$ (Table 3.1) were compared with the Hertz solution (Eqn. 3.9) and the results for $h_1/R_1 = 0.005$ (Table 3.1) were compared with the Reissner solution (Eqn. 3.11). As shown in Eqn. 3.9, the coefficient and exponent in the Hertz solution are 1.33 and 1.50, respectively, which match the ranges of C and n reported in Table 3.1 for $h_1/R_1 = 1$. Similarly, the coefficient and exponent in the Reissner solution are 2.19 and 1.00, respectively, which match the ranges of C and n reported in Table 3.1 for $h_1/R_1 = 0.005$.

The contact area between the spherical shell and the rigid flat plate is a circle of radius $a(t)$. Considering the isotropic, elastic spherical shell (E_1, ν_1, R_1, and h_1), the rigid flat plate and the deflection of the spherical shell, δ, there exist a total of five variables (E_1, ν_1, R_1, h_1 and δ) and two different units to describe the contact radius, a. Therefore, according to the Buckingham-II theory [111, 128, 19], the contact radius

must be a function of three dimensionless groups. Finite element calculations showed that the contact radius, a, in a dimensionless form of a/R_1, can be expressed by the following three dimensionless groups:

$$\frac{a}{R_1} = f(\frac{\delta}{R_1}, \frac{h_1}{R_1}, \nu_1), \tag{3.16}$$

Fig. 3.4 and Table 3.2 report the results of calculations over the following ranges of values for ν_1, δ/R_1, and h_1/R_1:

$$\begin{aligned} \nu_1 &= 0.3 \\ 0.0001 \leq \frac{\delta}{R_1} &\leq 1 \\ 0.005 \leq \frac{h_1}{R_1} &\leq 1. \end{aligned} \tag{3.17}$$

Table 3.2: The coefficient, D, and the exponent, m, for various h_1/R_1 in the dimensionless contact radius-interference relationship $a/R_1 = D\ (\delta/R_1)^m$ considering $\nu_1 = 0.3$.

h_1/R_1	Coefficient (D)	Exponent (m)
1	1.03±0.10	0.47±0.03
0.75	0.77±0.06	0.46±0.02
0.5	0.57±0.06	0.44±0.04
0.25	0.51±0.04	0.39±0.02
0.1	0.33±0.05	0.35±0.03
0.05	0.25±0.04	0.33±0.03
0.02	0.23±0.05	0.32±0.04
0.005	0.10±0.03	0.30±0.04

Fig. 3.4 is indeed the contact radius-deflection relationship in a dimensionless form:

$$\frac{a}{R_1} = D(\frac{\delta}{R_1})^m, \tag{3.18}$$

for four different values of h_1/R_1 (0.005, 0.02, 0.25, and 1). Fig. 3.4 and Table 3.2 illustrate the sensitivity of the contact radius-deflection relationship to varying h_1/R_1.

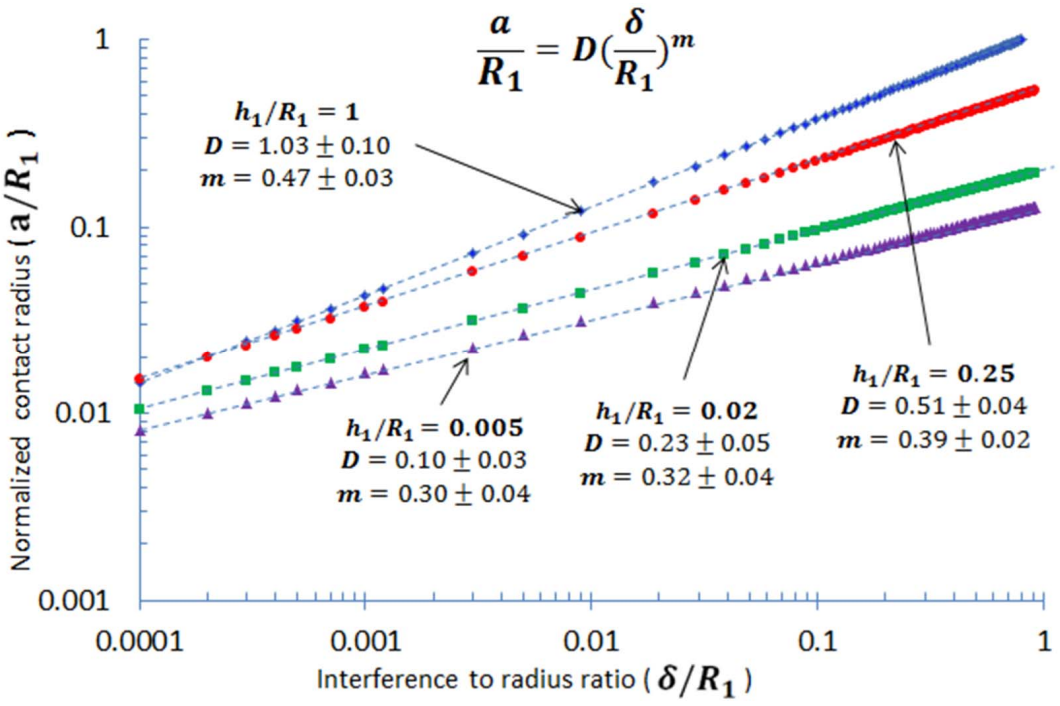

Figure 3.4: The contact radius-deflection relationship in dimensionless form: a/R_1 versus δ/R_1 for four different values of h_1/R_1 $(0.005, 0.02, 0.25$ and $1)$ and $\nu_1 = 0.3$.

The exponent, m, increases as the thickness to outer radius ratio, h_1/R_1, is increased. To verify the validity of the finite element model, the results for $h_1/R_1 = 1$ (Table 3.2) were compared with the Hertz solution in which the contact radius for a full sphere loaded by a flat plate is approximated as $a \approx \sqrt{R_1\delta}$ [55]. In this equation, the coefficient, D, and the exponent, m, are 1 and 0.5, respectively, which match the ranges of D and m reported in Table 3.2 for $h_1/R_1 = 1$. I am not comparing the area results with the Reissner solution due to the difference in loading conditions.

Finally, considering the isotropic, elastic spherical shell (E_1, ν_1, R_1, and h_1), the rigid flat plate, and the deflection of the spherical shell, δ, there exist a total of five variables (E_1, ν_1, R_1, h_1, and δ) and two different units to describe the contact pressure, P. Therefore, according to the Buckingham-II theory [111, 128, 19], the contact pressure must be a function of three dimensionless groups. Finite element calculations showed that the contact pressure, P, in a dimensionless form of P/E^*, can be expressed by the following three dimensionless groups:

$$\frac{P}{E^*} = f(\frac{\delta}{h_1}, \frac{h_1}{R_1}, \nu_1), \tag{3.19}$$

Fig. 3.5 reports the results of calculations over the following ranges of values for ν_1, δ/h_1, and h_1/R_1:

$$\begin{aligned} \nu_1 &= 0.3 \\ 0.0001 \leq \frac{\delta}{h_1} &\leq 0.01 \\ 0.005 \leq \frac{h_1}{R_1} &\leq 1. \end{aligned} \tag{3.20}$$

Fig. 3.4 is indeed the contact pressure-deflection relationship in a dimensionless

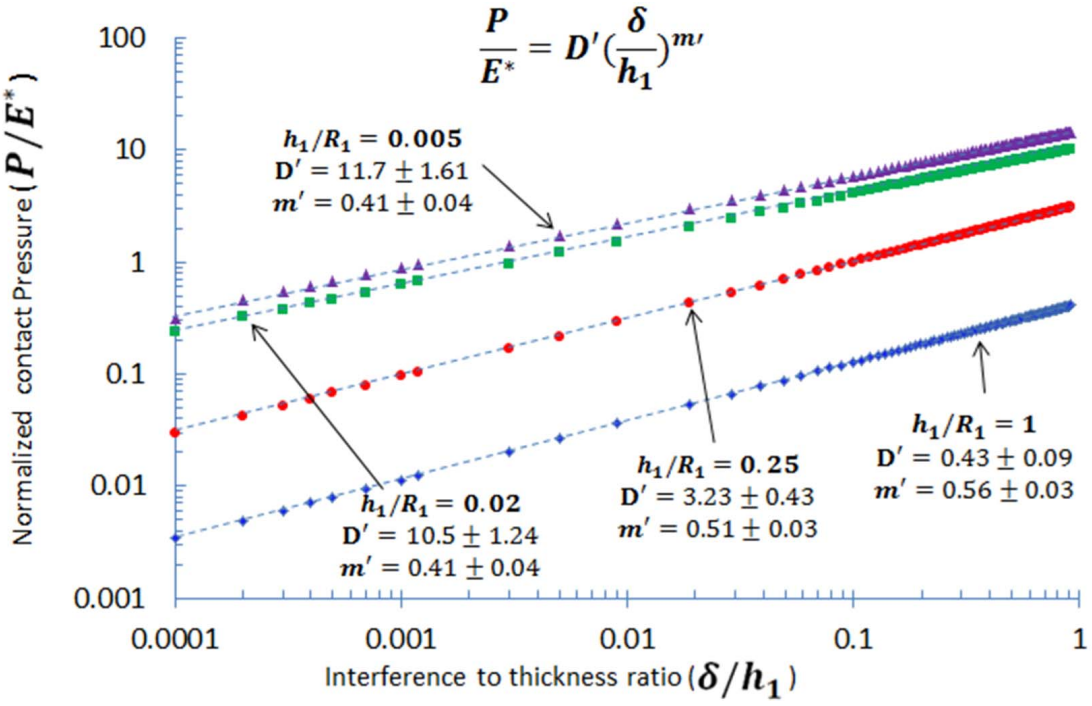

Figure 3.5: The contact pressure-deflection relationship in dimensionless form: P/E^* versus δ/h_1 for four different values of h_1/R_1 $(0.005, 0.02, 0.25$ and $1)$ and $\nu_1 = 0.3$.

Table 3.3: The coefficient, D', and the exponent, m', for various h_1/R_1 in the dimensionless contact pressure-interference relationship $P/E^* = D'\ (\delta/\delta)^{m'}$ considering $\nu_1 = 0.3$.

h_1/R_1	Coefficient (D')	Exponent (m')
1	0.43±0.09	0.56±0.03
0.75	1.17±0.13	0.57±0.02
0.5	2.82±0.15	0.58±0.04
0.25	3.23±0.43	0.51±0.03
0.1	7.05±0.52	0.47±0.03
0.05	9.93±1.10	0.43±0.03
0.02	10.5±1.24	0.41±0.04
0.005	11.7±1.61	0.41±0.04

form:

$$\frac{P}{E^*} = \acute{D}(\frac{\delta}{R_1})^{\acute{m}}, \tag{3.21}$$

for four different values of h_1/R_1 (0.005, 0.02, 0.25, and 1) and $\nu_1 = 0.3$. Fig. 3.5 and Table 3.3 illustrate the sensitivity of the contact average pressure-deflection relationship to varying h_1/R_1.

3.2.3 Generalized Formulae for Impact Characteristics of Intermediate Spherical Shells

In this Section, I use the load-deflection relationship calculated in Section 3.2.2 to work out the generalized formulae for the three major impact characteristics including impact overpressure P_o, duration t_o, and impulse I_o from the impact of intermediate spherical shells (having a Poisson's ratio of 0.3) with a rigid flat plate.

Consider an elastic spherical shell with mass of m_1 which contacts a rigid flat plate under frictionless conditions while traveling at a constant velocity V_o. The generalized

contact load-deflection relationship of Eqn. 3.15 is rewritten as

$$F(t) = C(\frac{E^* h_1^{3-n}}{R_1})\delta(t)^n = K\delta(t)^n, \tag{3.22}$$

where K is the effective stiffness that depends upon the geometry (h_1 and R_1) and elastic constants (E_1 and ν_1) of the shell along with the coefficient, C, and the exponent, n. According to Newton's second law of motion, the inertia force of the spherical shell is

$$m_1 \frac{d^2\delta(t)}{dt^2} = -K\delta(t)^n. \tag{3.23}$$

Integrating Eqn. 3.23 with respect to $\delta(t)$ gives

$$\frac{1}{2}\left[V_o^2 - (\frac{d\delta(t)}{dt})^2\right] = (\frac{1}{n+1})\frac{K}{m_1}\delta(t)^{n+1}. \tag{3.24}$$

The moment at which the maximum deflection (δ_{max}) of the spherical shell with respect to the rigid flat plate occurs, the instantaneous velocity of the center of the shell, $d\delta(t)/dt$, becomes zero. Therefore, the maximum elastic deflection of the shell is determined as

$$\delta_{max} = \left[\frac{n+1}{2}\frac{m_1 V_o^2}{K}\right]^{\frac{1}{n+1}}. \tag{3.25}$$

Substituting δ_{max} into Eqn. 3.22 gives us the maximum contact load, F_{max}, as

$$F_{max} = K(\delta_{max})^n. \tag{3.26}$$

F_{max} in terms of relative velocity, and material and geometrical parameters of the spherical shell is calculated as

$$F_{max} = (\frac{n+1}{2})^{\frac{n}{n+1}} C^{\frac{1}{1+n}} \left[\frac{m_1^n V_o^{2n} E^* h_1^{3-n}}{R_1}\right]^{\frac{1}{n+1}}. \tag{3.27}$$

On the other hand, the contact radius-deflection relationship of Eqn. 3.18 can be

rewritten as

$$a(t) = D\delta(t)^m {R_1}^{1-m}. \tag{3.28}$$

The maximum contact radius, a_{max}, can be calculated by substituting δ_{max} (Eqn. 3.25) into Egn. 3.28 to give

$$a_{max} = D\delta_{max}^m {R_1}^{1-m}. \tag{3.29}$$

Since the spherical shell is elastic, F_{max} and δ_{max} occur at the same time. Dividing the maximum contact load, F_{max}, (Eqn. 3.27) by the maximum contact area, πa_{max}^2, gives us the impact overpressure, P_o, as

$$P_o \approx \frac{(n+1)^{\frac{n-2m}{n+1}} C^{\frac{2m+1}{n+1}}}{2\pi D^2} \left[\frac{{m_1}^{n-2m} {V_o}^{2n-4m} {E^*}^{1+2m} {h_1}^{6m-2nm+3-n}}{{R_1}^{3+2n-2nm}} \right]^{\frac{1}{n+1}}. \tag{3.30}$$

Here, the impact duration, t_o, will be investigated. The relation between time, t, and the deflection, δ, is determined by integrating Eqn. 3.24 as [74]

$$t = \frac{1}{V_o} \int_0^{\delta} \frac{d\delta}{\sqrt{1 - (\frac{\delta}{\delta_{max}})^{n+1}}}. \tag{3.31}$$

The duration of the impact, t_o, which is an important parameter in the analysis of the impact, is

$$t_o = \frac{2}{V_o} \int_0^{\delta_{max}} \frac{d\delta}{\sqrt{1 - (\frac{\delta}{\delta_{max}})^{n+1}}}. \tag{3.32}$$

If the substitution $x = (\delta/\delta_{max})^{n+1}$ is made in Eqn. 3.32, the integral reduces to

$$t_o = \frac{2}{n+1} \frac{\delta_{max}}{V_o} \int_0^1 x^{\frac{-n}{n+1}} (1-x)^{-0.5} dx = \frac{2}{n+1} \frac{\delta_{max}}{V_o} B_x(\frac{1}{n+1}, 0.5), \tag{3.33}$$

where $B_x(1/(n+1), 0.5)$ is the Beta function, also known as an Euler integral of the

first kind. Rewriting Eqn. 3.33 leads to

$$t_o = \frac{2}{n+1} B_x(\frac{1}{n+1}, 0.5) \left[\frac{m_1 R_1}{{V_o}^{n-1} E^* {h_1}^{3-n}} \right]^{\frac{1}{n+1}}. \tag{3.34}$$

The final important characteristic of the impact is the impulse, I_o, which can be considered as the area under the load-time history of the impact, $F(t)$. The calculated impulse is in Newton.sec:

$$I_o = \int F(t)dt. \tag{3.35}$$

To solve the integral in Eqn. 3.35, I need to have the profile for $F(t)$. Deresiewicz [24] evaluated Eqn. 3.31 numerically and obtained the approximate deflection-time history, $\delta(t)$, as

$$\delta(t) \approx \delta_{max} sin(\frac{\pi t}{t_o}). \tag{3.36}$$

Therefore, the load-time profile of the impact, $F(t)$, which is a function of $\delta(t)$ as in Eqn. 3.22, has a sinusoidal profile with a total duration of t_o and the maximum contact load of F_{max} occurring at t_o / 2:

$$F(t) \approx K \delta_{max}^n sin^n(\frac{\pi t}{t_o}). \tag{3.37}$$

Substituting Eqn. 3.37 into Eqn. 3.35 gives

$$I_o \approx \left[\frac{n+1}{2} C^n \frac{m_1 {V_o}^2 {h_1}^{3n-n^2} E^{*n}}{R^n} \right]^{\frac{1}{n+1}} \int_0^{t_o} sin^n(\frac{\pi t}{t_o}) dt. \tag{3.38}$$

If I simplify Eqn. 3.38 by considering the load-time profile of the impact, $F(t)$, as a triangle with a total duration of t_o and the maximum contact load of F_{max} occurring

at t_o / 2, Eqn. 3.38 changes to

$$I_o \approx \frac{\sqrt{2\pi}(\frac{n+1}{2})^{\frac{n}{n+1}}}{n+1} \frac{(\frac{1}{n+1})^{\frac{1}{n+1}-0.5}}{(\frac{1}{n+1}+0.5)^{\frac{1}{n+1}}} [m_1 V_o]. \tag{3.39}$$

As shown in Eqn. 3.39, I_o is only a function of mass (m_1) and velocity (V_o), which confirms the physics of momentum.

P_o (Eqn. 3.30), t_o (Eqn. 3.34), and I_o (Eqn. 3.38) are the three major characteristics of the impact in generalized form for $\nu_1 = 0.3$. These three major characteristics are all functions of relative velocity (V_o) and material and geometrical parameters of the spherical shell (m_1, h_1, R_1, and E_1). The sensitivities of P_o, t_o, and I_o (simplified triangular form) with respect to each of these parameters (V_o, m_1, h_1, R_1, and E_1) are summarized in Table 3.4.

Table 3.4: The exponents for V_o, m_1, h_1, R_1 and E_1 in the derived generalized formulae for P_o, t_o, and I_o ($\nu_1 = 0.3$).

Parameter	$P_o(Pa)$	$t_o(sec)$	I_o (N.sec)
V_o	$\frac{2n-4m}{n+1}$	$-\frac{n-1}{n+1}$	1
m_1	$\frac{n-2m}{n+1}$	$\frac{1}{n+1}$	1
h_1	$\frac{6m-2nm+3-n}{n+1}$	$-\frac{3-n}{n+1}$	0
R_1	$-\frac{3+2n-2nm}{n+1}$	$\frac{1}{n+1}$	0
E_1	$\frac{1+2m}{n+1}$	$-\frac{1}{n+1}$	0

Considering the limiting case of Reissner contact theory with $n = 1$, P_o and t_o become

$$P_o \approx \frac{C^{0.8} E^{*0.8} h_1^{1.61} V_o^{0.38} m_1^{0.19}}{2\pi D^2 R_1^{2.19}},$$

$$t_o \approx \frac{1}{h_1}\sqrt{\frac{2\pi m_1 R_1}{C E^*}}.$$

Considering the other limiting case, the Hertz contact theory, with $n = 3/2$ and

$R_1 = h_1$, P_o and t_o become

$$P_o \approx \frac{C^{0.8} m_1^{0.2} V_o^{0.4} E^{*0.8} h_1^{1.2}}{2\pi D^2 R_1^{1.8}},$$

$$t_o \approx 1.3 \frac{m_1^{0.4}}{C^{0.4} V_o^{0.2} E^{*0.4} R_1^{0.2}}.$$

CHAPTER IV

Mechanics of Damage to a Behind-Armor Target as a Result of Blast/Impact

Recently, there has been much publicity about the damage that can be caused to brain tissue by blast or by impact to the head in sports or vehicle crashes. The physiological origin of the damage is not well understood, although it is generally agreed to be the consequence of excessive axonal deformation arising from local deviatoric stresses [114, 88, 56]. Local stresses may also be responsible for the failure of delicate mechanical objects located within or behind a protective structure (or armor). Therefore, for the purposes of evaluating possible mitigation strategies, it is necessary to identify the important features of any pressure waves induced by blast or impact that may travel through armor to damage a behind-armor target.

There is a general tendency in the brain injury literature to measure the acceleration of the head as a proxy for the stresses acting on the brain [37, 82, 50, 17, 38]. However, it was recognized more than 70 years ago [53] that this is valid only for impacts of long duration. For short impacts and blasts, it is the change in velocity (impulse) of the head that indicates the level of the stresses in the brain. The head is a complex dynamical system, so the force transmitted to the brain cannot simply be taken to be the force applied to or transmitted to the skull. Here, I am using a

very simple dynamical system to illustrate this point, since identifying the correct mechanics is crucial for evaluating design concepts for armor.

4.1 Basic Definitions

The *mathematical description* of any dynamic system is obtained by first drawing a schematic diagram of the system and defining variables and then using physical laws (e.g. Newton's laws) to write equations for each component. For a *linear system*, the equations that constitute the mathematical model are linear. The *Laplace transform* is one of the most important mathematical tools available for modeling and analyzing linear systems. The main advantage of the Laplace transform is that differential equations in the time domain become algebraic equations in the Laplace domain because differentiation of the time function corresponds to the multiplication of the Laplace transform by a complex number s. Let's define $f(t)$ as a time function such that $f(t) = 0$ for $t < 0$, s as a complex variable and Ł as an operational symbol indicating that the quantity upon which it operates is to be transformed by the Laplace integral:

$$\int_0^\infty \mathrm{e}^{-st}\,\mathrm{d}t. \tag{4.1}$$

Then, the Laplace transform of $f(t)$, shown by $F(s)$, is calculated as:

$$Ł[f(t)] = F(s) = \int_0^\infty f(t)\mathrm{e}^{-st}\,\mathrm{d}t. \tag{4.2}$$

According to *differentiation theorem*, the Laplace transform of the derivative of a function $f(t)$ is given by [90]:

$$Ł[\frac{d}{dt}f(t)] = sF(s) - f(0), \tag{4.3}$$

where $f(0)$ is the initial value of $f(t)$, evaluated at $t = 0$. A *transfer function* is one common approach for modeling and analyzing dynamic systems which is defined as the ratio of the Laplace transform of the output to the Laplace transform of the input.

4.2 Dynamic Model of an Elastic Behind-armor Target Exposed to Blast

A simplified, but typical, system that might need to be protected from blast and impact can be modelled as a two-component dynamical system consisting of the target and it's supporting structure. The supporting structure and target are masses coupled by a spring, and the structure is attached to a rigid foundation by a second spring. The motivation for this assumption is a simple model of a head that can be envisaged as a brain coupled to a skull through cerebrospinal fluid, with the motion of the skull being resisted by its attachment to the rest of the body by the neck. Fig. 4.1 demonstrates such a system that included a delicate target (m_2) supported by a structural support (m_1) coupled with each other by a spring (k_2) and to a rigid foundation by a spring (k_1), where m represents mass and k represents geometric stiffness. The force pulse transmitted from the blast, either directly or as modified by passage through the armor, $F(t)$, is applied to the structural support. In a simple model of the head, this structural support m_1 is the skull, and the spring k_1 represents the stiffness of the neck. The importance of this spring has been demonstrated experimentally by showing that bracing the neck decreases the severity of brain damage [37, 23]. In this simple model of the head, the target m_2 is the brain, and the spring k_1 represents the cerebrospinal fluid.

Equations of motion for the two masses, m_1 and m_2, are obtained by applying the

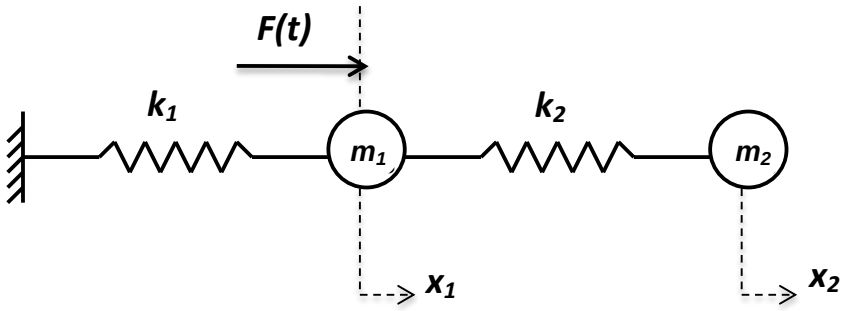

Figure 4.1: Dynamic model of a structural support of mass m_1 attached to a rigid foundation by a spring of stiffness k_1, and coupled to a delicate target of mass m_2 through a spring of stiffness k_2. A pressure force $F(t)$ is transmitted to the structure either directly from the blast, or through the armor.

Newton's second law to the system:

$$m_1\ddot{x}_1 = F(t) - K_1x_1 - K_2[x_1 - x_2], \tag{4.4}$$

$$m_2\ddot{x}_2 = K_2[x_1 - x_2], \tag{4.5}$$

where x_2 is the displacement of the target, and x_1 is the displacement of the structure (Fig. 4.1). In Eqn. 4.5, $\ddot{x}_2$ is the acceleration of the target which is linearly proportional to the total force ($K_2(x_1$ - $x_2)$) applied to the target. Therefore, the load that can cause damage (acceleration) to the target is given by

$$F_2(t) = K_2(x_1 - x_2). \tag{4.6}$$

Consequently, the relationship between the force imposed on the structure, $F(t)$, and the force acting on the target, $F_2(t)$, is given by

$$F_2(t) = F(t) - [m_1\ddot{x}_1 + k_1x_1]. \tag{4.7}$$

A calculation of the force that acts on the target is obtained by solving these two

equations, subject to an assumption that the structure and target are assumed to be initially at rest ($x_1 = x_2 = \dot{x}_1 = \dot{x}_2 = 0$), and the transmitted force, $F(t)$, is a decaying triangular pulse with a peak force F_t, a duration of t_t and an impulse of I_t ($= F_t t_t$ / 2).

Eqns. 4.4 and 4.5 are the mathematical models of the system. The Laplace transforms of these equations are

$$m_1[s^2X_1(s) - sx_1(t=0) - \dot{x_1}(t=0)] + K_1X_1(s) + K_2[X_1(s) - X_2(s)] = P(s), \quad (4.8)$$

$$m_2[s^2X_2(s) - sx_2(t=0) - \dot{x_2}(t=0)] - K_2[X_1(s) - X_2(s)] = 0. \quad (4.9)$$

Since the displacement initial conditions (x_1 (t = 0) and x_2 (t = 0)) and velocity initial conditions ($\dot{x_1}$ (t = 0) and $\dot{x_2}$ (t = 0)) are zero, Eqns. 4.8 and 4.9 can be written as

$$X_1(s)[K_1 + K_2 + m_1s^2] + X_2(s)[-K_2] = F(s), \quad (4.10)$$

$$X_1(s)[K_1] + X_2(s)[-K_2 - m_2s^2] = 0. \quad (4.11)$$

The input of the protected system is the transmitted force, $F(t)$, while the output is the acceleration of the target, $\ddot{x}_2$. As mentioned before, $\ddot{x}_2$ is linearly proportional to $F_2(t)$ which itself is linearly proportional to $x_1 - x_2$. Once x_1 and x_2 are found, $F_2(t)$ and consequently $\ddot{x}_2$ can be found. Therefore, the displacements x_1 and x_2 are the actual outputs of the system. Since there exist two output variables, there shall be two transfer functions: the ratio of the Laplace transform of x_1 to the Laplace transform of $F(t)$ and the ratio of the Laplace transform of x_2 to the Laplace transform of $F(t)$. These two ratios can be obtained by combining Eqns. 4.10 and 4.11 to get

$$G(s) = \frac{X_1(s)}{F(s)} = \frac{K_2 + m_2 s^2}{m_1 m_2 s^4 + (K_2 m_2 + K_1 m_2 + K_2 m_1)s^2 + (K_1 K_2)}, \tag{4.12}$$

$$K(s) = \frac{X_2(s)}{F(s)} = \frac{K_2}{m_1 m_2 s^4 + (K_2 m_2 + K_1 m_2 + K_2 m_1)s^2 + (K_1 K_2)}. \tag{4.13}$$

A system's transfer function is a property of the system itself, independent of the magnitude and nature of the input. If a transfer function of a system is known, the output or response can be studied for various forms of inputs with a view towards understanding the nature of the system. MATLAB Simulink [3] is a powerful tool enabling us to analyze the output or response once the transfer functions are identified. The MATLAB SIMULINK code developed to analyze the protected structure system is presented in APPENDIX A.

The behind-armor system involves two point masses, m_1 and m_2, and two springs, k_1 and k_2. These properties plus the two characteristics (F_t and t_t) of the transmitted force, $F(t)$, make a total of six variables and three different units to describe the maximum force acting on the supporting structure, $F_{1_{max}}$, and the maximum force acting on the target, $F_{2_{max}}$. Therefore, according to the Buckingham-Π theory [111, 128, 19], the resultant maximum acting forces must be a function of three dimensionless groups:

$$\frac{F_{i_{max}}}{F_t} = f\left(\frac{m_1}{m_2}, \frac{k_1}{k_2}, \sqrt{\frac{k_2}{m_2}}t_t\right) \ , \tag{4.14}$$

where i = 1 indicates the supporting structure, i = 2 indicates the target, $\sqrt{m_2/k_2}$ represents the natural period of the target and $\sqrt{\frac{k_2}{m_2}}t_t$ is the normalized impact duration by the natural period of the target.

MATLAB SIMULINK (APPENDIX A) calculations show how $F_{1_{max}}$ and $F_{2_{max}}$ vary with $\sqrt{k_2/m_2}t_t$ for a range of masses and spring constants. Fig. 4.2 shows the maximum force exerted on the structure, $F_{1_{max}}/F_t$, and on the target, $F_{2_{max}}/F_t$, as a function of normalized time, $\sqrt{k_2/m_2}t_t$, and mass ratio, m_1/m_2, for $k_1/k_2 = 10$. Moreover, Fig. 4.3 shows the maximum force exerted on the structure, $F_{1_{max}}/F_t$, and on the target, $F_{2_{max}}/F_t$, as a function of normalized time, $\sqrt{k_2/m_2}t_t$, and spring constant ratio, $k_1/k_2 = 10$, for $m_1/m_2 = 1$. Figs. 4.2 and 4.3 demonstrate:

1. The maximum force acting on the supporting structure is relatively constant and approximately equal to F_t. This is what would be measured by placing an accelerometer on the supporting structure.

2. The maximum force on the target depends on the transmitted impulse, I_t, when the duration of the pulse is shorter than the natural period of the target ($t_t < \sqrt{m_2/k_2}$).

3. The maximum force on the target depends on the amplitude of the transmitted force, F_t when the duration of the pulse is longer than the natural period of the target ($t_t > \sqrt{k_2/m_2}$).

Although this is a relatively simple dynamical model, it provides several important conclusions about protecting targets from damage arising from blast:

1. The maximum force on the target does not necessarily correlate with the maximum force applied to the structure. A practical implication of this is that a simple measurement of maximum acceleration of a skull may give no indication of the force that a brain experiences. Skull acceleration measurements are a useful part of the time-history record, and not the complete record.

2. The correct protective strategy depends on the duration of the blast compared to the natural period of the target one is trying to protect. If the duration of

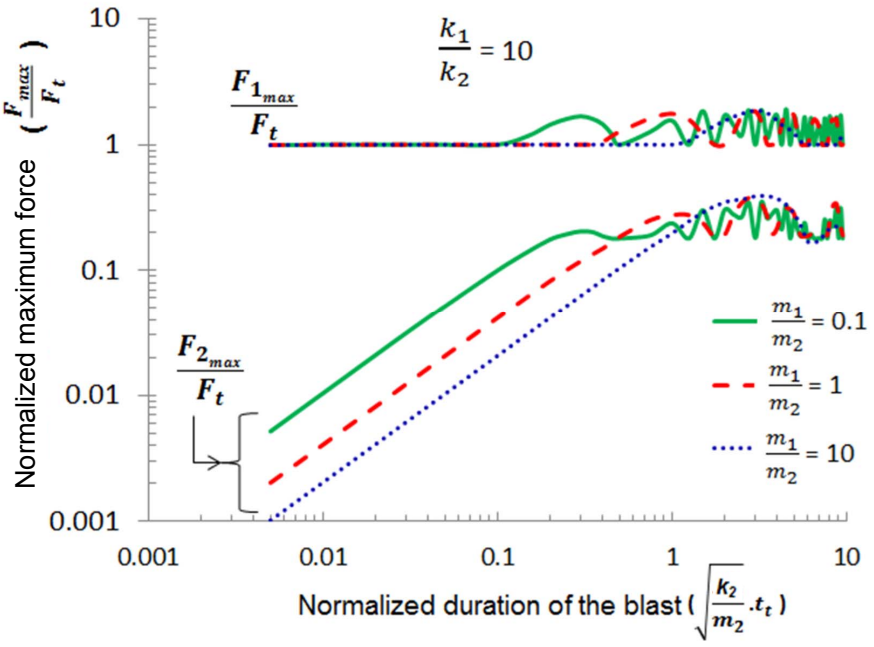

Figure 4.2: Maximum force exerted on the structure, $F_{1_{max}}/F_t$, and on the target, $F_{2_{max}}/F_t$, as a function of normalized time, $\sqrt{k_2/m_2}t_t$, and mass ratio, m_1/m_2, for $k_1/k_2 = 10$. The maximum force on the structure is relatively constant and approximately equal to the amplitude of the transmitted force. The maximum force on the target depends on the transmitted impulse when the transmitted pulse is shorter than the natural period of the target. It depends on the amplitude of the transmitted force only when the pulse is longer than the natural period of the target.

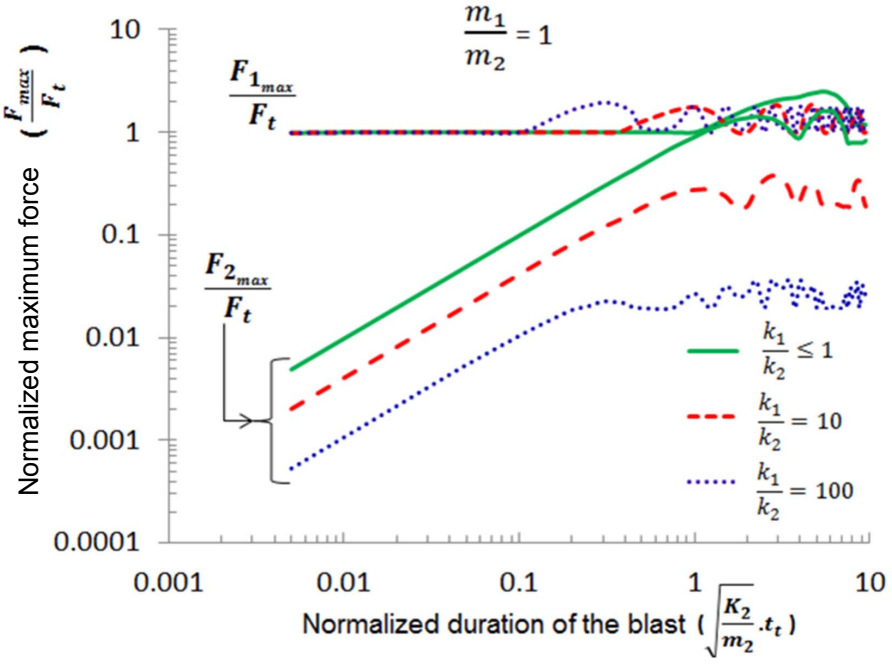

Figure 4.3: Maximum force exerted on the structure, $F_{1_{max}}/F_t$, and on the target, $F_{2_{max}}/F_t$, as a function of normalized time, $\sqrt{k_2/m_2}t_t$, and spring constant ratio, $k_1/k_2 = 10$, for $m_1/m_2 = 1$. The maximum force on the structure is relatively constant and approximately equal to the amplitude of the transmitted force. The maximum force on the target depends on the transmitted impulse when the transmitted pulse is shorter than the natural period of the target. It depends on the amplitude of the transmitted force only when the pulse is longer than the natural period of the target.

the blast is relatively long, then it is the amplitude of the transmitted force that has to be reduced. If the duration of the blast is relatively short, then it is the transmitted impulse that has to be minimized.

3. The duration of a blast event is generally very short (a few tens or hundreds of microseconds). In the case of a brain as the target, the exact value for the natural period of the brain is not well understood, however, the relaxation times of the brain are in the range of 30 - 1000 msec [101]. Therefore the duration of the blast is expected to be shorter than the natural period of the brain as well. Thus the impulse becomes the damage-causing feature of the blast that has to be minimized in the armor design.

4. Neurological studies of the blast-born TBI have shown that blast-induced learning and memory deficits can be reduced by immobilizing the head [37]. This finding has been demonstrated in Fig. 4.3 in which both damaging features of a blast (transmitted force and transmitted impulse) reduce as the ratio of k_1/k_2 increases by stiffening the "neck". As Fig. 4.3 shows, as k_1/k_2 increases, the force transmitted to the brain decreases.

4.3 Dynamic Model of an Elastic Behind-armor Target Exposed to Impact

In Section 4.2, I investigated the dynamic response of the protected system (Fig. 4.1) to the transmitted force, $F(t)$, which was modelled as a decaying triangular pulse with a peak force of F_t (at time $t = 0$), a duration of t_t, and an impulse of I_t ($= F_t t_t$ / 2). The transmitted force, $F(t)$, was a simplified representation of a blast load. Here, in this section, I study the dynamic response of the same protected system (Fig. 4.1) to a transmitted force, $F(t)$, which is a representative of an impact load. Therefore, $F(t)$ is an isosceles triangular pulse with a duration of t_t, a peak force of F_t occurring

at $t = t_t$ / 2, and an impulse of I_t (= $F_t t_t$ / 2). MATLAB SIMULINK (APPENDIX A) was applied again to demonstrate how the maximum force exerted on the structure, $F_{1_{max}}/F_t$, and on the target, $F_{2_{max}}/F_t$, vary with normalized impact duration, $\sqrt{k_2/m_2}t_t$, for a range of masses and spring constants.

Fig. 4.4 shows the maximum force exerted on the behind-armor supporting structure, $F_{1_{max}}/F_t$, and on the target, $F_{2_{max}}/F_t$, as a function of normalized time, $\sqrt{k_2/m_2}t_t$, and mass ratio, m_1/m_2, for $k_1/k_2 = 10$. This figure demonstrates:

1. The maximum force acting on the supporting structure is relatively constant and approximately equal to F_t when the duration of the pulse is shorter than the natural period of the target ($t_t < \sqrt{m_2/k_2}$).

2. The maximum force on the target depends on the transmitted impulse, I_t, when the duration of the pulse is shorter than the natural period of the target ($t_t < \sqrt{m_2/k_2}$).

3. The maximum force on the target and on the supporting structure relates directly to the amplitude of the transmitted force, F_t, and relates inversely to the duration of the pulse, t_t, when the duration of the pulse is longer than the natural period of the target ($t_t > \sqrt{m_2/k_2}$).

The important conclusions about protecting targets from damage arising from impact are:

1. The maximum force on the target does not necessarily correlate with the maximum force applied to the structure.

2. The correct protective strategy depends on the duration of the impact compared to the natural frequency of the target one is trying to protect. If the duration of the impact is long, then it is the amplitude of the transmitted force that has

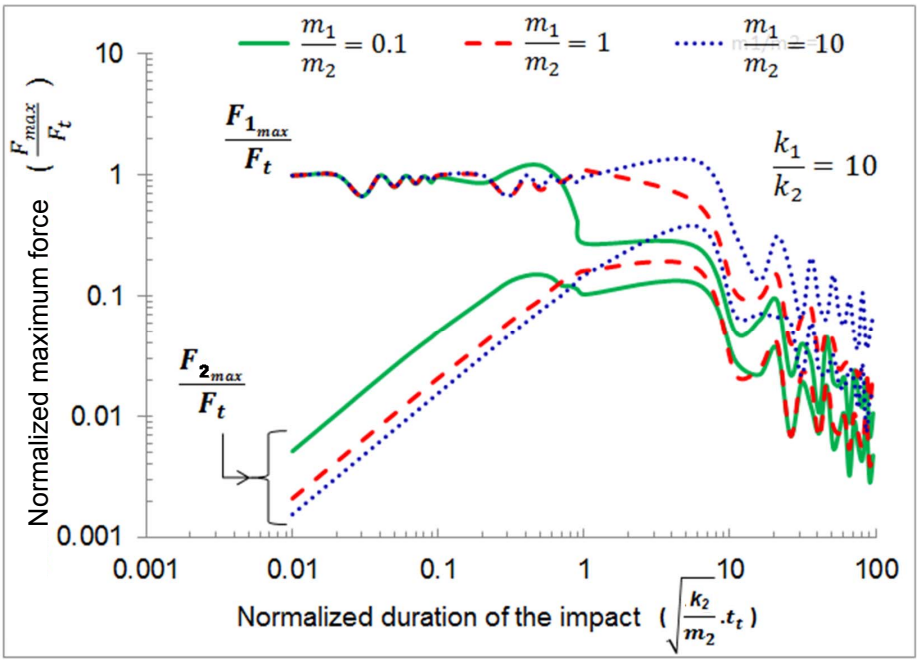

Figure 4.4: Maximum force exerted on the structure, $F_{1_{max}}/F_t$, and on the target, $F_{2_{max}}/F_t$, as a function of normalized time, $\sqrt{k_2/m_2}t_t$, and mass ratio, m_1/m_2, for $k_1/k_2 = 10$. When the duration of the pulse is longer than the natural period of the target, the maximum force on the target and on the supporting structure relates directly to the amplitude of the transmitted force and relate inversely to the duration of the pulse. When the duration of the pulse is shorter than the natural period of the target, the maximum force acting on the supporting structure is relatively constant while the maximum force on the target depends on the transmitted impulse.

to be reduced. If the duration of the impact is short, then it is the transmitted impulse that has to be minimized. This important appreciation that either the pressure or the impulse can cause damage was recognized as long ago as 1941 [53], and is reflected in empirical head-injury criteria [44, 47, 104]. However, it is often only the peak acceleration of the supporting structure (skull) that is measured in instrumented studies of impact [37, 82, 50, 17, 38], assuming that it is only this that determines the acceleration of the brain and therefore acts as a proxy for the damaging stresses.

4.4 Dynamic Model of a Visco-elastic Behind-armor Target Exposed to Impact

In Section 4.3, I investigated the dynamic response of a protective system including two point masses and two elastic springs (Fig. 4.1) to the transmitted impact load, $F(t)$. In that system, the response is fully elastic. In order to involve the visco-elastic response of the system, here, in this section, I am adding to the protective system a visco-elastic damper with a damping coefficient of C. Fig. 4.5 demonstrates such a system. As shown in this figure, the supporting structure and the target, m_1 and m_2, are coupled by an elastic spring of stiffness k_2 and a dissipative dash pot with a damping coefficient C. The motivation for this modification is a simple model of a head in which the brain and the cerebrospinal fluid are made of viscoelastic materials.

In this system, equations of motion for the two masses, m_1 and m_2, are:

$$m_1\ddot{x}_1 = F(t) - K_1x_1 - K_2[x_1 - x_2] - C[\dot{x_1} - \dot{x_2}], \tag{4.15}$$

$$m_2\ddot{x}_2 = K_2[x_1 - x_2] + C[\dot{x_1} - \dot{x_2}], \tag{4.16}$$

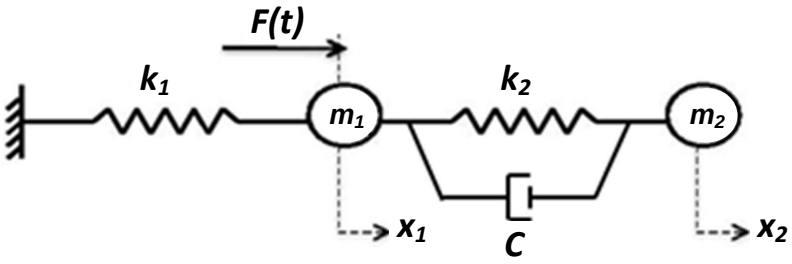

Figure 4.5: Dynamic model of a structural support of mass m_1 attached to a rigid foundation by a spring of stiffness k_1, and coupled to a delicate target of mass m_2 through a spring of stiffness k_2 and a dash pot of coefficient C. A force $F(t)$ is transmitted to the structure either directly from the impact, or through the armor.

where x_2 is the displacement of the target, x_1 is the displacement of the structure and $\ddot{x}_2$ is the acceleration of the delicate target. The load that can cause damage (acceleration) to the target is

$$F_2(t) = K_2(x_1 - x_2) + C[\dot{x_1} - \dot{x_2}]. \tag{4.17}$$

Consequently, the relationship between the impact force imposed on the structure, $F(t)$, and the force acting on the target, $F_2(t)$, is given by Eqn. 4.7. Assuming that the structure and target are initially at rest ($x_1 = x_2 = \dot{x}_1 = \dot{x}_2 = 0$), the Laplace transforms of Eqns 4.15 and 4.16 become

$$m_1[s^2X_1(s)] + C[sX_1(s) - sX_2(s)] + K_1X_1(s) + K_2[X_1(s) - X_2(s))] = P(s), \tag{4.18}$$

$$m_2[s^2X_2(s)] - C[sX_1(s) - sX_2(s)] - K_2[X_1(s) - X_2(s)] = 0. \tag{4.19}$$

The displacements x_1 and x_2 are still the outputs of the system. Therefore, there shall be two transfer functions: the ratio of the Laplace transform of x_1 to the Laplace transform of $F(t)$ and the ratio of the Laplace transform of x_2 to the Laplace transform

of $F(t)$. These transfer functions are given by

$$G(s) = \frac{X_1(s)}{F(s)} = \frac{K_2 + Cs + m_2 s^2}{m_1 m_2 s^4 + [Cm_1 + Cm_2]s_3 + [K_2 m_2 + K_1 m_2 + K_2 m_1]s^2 + (Ck_1)s + (K_1 K_2)}, \tag{4.20}$$

$$K(s) = \frac{X_2(s)}{F(s)} = \frac{K_2 + Cs}{m_1 m_2 s^4 + [Cm_1 + Cm_2]s_3 + [K_2 m_2 + K_1 m_2 + K_2 m_1]s^2 + (Ck_1)s + (K_1 K_2)}. \tag{4.21}$$

Again, MATLAB SIMULINK was used to analyze the protected structure system and the code is presented in APPENDIX B.

The protected system involves two point masses, m_1 and m_2, two springs, k_1 and k_2 and one dashpot, C. These properties plus the two characteristics of the transmitted force, $F(t)$, make a total of seven variables and three different units to describe the maximum force acting on the supporting structure, $F_{1_{max}}$, and the maximum force acting on the target, $F_{2_{max}}$. Therefore, according to the Buckingham-Π theory [111, 128, 19], the resultant maximum forces must be a function of four dimensionless groups:

$$\frac{F_{i_{max}}}{F_t} = f\left(\frac{m_1}{m_2}, \frac{k_1}{k_2}, \sqrt{\frac{k_2}{m_2}}t_t, \frac{C}{m_2}t_t\right) , \tag{4.22}$$

where i = 1 indicates the supporting structure, i = 2 indicates the delicate target, $\sqrt{m_2/k_2}$ represents the natural period of the delicate target and m_2 / C is the relaxation time of the target. In fact, the main difference between the two presented systems (Fig. 4.1 versus Fig. 4.5) is in the number of time scales involved in the system. In Fig. 4.1, the only time scale is the natural period of the target, $\sqrt{m_2/k_2}$, while in Fig. 4.5, there are two time scales: the natural period of the target, $\sqrt{m_2/k_2}$, and the relaxation time of the delicate target, m_2 / C.

MATLAB SIMULINK calculations show how $F_{1_{max}}$ and $F_{2_{max}}$ vary with $\sqrt{k_2/m_2}t_t$ for a range of $(C/m_2)t_t$. Fig. 4.6 shows the maximum force exerted on the structure, $F_{1_{max}}/F_t$ as a function of normalized times $\sqrt{k_2/m_2}t_t$ and $(C/m_2)t_t$, for $k_1/k_2 = 10$ and $m_1/m_2 = 1$. Fig. 4.7 shows the maximum force exerted on the target, $F_{2_{max}}/F_t$, as a function of normalized times $\sqrt{k_2/m_2}t_t$ and $(C/m_2)t_t$, for $k_1/k_2 = 10$ and $m_1/m_2 = 1$. Figs. 4.6 and 4.7 demonstrate:

1. The maximum force acting on the supporting structure is relatively constant and approximately equal to F_t when the duration of the pulse is shorter than both the natural period of the target and the relaxation time of the target ($t_t < \sqrt{m_2/k_2}$ and $t_t < m_2/C$).

2. The maximum force acting on the supporting structure depends on the amplitude of the transmitted force, F_t when the duration of the pulse is shorter than the natural period of the target ($t_t < \sqrt{m_2/k_2}$) and larger than the relaxation time of the target ($t_t > m_2/C$).

3. The maximum force on the target and on the supporting structure is directly proportional to the amplitude of the transmitted force, F_t, and inversely proportional to the duration of the pulse, t_t, when the duration of the pulse is longer than the natural period of the target ($t_t > \sqrt{k_2/m_2}$).

4. The maximum force on the target depends on the transmitted impulse, I_t, when the duration of the pulse is shorter than the natural period of the target which itself is shorter than the relaxation time of the target ($t_t < \sqrt{k_2/m_2} < m_2$ / C).

5. The maximum force on the target only depends on the amplitude of the transmitted force, F_t, when the duration of the pulse is shorter than the natural period of the target which itself is longer than the relaxation time of the target ($t_t < \sqrt{k_2/m_2}$ and $\sqrt{k_2/m_2} > m_2$ / C).

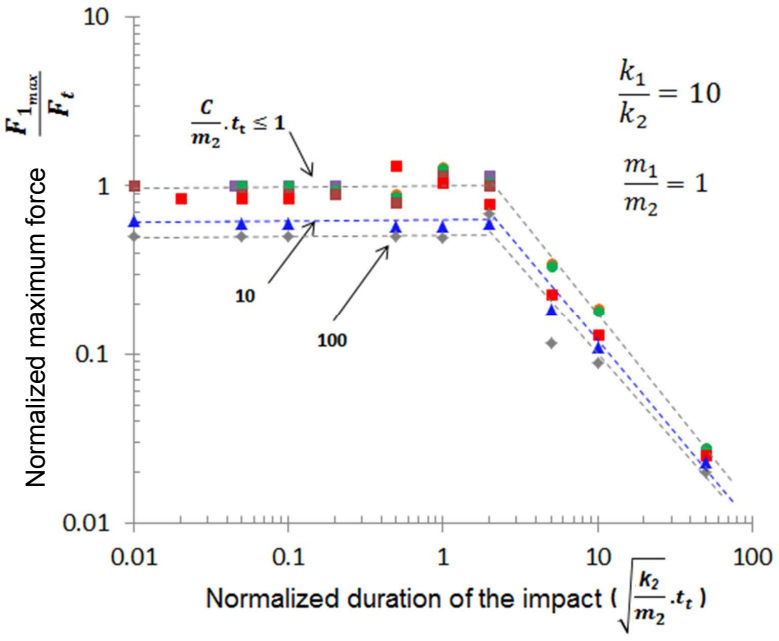

Figure 4.6: Maximum force exerted on the structure, $F_{1_{max}}/F_t$ as a function of normalized times $\sqrt{k_2/m_2}t_t$ and $(C/m_2)t_t$, for $k_1/k_2 = 10$ and $m_1/m_2 = 1$. The maximum force acting on the supporting structure is relatively constant and approximately equal to the amplitude of the transmitted force when the duration of the pulse is shorter than both the natural period of the target and the relaxation time of the target. It depends on the amplitude of the transmitted force when the duration of the pulse is shorter than the natural period of the target and larger than the relaxation time of the target. Finally, it is directly proportional to the amplitude of the transmitted force and inversely proportional to the duration of the pulse when the duration of the pulse is longer than the natural period of the target.

Although this is still a relatively simple dynamical model, there are several important conclusions:

1. The maximum force on the target does not necessarily correlate with the maximum force applied to the structure.

2. The correct protective strategy depends on the relative values for the duration of the impact, the natural period of the target and the relaxation times of the target one is trying to protect. If the duration of the impact is long relative to the natural period of the target, then it is the amplitude of the transmitted

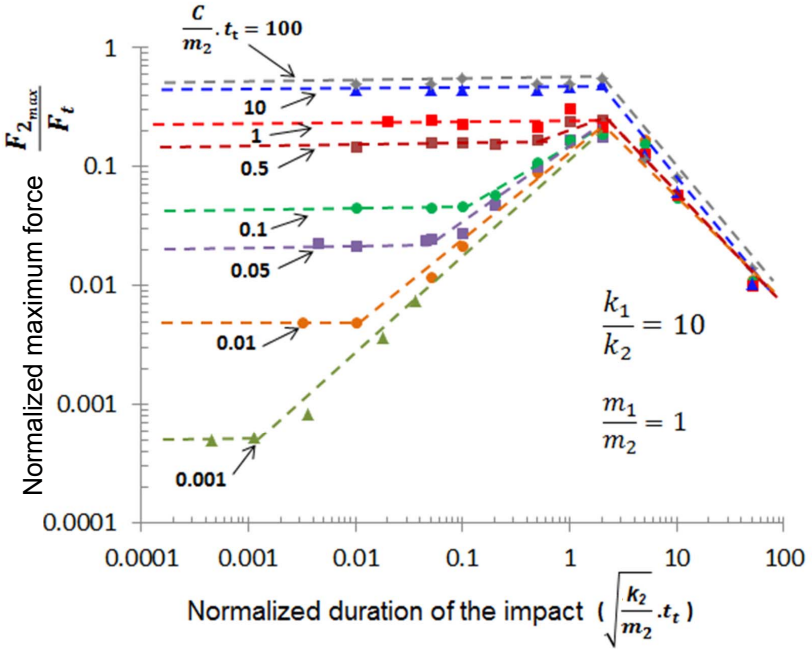

Figure 4.7: Maximum force exerted on the delicate target, $F_{2_{max}}/F_t$ as a function of normalized times $\sqrt{k_2/m_2}t_t$ and $(C/m_2)t_t$, for $k_1/k_2 = 10$ and $m_1/m_2 = 1$. The maximum force acting on the target depends on the transmitted impulse when the duration of the pulse is shorter than the natural period of the target which itself is shorter than the relaxation time of the target. It depends on amplitude of the transmitted force when the duration of the pulse is shorter than the natural period of the target which itself is longer than the relaxation time of the target Finally, it is directly proportional to the amplitude of the transmitted force and inversely proportional to the duration of the pulse when the duration of the pulse is longer than the natural period of the target.

pressure that has to be reduced. If the duration of the impact is short relative to the natural period of the target, then depending on the relative values for the natural period of the target and the relaxation times of the target, it is either the transmitted impulse or the amplitude of the transmitted pressure that has to be minimized.

3. In the case of the human brain as the target, the values for its natural periods are not well understood, however, the relaxation times of the brain are in the range of 30 - 1000 msec [101]. Since the relative values for the natural period of the brain and the relaxation times of the brain are not well identified, the conservative design approach is to minimize both damaging features of the impact including the transmitted impulse and the transmitted pressure.

CHAPTER V

Mechanics of Blast/Impact Mitigation

As discussed in Chapter IV, the damage (stress or acceleration) on the delicate target (i.e. brain) is controlled by either the amplitude of the transmitted pressure or the transmitted impulse to the structural support (i.e. skull). The relative importance between the two parameters depends on the relative values for the duration of the blast/impact, the natural period of the target, and the relaxation times of the target. No matter what the relative values for the three time scales of the system are, if the duration of the blast/impact is long relative to the natural period of the target, it is the amplitude of the transmitted pressure responsible for the damage to the brain. In the case where there is not enough information available about the exact values for the three time scales of the system, the conservative approach is to design a protective structure that can mitigate both the impulse and pressure amplitude to minimize the transmission of these parameters to the structural support.

5.1 Pressure Mitigation

5.1.1 Impedance Mismatch

Here I start with the investigation of the wave propagation in a linear elastic thin plate having Young's modulus of E, density of ρ and length of L. With the definition

of a thin plate, I make the assumption that the transverse displacements can be neglected in comparison to the longitudinal displacement. To investigate, I need to solve the second-order linear partial differential wave equation. In its simplest 1D form, the wave equation concerns a time variable t, a spatial variable x and a scalar function $u = u\ (x,\ t)$, whose values could model the displacement of a wave:

$$\frac{\partial^2 u}{\partial x^2} = \frac{1}{C^2}\frac{\partial^2 u}{\partial t^2}, \tag{5.1}$$

where the constant C is the propagation speed of the wave calculated as $\sqrt{E/\rho}$. Eqn. 8.1 alone does not specify a solution; a unique displacement solution, $u(x,t)$, is usually obtained by setting a problem with further conditions: initial conditions and boundary conditions. Once displacement, $u(x,t)$, is solved, particle velocity $v(x,t)$ and stress wave $\sigma(x,t)$ can be easily calculated as

$$v(x,t) = \frac{\partial u(x,t)}{\partial t}, \tag{5.2}$$

$$\sigma(x,t) = E\frac{\partial u(x,t)}{\partial x}. \tag{5.3}$$

For the purposes of this thesis, which mostly focuses on one-dimensional geometries, instead of solving the actual wave equation (Eqn. 8.1), an alternative method of 1D x-t diagram is applied to identify how the stress wave, $\sigma(x,t)$, propagates in the plate. The x-t diagram provides a systematic presentation of the progress of a family of stress waves such that it is easy to identify the stress level at any point x in a system at a chosen time t [11]. One example of the x-t diagram is shown in Fig. 5.1. This figure demonstrates how the stress wave, $\sigma(x,t)$, propagates in a free-free plate (a plate free to move on both sides with no adjacent plates) and a free-fixed plate (a plate free to move in one side and adjacent to a rigid massive wall on the other

side) exposed to a square pressure wave with over-pressure P_o and duration t_o. t_o is assumed to be half the propagation time of the elastic wave, t_1, which is defined as L/C. t_1 is the time it takes for the stress wave to pass though the whole length of the plate and C is the propagation wave speed. A compressive pulse of intensity -P_o is reflected as a tensile wave $+P_o$ when it strikes a free surface. However, if a compressive pulse of intensity -P_o travels towards a fixed end, the reflected wave is also compressive and for the duration of the interaction of the pulse with the fixed surface, the wall experiences a stress of intensity -$2P_o$. Fig. 5.1 shows that the natural period, T_n, of the propagating stress wave for a free-free plate and a free-fixed plate are $2t_1$ and $4t_1$, respectively. Later in chapter VI, I will take advantage of the calculated natural period of the propagating stress wave in a free-free plate for tuning blast/impact.

When an incident compressive stress wave of amplitude σ_i travelling in material A strikes an interface with material B, the stress wave is partially reflected to material A as σ_r and partially transmitted to material B as σ_t. Equilibrium at the interface assuming all waves are compressive and positive yields

$$\sigma_i + \sigma_r = \sigma_t. \tag{5.4}$$

In general, the particle velocity, v, in an elastic material, as a function of stress amplitude, σ, Young's modulus, E, and density, ρ, is in the form of [66]

$$v = \frac{\sigma}{\sqrt{E\rho}}. \tag{5.5}$$

Compatibility at the interface of material A and B requires

$$v_i - v_r = v_t. \tag{5.6}$$

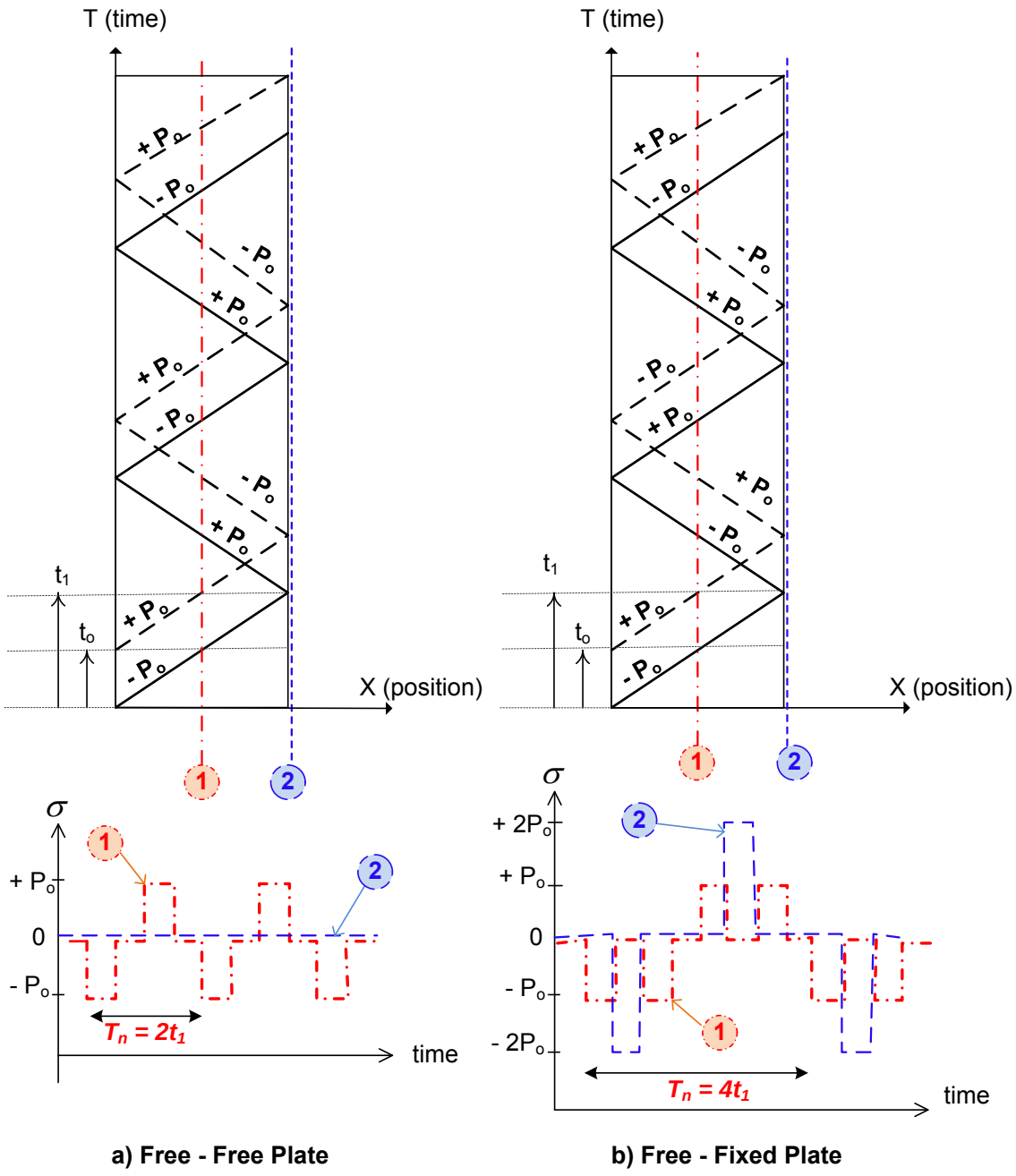

Figure 5.1: X-T diagram for the propagating stress wave in a free-free plate and a free-fixed plate exposed to a square blast with over-pressure P_o and duration t_o: $t_o = t_1/2$ where t_1 is the time it takes for the pressure wave to pass through the length of the plate. The natural period, T_n, of the propagating stress wave for a free-free plate and a free-fixed plate are $2t_1$ and $4t_1$, respectively.

Substituting Eqn. 5.5 into Eqn. 5.6 gives

$$\frac{\sigma_i}{\sqrt{E_A\rho_A}} - \frac{\sigma_r}{\sqrt{E_A\rho_A}} = \frac{\sigma_t}{\sqrt{E_B\rho_B}}, \tag{5.7}$$

where E is the Young's modulus, ρ is the density, and the subscripts A and B indicate the two materials. Combining Eqns. 5.4 and 5.7 and solving for the magnitude of the transmitted stress wave, σ_t, and the magnitude for the reflected stress wave, σ_r, gives us

$$\sigma_t = \frac{2\sqrt{E_B\rho_B}}{\sqrt{E_A\rho_A} + \sqrt{E_B\rho_B}}\sigma_i, \tag{5.8}$$

and

$$\sigma_r = \frac{\sqrt{E_B\rho_B} - \sqrt{E_A\rho_A}}{\sqrt{E_A\rho_A} + \sqrt{E_B\rho_B}}\sigma_i, \tag{5.9}$$

where $\sqrt{E_A\rho_A}$ and $\sqrt{E_B\rho_B}$ are the acoustic impedances of material A and material B, respectively. As indicated by Eqn. 5.8, the magnitude of a transmitted stress wave is reduced by making the acoustic impedance of material B much smaller than that of material A. This is called impedance mismatch approach to minimize the transmission of stress amplitude. The impedance-mismatch approach has no effect on mitigating impulse.

5.1.2 Plateau Compressive Yield Stress in Cellular Foams

Cellular materials including metal foams and elastomer foams are an alternative in mitigating the transmitted stress amplitude due to their unique constitutive behavior. Three stages can be identified in the uniaxial compression stress-strain curve of cellular materials (see Fig. 5.2). In *Stage I*, deformation is in the form of bending of the cell walls and edges and in general, is linear and reversible. In *Stage II*, deformation proceeds at almost constant yield stress, σ_y, over a broad strain range. The deformation in this stage is unrecoverable. The favorable design regime is *Stage II*

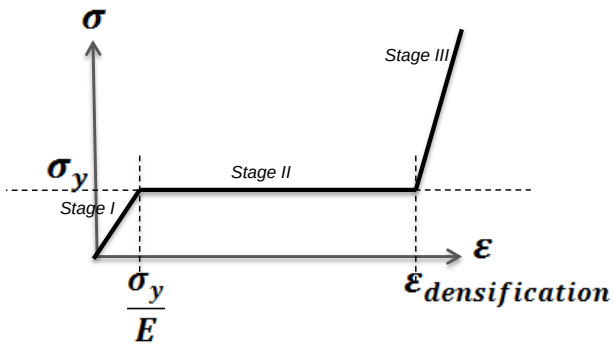

Figure 5.2: General stress-stain curve for cellular materials.

where the transmitted stress amplitude is limited to σ_y. Finally, in *Stage III*, cell walls and edges contact each other, giving rise to a steeply rising stress [11]. Fig. 5.2 shows a schematic stress-strain curve for compression in cellular foams.

In cellular foams, plastic deformation is irreversible and limited to a single use. Once an element of material has plastically deformed, it is unavailable to absorb energy from subsequent stress waves of the same magnitude. Fig. 5.3 (b) demonstrates this limitation aspect of cellular foams. After the first loading into the plastic region up to the densification strain, $\varepsilon_{densification}$, a subsequent unloading results in a plastic strain, ε_{pl}. For the second loading, the material has been densified and the starting point in the stress-strain curve would be the point at which the first unloading ends (ε_{pl}). The response of the foam would proceed elastically into the densification region with little or no further dissipation.

5.1.3 Stress Relaxation in Visco-elastic Polymers

Linear visco-elastic response is modeled as a Standard Linear Solid (SLS) which consists of a linear spring in parallel with one Maxwell element (one spring and one viscous damper connected in series). The parameters describing the constitutive properties are an unrelaxed modulus, E_u, a relaxed modulus, E_r, and a relaxation time, τ. The constitutive partial differential equation (PDE) for SLS materials is of

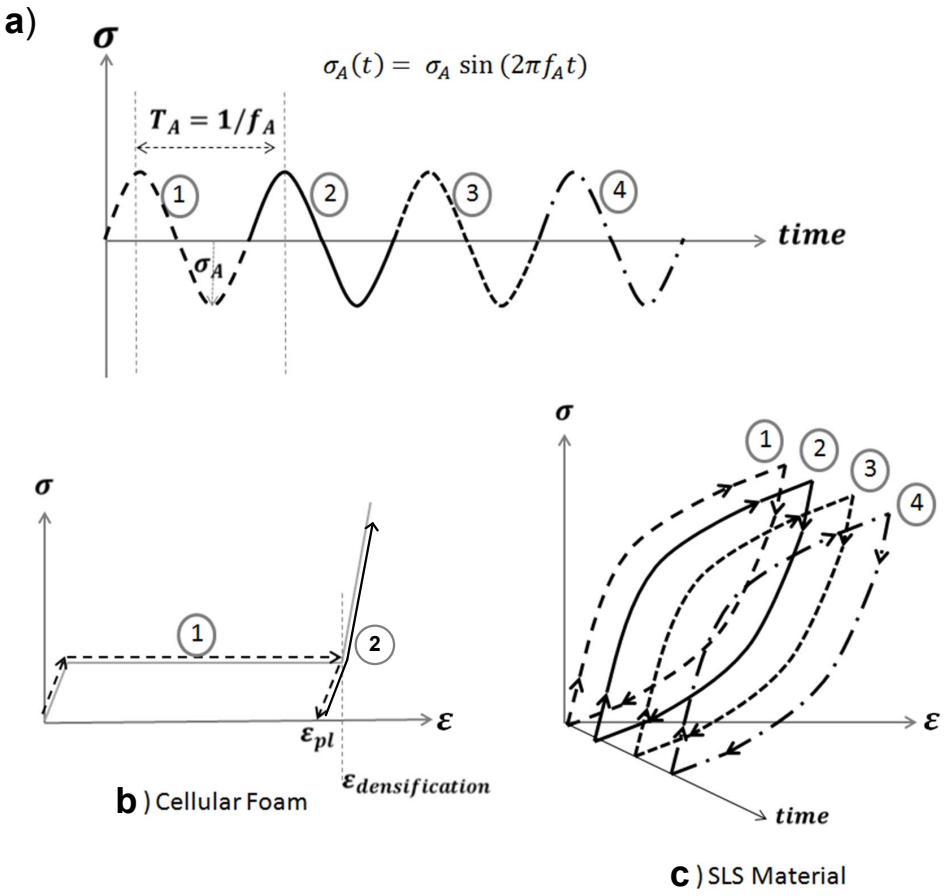

Figure 5.3: Cellular foams versus visco-elastic SLS materials: plastic deformation is irreversible and limited to a single use, while visco-elastic deformation is reversible and able to dissipate energy over multiple cycles.

the form [139]

$$\dot{\sigma}(\tau) + \sigma = \dot{\varepsilon}(\tau E_u) + \varepsilon(E_r). \tag{5.10}$$

In response to a constant strain input, $\varepsilon\ (t) = \varepsilon_o$, the PDE simplifies to

$$\dot{\sigma}(\tau) + \sigma = \varepsilon_o(E_r), \tag{5.11}$$

and the output stress becomes

$$\sigma(t) = \varepsilon_o[E_r + (E_u - E_r)e^{\frac{-t}{\tau}}]. \tag{5.12}$$

Stress relaxation describes how polymers relieve stress under constant strain. As shown in Eqn. 5.12, stress relaxes over time from $\varepsilon_o E_u$ to $\varepsilon_o E_r$ therefore the transmitted stress amplitude reduces to $\varepsilon_o E_r$ if enough time for full stress relaxation is available.

5.2 Impulse Mitigation

5.2.1 Energy Dissipation

The transmitted impulse is affected by energy dissipation within the armor, and by the relative masses of the armor and protected system. To investigate, a simple, rigid-body-dynamics analysis in which an armor collides with a protected structure is considered first with no energy dissipation involved in the armor (perfectly-elastic collision) and then with energy dissipation in the armor (perfectly-inelastic collision).

I start with a perfectly-elastic collision in which the armor is a rigid body with a concentrated mass of m_a exposed to a zero-period pressure pulse with impulse of I_o to protect a rigid protected structure with a concentrated mass of m_s. As the original

pressure pulse hits the armor, by conservation of momentum, the armor reaches an initial velocity of V_o while the target is still stationary. The equation for V_o is

$$V_o = \frac{I_o}{m_a}. \tag{5.13}$$

As the armor with an initial velocity of V_o and kinetic energy of $\frac{1}{2}m_a V_o^2$ impinges upon the target structure, a part of the armor's momentum and kinetic energy is transmitted to the target causing the target to move with a velocity of V_s, while the velocity of the armor changes to V_a. Conservation of momentum tells us

$$m_a V_o = m_a V_a + m_s V_s. \tag{5.14}$$

By substituting Eqn. 5.13 into Eqn. 5.14 and rearranging the terms, the expression for V_a becomes

$$V_a = \frac{I_o - m_s V_s}{m_a} \tag{5.15}$$

Conservation of energy is

$$\frac{1}{2}m_a V_o^2 = \frac{1}{2}m_a V_a^2 + \frac{1}{2}m_s V_s^2. \tag{5.16}$$

By combining Eqns. 5.15 and 5.16, an expression for V_s independent of V_a is obtained as

$$V_s = \frac{I_o}{m_s}\left(\frac{2\frac{m_s}{m_a}}{1+\frac{m_s}{m_a}}\right), \tag{5.17}$$

where $V_s m_s$ is the transmitted impulse from the armor to the protected structure and I call it I_t. Therefore, the ratio between the impulse transmitted to the structure, I_t,

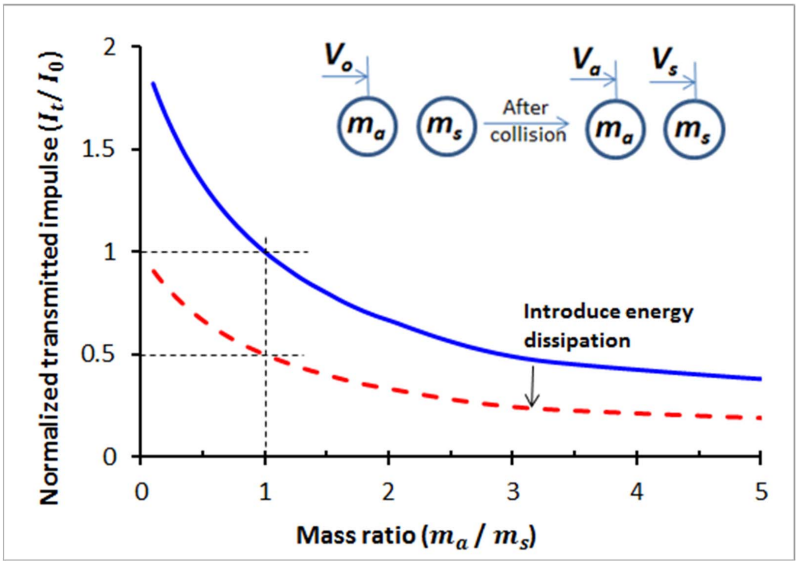

Figure 5.4: The ratio between the impulse transmitted to the structure and the original impulse imparted to the armor, I_t/I_o versus the mass ratio, m_s/m_a for perfectly elastic collision (blue solid line) and perfectly plastic collision (red dash line).

and the original impulse imparted to the armor, I_o, is [52]

$$\frac{I_t}{I_o} = \frac{2\frac{m_s}{m_a}}{1+\frac{m_s}{m_a}}. \tag{5.18}$$

Fig. 5.4 demonstrates I_t/I_o versus the mass ratio, m_s/m_a, for a perfectly-elastic collision (Eqn. 5.18). As shown in this figure, one approach for mitigating impulse is to use massive armor ($m_a >> m_s$).

An approach that relies on heavy armor conflicts with a common design criterion of minimizing mass. An alternative approach is to reduce the transmitted impulse by dissipating energy within the armor. Here, I introduce energy dissipation in the armor and consider a perfectly-inelastic collision between the armor, m_a, and the protected structure, m_s. As the original pressure pulse with impulse, I_o, hits the armor, by conservation of momentum, the armor reaches an initial velocity of V_o while the target is still stationary. V_o is still calculated as Eqn. 5.13. As the armor

with this initial velocity of V_o impinges upon the target structure, the armor and the target structure move with the same velocity ($V_s = V_a$). Conservation of momentum tells us

$$m_a V_o = (m_a + m_s) V_s. \tag{5.19}$$

Therefore, the ratio between the impulse transmitted to the structure, I_t, and the original impulse imparted to the armor, I_o, becomes [52]

$$\frac{I_t}{I_o} = \frac{\frac{m_s}{m_a}}{1 + \frac{m_s}{m_a}}. \tag{5.20}$$

Fig. 5.4 demonstrates I_t/I_o versus the mass ratio, m_s/m_a, for a perfectly-inelastic collision (Eqn. 5.20). As shown in this figure, introducing energy dissipation results in lower transmitted impulse for any given mass ratio. For instance, assuming equal masses for the armor and the protected structure ($m_s/m_a = 1$), the normalized transmitted impulse, I_t/I_o, drops from unity for a perfectly-elastic collision to 0.5 for a perfectly-inelastic collision.

If this reduction in impulse is not enough to protect the target, an alternative design approach is needed: either more massive armor, or an increase in the interaction time (t_o) to move the design space to one in which it is the pressure, not the impulse, that needs to be mitigated (refer to Chapter IV).

An additional consideration raised by Eqns. 5.18 and 5.20 is that there is a limit to the possible reduction in transmitted impulse, which depends on the mass of the armor. However, as mentioned above, if the time scale of a pressure pulse is increased, it may be possible to move the design space to the regime in which damage is definitely correlated to the amplitude of the pressure. Unlike impulse that has a dissipation limited to the conservation of momentum and energy, there is no limita-

tion with dissipating pressure.

5.2.2 Plastic Foams versus Visco-elastic Polymers

Energy can be dissipated in armor using mechanisms such as plasticity and visco-elasticity, as well as friction and delamination. Here, I am focusing on the energy dissipation mechanism in visco-elastic polymers and its advantages relative to the energy dissipation mechanism in plastic foams.

When a sinusoidally varying strain $\varepsilon(t) = \varepsilon_o \sin(\omega t)$ is applied to a SLS material, the stress will lag behind the strain such that $\sigma(t) = \sigma_o \sin(\omega t - \delta)$ where δ is the phase lag. The stress equation $\sigma(t)$ may be expanded to give

$$\sigma(t) = \sigma_o \sin(\omega t)\cos(\delta) + \sigma_o \cos(\omega t)\sin(\delta), \tag{5.21}$$

where ω is the angular velocity equal to $2\pi f$ or $2\pi/T$, where f is the cyclic frequency in hertz (Hz) and T is the period of the sinusoidal oscillation. Stress in Eqn. 5.21 can be considered to have two components:

- $\sigma_o \cos(\delta)$ which is in phase with the strain,
- $\sigma_o \sin(\delta)$ which is 90 degree out of phase with strain.

This leads to the definition of two dynamic moduli:

- *storage modulus* : $E' = \sigma_o \cos\delta/\varepsilon_o$,
- *loss modulus* : $E" = \sigma_o \sin\delta/\varepsilon_o$.

From these two moduli, it is possible to define a complex modulus, $\tilde{E}$ as

$$\tilde{E} = \frac{\sigma}{\varepsilon} = \sqrt{E'^2 + E"^2} = E' + iE", \tag{5.22}$$

where i $= \sqrt{-1}$. Here, I am interested in tanδ known as the loss tangent which is a measure of viscous energy dissipation in visco-elastic materials. After some derivations, tanδ is obtained as [139]

$$\tan\delta = \frac{E"}{E'} = \frac{\tau\omega(E_u - E_r)}{E_r + E_u(\tau\omega)^2}. \tag{5.23}$$

As shown in Eqn. 5.23, tanδ is a function of SLS material parameters (E_r, E_u, and τ) and the excitation angular frequency, ω in rad/sec. Considering any three combination of E_r, E_u, and τ, tanδ reaches its maximum limit at a particular angular frequency called the critical damping angular frequency, ω_{crit}:

$$\omega_{crit} = \frac{\sqrt{\frac{E_r}{E_u}}}{\tau} = 2\pi f_{crit}, \tag{5.24}$$

where f_{crit} is the critical damping frequency in Hz. The maximum value of tanδ at f_{crit} represents the maximum energy dissipation possible and is calculated as

$$\tan\delta_{max} = \frac{E_u - E_r}{2\sqrt{E_r E_u}}. \tag{5.25}$$

Hence, to achieve optimal viscous energy dissipation:

- the excitation frequency of the stress wave in a visco-elastic material should match the critical damping frequency of the material, f_{crit}, and
- the difference in the relaxed and unrelaxed moduli should be as large as possible.

Therefore, the limitation in the viscous energy dissipation mechanism is that the efficiency with which energy is dissipated within visco-elastic materials depends on the amplitudes and frequencies of the stress waves traveling through them. In general, the stresses induced by a blast or impact exhibit a broad range of frequency components, only a few of which will be associated with the optimal damping of a

particular visco-elastic material. Therefore, the introduction of a layer of visco-elastic material into armor, without thought about its characteristic frequencies, may not be useful. The challenge is to tune the stresses induced by a blast or impact to a controllable characteristic frequency in the visco-elastic material and to match this characteristic frequency to the critical damping frequency of the material.

The attractive aspect of energy dissipation in visco-elastic materials is that visco-elastic deformation is reversible, not limited to single use and most importantly, can dissipate energy over multiple cycles as shown in Fig. 5.3 (b). A higher excitation frequency leads to more loading-unloading cycles and therefore, a higher cumulative dissipation. In other words, energy dissipation capabilities of visco-elastic materials can accumulate significantly if the period of the excitation stress wave is small relative to the time it takes for the wave to pass through the visco-elastic layer. This attractive aspect does not exist is cellular foams in which plastic deformation is irreversible and limited to single use. The comparison of loading-unloading in the stress-strain curves of visco-elastic SLS materials and cellular foams is depicted in Fig. 5.3.

The final consideration in energy dissipation management of visco-elastic materials is associated with the characteristic relaxation time, τ and its effect on $\tan\delta$ in Eqn.5.23. Fig. 5.5 plots $\tan\delta$ versus ω for different values of τ, considering constant values for E_u and E_r. As τ gets smaller, the critical damping frequency, f_{crit}, increases (Eqn. 5.24) and most interestingly, the $\tan\delta$ peak broadens and a wider range of frequencies experience large $\tan\delta$s.

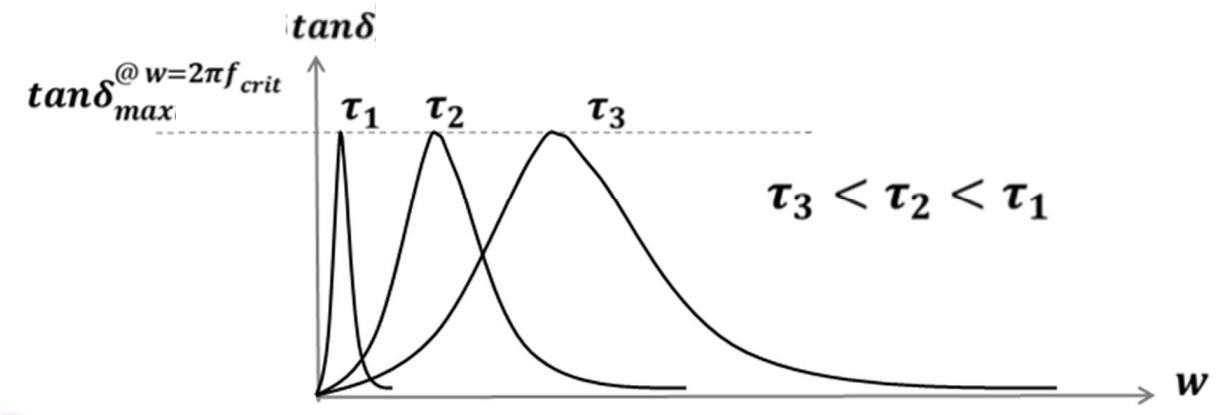

Figure 5.5: $\tan\delta$ versus frequency for different values of τ : E_u and E_r are constant.

CHAPTER VI

Novel Design Concept: Blast/Impact Tuning and Mitigation

6.1 The Concept of Tuning

As discussed in Section 5.2.2, an optimally dissipative visco-elastic material is one in which the frequency of the excitation stress wave matches the critical damping frequency. The problem with using visco-elastic materials to dissipate the energy of a blast or impact is that the impulse is usually delivered to the protective structure in the form of a single pulse, which induces stress waves that are represented by a wide range of frequencies in the Fourier domain. Both of these considerations, the single pulse and the wide range of characteristic frequencies, might appear to make visco-elastic materials unattractive for energy dissipation in this application. However, as will be explained in this chapter, it is possible to use a multi-layered structure to tune the stresses to characteristic frequencies that can then be dissipated by an appropriate choice of visco-elastic materials [122, 99].

To achieve the tuning required to realize optimal damping, two layers of materials need to be placed between the threat and the visco-elastic layer. Therefore, the protective structure has three layers:

- The first layer, closest to the threat, should be a stiff, linear-elastic material (here, I also assume it to be isotropic), having a large acoustic impedance relative to the second layer. The length of the first layer in the direction of wave propagation is L_1, the modulus is E_1, and the density is ρ_1.

- The second layer should also be elastic. The length of this second layer is L_2, the modulus is E_2, and the density is ρ_2. The acoustic impedance of the second layer needs to be much less than that of the first layer to ensure tuning: $\sqrt{E_1\rho_1} >> \sqrt{E_2\rho_2}$. As a result of this acoustic mismatch, the internal stress reflections between this interface and the surface of the protective structure will tune the stress vibrations to a characteristic value of

$$f_A = \frac{\sqrt{E_1/\rho_1}}{2L_1}. \tag{6.1}$$

  Numerical simulations using the commercial finite-element code ABAQUS [1] confirmed that Eqn. 6.1 provides an accurate description of this characteristic frequency provided the ratio between the impedances of the two layers is about 70.

- The third layer should be the visco-elastic layer that dissipates the energy of the tuned blast/impact. This layer has length L_3, density ρ_3, unrelaxed modulus E_u, relaxed modulus E_r, and time constant τ. The properties of this layer should be such that its characteristic damping frequency, f_{crit}, matches the tuned frequency, f_A, given by Eqn. 6.1.

The energy dissipated in a visco-elastic material increases with the number of loading and unloading cycles, and with their amplitude as long as the respond remains in the visco-elastic layer. This adds some additional considerations to the design of

multi-layered protective structure. First, the impedance mismatch between the first and second layers must be just large enough to provide good tuning without excessively reducing the amplitude of the stresses that eventually get transmitted into the energy-absorbing layer. For a similar reason, to ensure a reasonable amplitude of stress waves for dissipation, the impedance of the third layer must be relatively high compared to the impedance of the second layer. Furthermore, the need to have many stress cycles within the visco-elastic layer suggests that the tuned frequency should be as high as possible, consistent with finding a material with a suitable time constant. The higher the frequency, the less material is needed to dissipate the energy (for a given wave speed). The potential materials challenge from a development perspective is that the frequencies associated with this tuning will be in a range for which the properties of polymers have only received limited study [5, 102, 15, 54].

6.2 Finite Element Analysis Preparation

In this thesis, I used a commercial finite-element code, ABAQUS Explicit [1], to analyze blast/impact mitigation. In these analyses, the internal interactions within the protected structure, between the supporting structure and the delicate target, were not addressed. It was assumed that the characteristics of the pressure pulse that the structure can support without damage to the target are known from a separate analysis of the protective structure. I, therefore, compared the maximum amplitude of the stress wave, P_t, and impulse, I_t, transmitted through the protective structure to an elastic structure behind it, to the corresponding values of P_o and I_o of the original pressure pulse applied to the surface of the protective structure. The relative ratios of P_t/P_o and I_t/I_o were taken as the two primary measures of performance of the protective structure, and used for comparisons between different designs.

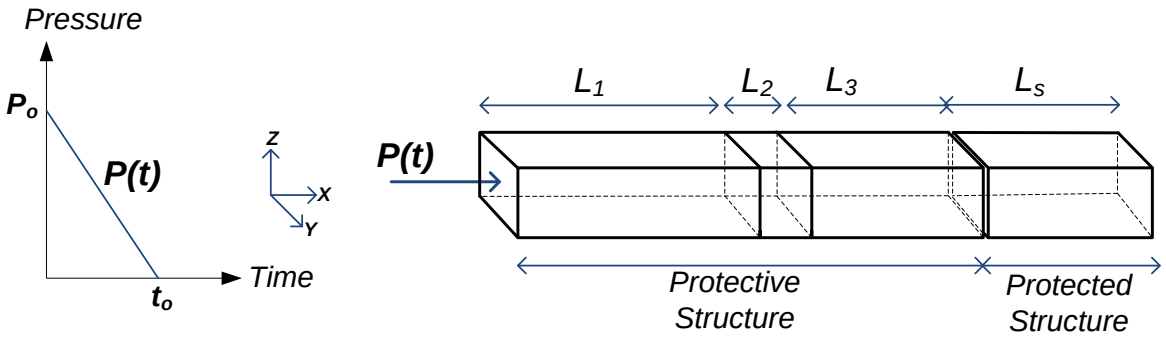

Figure 6.1: Geometry of the protective structure and protected structure exposed to a time-varying normal load, $P(t)$, analyzed in the finite-element model.

The protective structure and the protected structure were modeled using three-dimensional, eight-node brick elements with reduced integration. The geometry is shown in Fig. 6.1. The displacements along one set of *xz*- and *xy*-faces were constrained in the *y*- and *z*- directions, respectively. The other *xz*- and *xy*-faces were traction-free. The interfaces between the internal layers of the protective structure were bonded. The protected structure was a solid, linear-elastic block. The interface between the protected structure and the protective structure was frictionless. A pressure $P(t)$ was applied to the external surface of the protective structure along the x -direction (Fig. 6.1). This pressure decayed linearly to zero from an initial value of P_o during a time t_o. It was verified that the major conclusions of the study were not sensitive to this particular choice of $P(t)$.

The peak pressure transmitted to the protected structure, P_t, was taken to be the maximum value of the longitudinal stress at the internal surface of the protective structure as calculated from the finite-element calculations. Determining the transmitted impulse was more complicated. As will be discussed in more detail later, two distinct types of behavior were observed. In one type of behavior, momentum was transferred to the protected structure in a single broad pulse. In the other type of behavior, momentum was transferred over a large number of broad pulses separated

by significant periods of time. Owing to the time scales involved, only the impulse delivered in the first broad pulse was considered. Therefore, rather than comparing I_o to the total transmitted impulse, I compare it to the effective transmitted impulse I_{eff}, determined by integrating the longitudinal stress at the internal surface of the protective structure over the first broad pulse delivered to the structure. The calculations for the transmitted impulse were verified by comparing it to the momentum of the protected structure.

Since a commercial code was used, considerable care was taken to reduce the effects of any spurious numerical artifacts to below an acceptable level of numerical uncertainty that I indicate on the plots. For example, the bulk viscosity parameter (which by default is 0.06 in ABAQUS Explicit, resulting in some artificial dissipation) was changed to zero, and double-precision was used for the solutions. Additional concerns were to ensure that the effects of the two non-dimensional groups involving the time-step and mesh size were no larger than the uncertainties introduced by any of the other unspecified non-dimensional groups (see Section 6.3.1). I did this by ensuring an adequate number of time steps and nodes for the highest frequency and shortest wavelength of interest. To satisfy the first requirement, the highest frequency and its associated period were identified, and the time increment was set to be no more than 20% of the period. To satisfy the second requirement, the shortest wavelength in a simulation was identified, and the largest element size was set to be no more than 20% of that wavelength. Since the incoming blast/impact sets up a spectrum of (unknown) frequencies in layer 1 initially, the highest frequency cannot be easily identified. In this analysis, I have assumed the highest frequency to be f_A. I also ensured that the Courant-Friedrichs-Lewy (CFL) [109] condition was met by setting the Courant number to 0.2. Finally, I verified that any change in the solution introduced by further mesh or temporal refinement was insignificant within the limits

of the error bars I quote in the results.

6.3 Analysis of the Three-Layered Protective Structure

6.3.1 Non-dimensional Analysis

In the analyses of the protective structure, it was assumed that each layer was isotropic. Layer 1 had a Young's modulus of E_1, a density of ρ_1, and a length of L_1. Layer 2 had a Young's modulus, of E_2, a density of ρ_2, and a length of L_2. The visco-elastic layer was modeled as a standard-linear solid with an unrelaxed modulus of E_u, a relaxed modulus of E_r, a characteristic relaxation time of τ, a density of ρ_3, and a length of L_3. The plate representing the supported structure had a Young's modulus of E_s, a density of ρ_s, and a mass of m_s. These properties, plus the two characteristics of the blast/impact, P_o and t_o, make a total of sixteen variables and three different units to describe the propagation of the stress wave through the protective structure. Therefore, according to the Buckingham-Π theory [111, 128, 19], the resultant impulse and pressure must be a function of thirteen dimensionless groups.

A series of finite-element calculations indicated that seven groups could be reasonably neglected for the calculations that are presented, leaving I_{eff} and P_t as functions of six dimensionless groups:

$$\begin{aligned} \frac{I_{eff}}{I_o} &= f\left(\frac{E_1\rho_1}{E_2\rho_2}, \frac{m_s}{\rho_1 L_1 + \rho_2 L_2 + \rho_3 L_3}, \frac{f_{crit}}{f_A}, \frac{t_3}{t_1}, \frac{E_{crit}\rho_3}{E_2\rho_2}, \frac{E_r}{E_u},\right) \\ \frac{P_t}{P_o} &= f\left(\frac{E_1\rho_1}{E_2\rho_2}, \frac{m_s}{\rho_1 L_1 + \rho_2 L_2 + \rho_3 L_3}, \frac{f_{crit}}{f_A}, \frac{t_3}{t_1}, \frac{E_{crit}\rho_3}{E_2\rho_2}, \frac{E_r}{E_u}\right) \end{aligned} \tag{6.2}$$

In these expressions, the critical frequency, f_{crit}, and the tuned frequency, f_A, have been defined in Eqns. 5.24 and 6.1. E_{crit} is the storage modulus of the third layer at the critical frequency [139], t_1 is the time for a stress wave to travel through layer 1,

and t_3 is the time for a stress wave at the critical frequency to travel through layer 3:

$$E_{crit} = (2E_u E_r)/(E_u + E_r),$$
$$t_1 = L_1\sqrt{\rho_1/E_1} = 1/2f_A,$$
$$t_3 = L_3\sqrt{\rho_3/E_{crit}}\ . \tag{6.3}$$

The first non-dimensional group, $E_1\rho_1/E_2\rho_2$, is the square of the impedance mismatch between the first two layers. As discussed earlier, this needs to be large enough to ensure tuning, but small enough to make sure that the stress waves pass through to the visco-elastic layer where they can be damped. A series of finite-element calculations indicated that the optimal level for the impedance mismatch is about 70. So, in all the calculations that follow, I set:

$$\frac{E_1\rho_1}{E_2\rho_2} = 5,000. \tag{6.4}$$

The second non-dimensional group is the relative mass of the protected structure to the mass of the protective structure. As indicated in Section 5.2.1, the transmitted impulse decreases with the relative mass of the protective structure. Therefore, to provide a point of comparison between the different calculations, I set:

$$\frac{m_s}{\rho_1 L_1 + \rho_2 L_2 + \rho_3 L_3} = 1. \tag{6.5}$$

The effects of the other four important non-dimensional groups will be seen in the results that follow.

During the calculations, the remaining seven non-critical groups were allowed to vary within fairly broad ranges:

$$0.1 < t_o/t_1 < 10,$$

$$0.08 < L_1/L_2 < 10,$$

$$5 < E_1/E_2 < 25,000,$$

$$7 \times 10^{-5} < E_{crit}/E_2 < 60,$$

$$E_s\rho_s/E_{crit}\rho_3 > 8,000,$$

$$0.8 < \rho_s/\rho_3 < 2,$$

$$10^{-5} < P_o/E_1 < 0.4.$$

From a materials design perspective, the above range limits were chosen considering the proposed protective structure made of a tough plastic polymer with a density in the range of 900 - 2000 kg/m^3 and a Young's modulus in the range of 0.1 - 5 GPa (first layer), a compliant elastic foam with a density in the range of 10 - 500 kg/m^3 and a Young's modulus in the range of 0.2 - 20 MPa (second layer), and a visco-elastic polymer with a density in the range of 800 - 1500 kg/m^3 (third layer), whereas the supporting structure is made of a hard, dense elastic material with material properties close to the ones for skull. The error bars shown on the figures are the result of both numerical uncertainties and the variations of these non-critical groups.

6.3.2 Temporal Stress Distributions

A well-tuned wave is expected to be optimally damped at $f_{crit}/f_A = 1$, and the effectiveness of the damping is expected to increase with the number of cycles that the pressure wave experiences in the visco-elastic layer. The first concept is illustrated by the plots in Figs. 6.2 and 6.3 that show minima in the effective impulse and

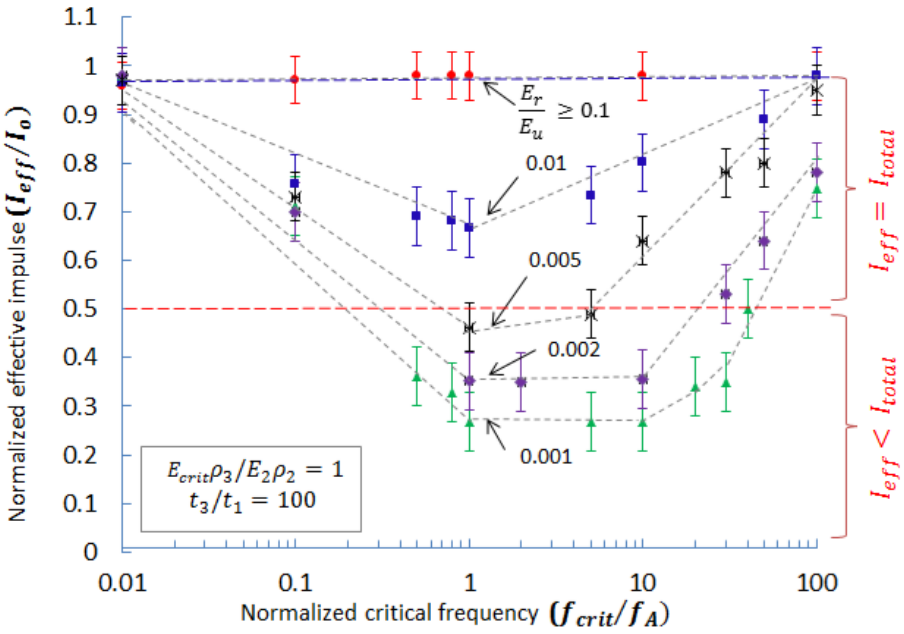

Figure 6.2: The effective impulse is minimized after passage through a three-layer visco-elastic protective structure when $f_{crit}/f_A = 1$. The transmitted impulse occurs in a single pulse for $E_r/E_u > 0.005$. For lower values of E_r/E_u, the impulse is transmitted in a series of pulses, so $I_{eff} < I_o/2$. When $E_r/E_u > 0.1$, there is negligible dissipation in the protective structure, and there is no reduction in the transmitted impulse.

transmitted pressure at $f_{crit}/f_A = 1$. The second concept is illustrated by the plots in Figs. 6.4 and 6.5 that show how the effective impulse and transmitted pressure decrease as the time for the stress wave to traverse the visco-elastic layer is increased. This travel time can be increased either by increasing the thickness of the visco-elastic layer, or by decreasing the wave speed.

Figs.6.2 and 6.4 show that there is no significant reduction in the effective impulse if $E_r/E_u \geq 0.1$, because there is no energy dissipation, even for a well-tuned protective structure. Correspondingly, the drop in the amplitude of the transmitted pressure for $E_r/E_u \geq 0.1$ shown in Figs. 6.3 and 6.5 is determined only by impedance mismatch. Finally, it will be noted from the plots in Figs. 6.2 and 6.3 that, when

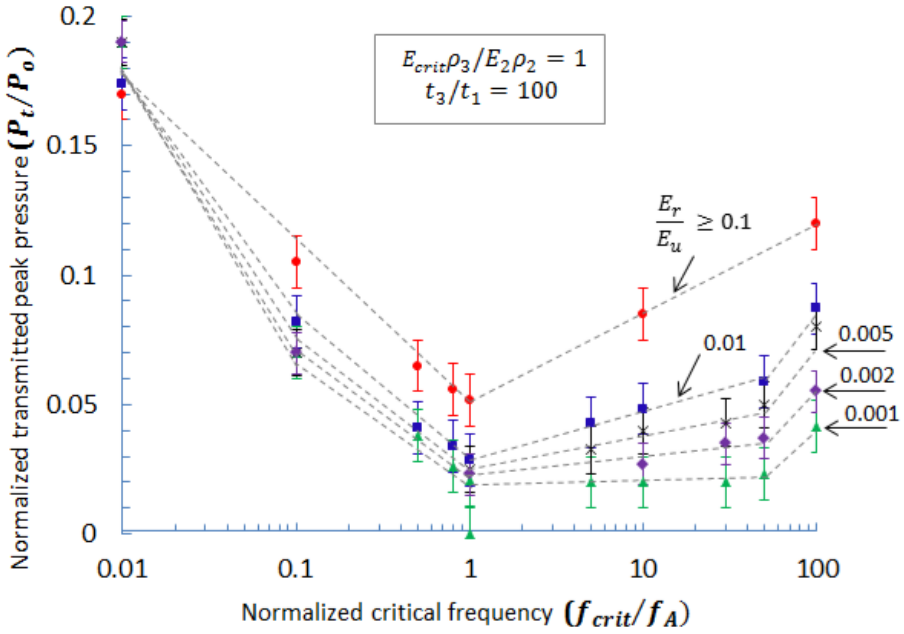

Figure 6.3: A significant reduction in the transmitted peak pressure can be achieved with a well-tuned, three-layer visco-elastic protective structure. The reduction in this peak pressure is increased as the ratio E_r/E_u is reduced. When $E_r/E_u > 0.1$, there is negligible dissipation in the protective structure, and any reduction in the pressure pulse occurs only because of impedance mismatch.

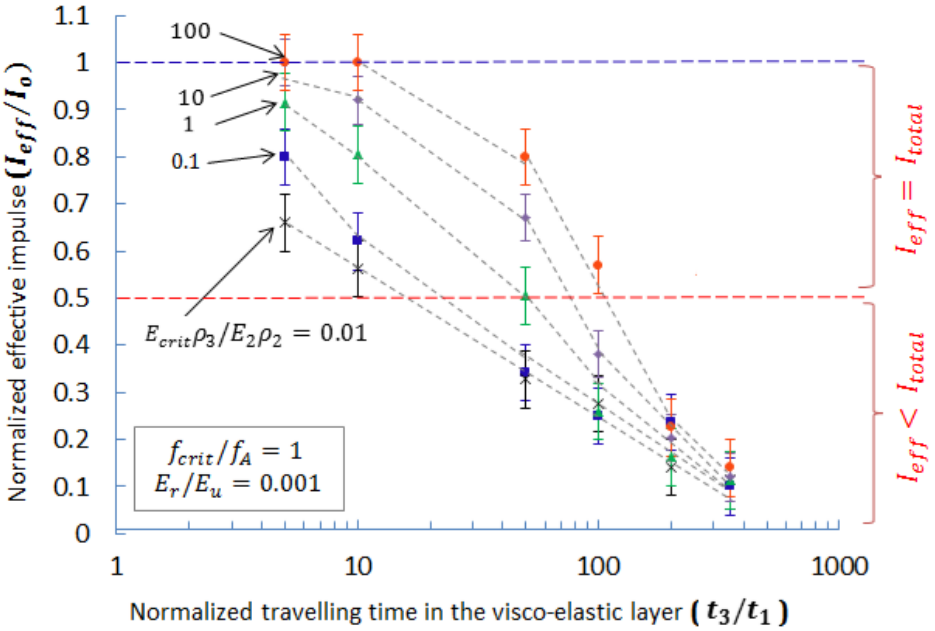

Figure 6.4: For a well-tuned three-layer protective structure, the effective impulse drops with the time taken for the stress wave to traverse the visco-elastic layer.

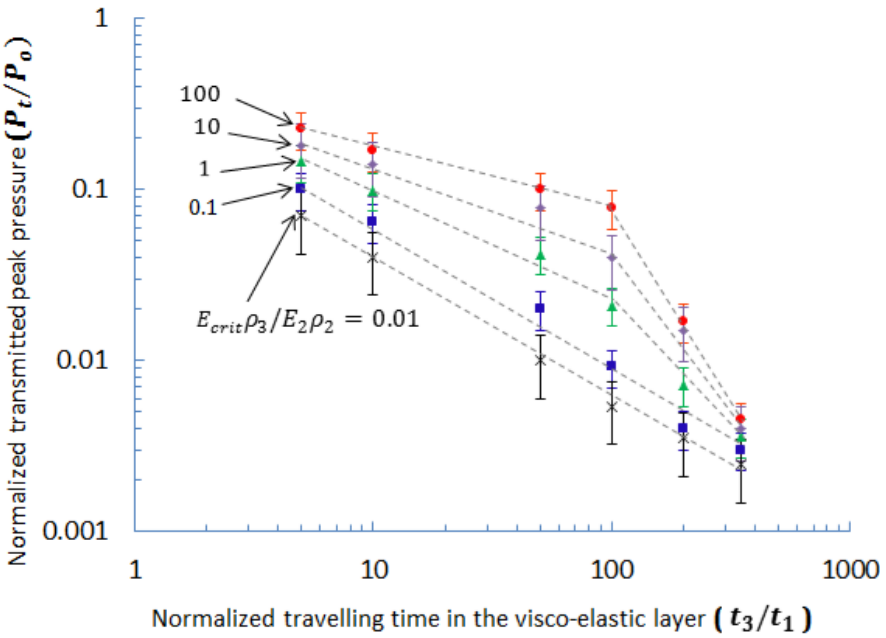

Figure 6.5: For a well-tuned three-layer protective structure, the maximum amplitude of the transmitted pressure drops with the time taken for the stress wave to traverse the visco-elastic layer, since this allows an increase in energy dissipation.

E_r/E_u is small, the minima are fairly broad for values of $f_{crit}/f_A > 1$. This can be explained by reference to Eqns. 5.23 and 5.24; as E_r/E_u becomes smaller, $\tan\delta$ exhibits a broader peak skewed to $f_{crit}/f_A > 1$. As will be discussed later, this may have significant practical importance from a design perspective in reducing the sensitivity of the performance of the protective structure to variations in operating conditions.

6.3.3 Spatial Stress Distributions

In the results that follow, it will be observed that there are regimes in which the transmitted impulse appears to be less than $0.5I_o$; less than that expected to be transmitted by a perfectly-inelastic protective structure. This can be explained by reference to Fig. 6.6, which shows how the pressure can be transmitted to the protected structure through widely spaced pulses. This figure illustrates finite-element results of how the pressure varies with time for three different elements within the

visco-elastic layer: at the front edge of the layer (element 1), in the middle of the layer (element 2), and at the back of the layer (element 3). The magnitude of the peak pressure that enters the visco-elastic layer depends on the impedance mismatch between layers 2 and 3. This pressure is then attenuated as it travels through the visco-elastic material.

- Poorly-tuned protective structure transmits the impulse over a single broad pulse, after which contact is lost (in the scenario used here of an untethered protected structure). The transmitted impulse in such a case can be anywhere between 100 and 50 % of the incident impulse (in this case of equal masses), depending on the amount of damping (refer to Fig. 6.6 (c)).

- Good tuning and dissipation results in only some of the impulse being transmitted in the first pulse before contact is lost with the protected structure; the rest of the impulse is then transmitted when there is subsequent contact, sometimes after multiple internal reflections within the protective structure. The impulse transmitted to the protective structure in the initial pulse is the "effective" impulse, I_{eff}, since the subsequent pulses occur so much later that they will probably have no significant effect on the target. The transmitted impulse in the first pulse can be less than 50 % of the incident pulse. However, contact is subsequently re-established and further increments of momentum are transferred to the protected structure at intervals of $1/f_B$, until the full 50 % has been transmitted (refer to Fig. 6.6 (a) and (b)). f_B has been explained in Section 6.3.4.

Examples of the form of the stress waves at different locations within the protective structure are given in Fig. 6.7 at a normalized time of $f_A t = 46$. This time is chosen to be somewhere within a regime for which the stress wave is fully within layer

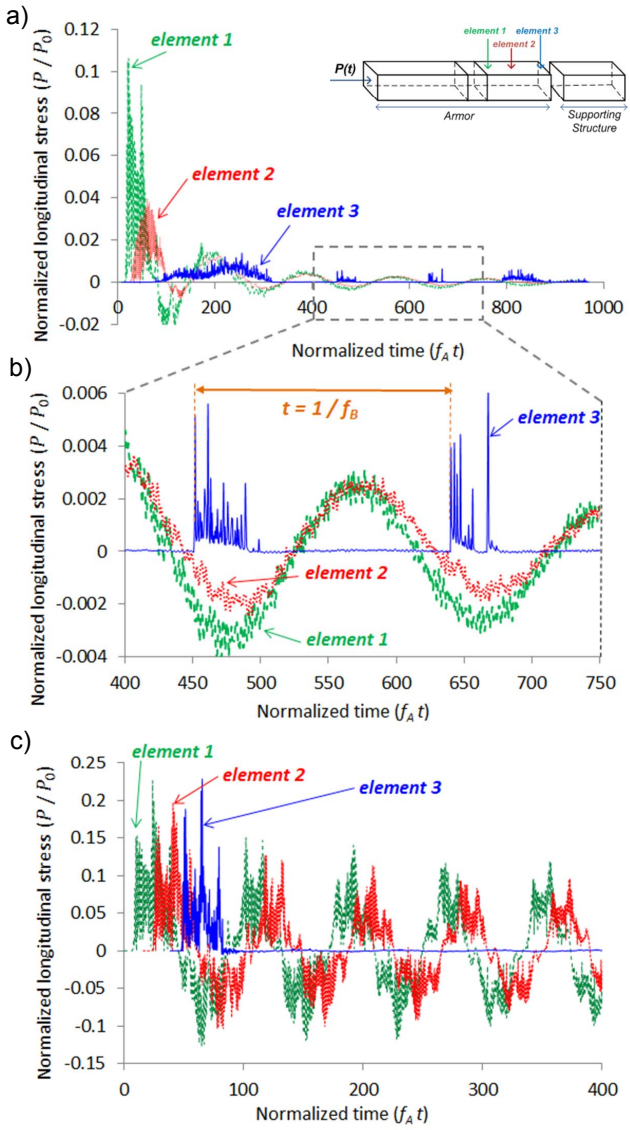

Figure 6.6: Pressure waves at the beginning, middle, and end of the visco-elastic layer: (**a** and **b**) in a well-tuned system with $f_A/f_{crit} = 1$, (**c**) in a poorly-tuned system with $f_A/f_{crit} = 0.01$. The values of the other groups are given by $E_{crit}\rho_3/E_2\rho_2 = 1$, $E_r/E_u = 0.001$, $t_3/t_1 = 100$ in **a**, **b**, and **c**. A detail of the stress waves for the first case **(a)** is shown in **(b)**. These figures show how, in a well-tuned system, the latter parts of the impulse can be transmitted to the protected structure in pulses separated by time intervals that are increments of $1/f_B$. While in a poorly-tuned system, the impulse gets transmitted to the protected structure over a single broad pulse.

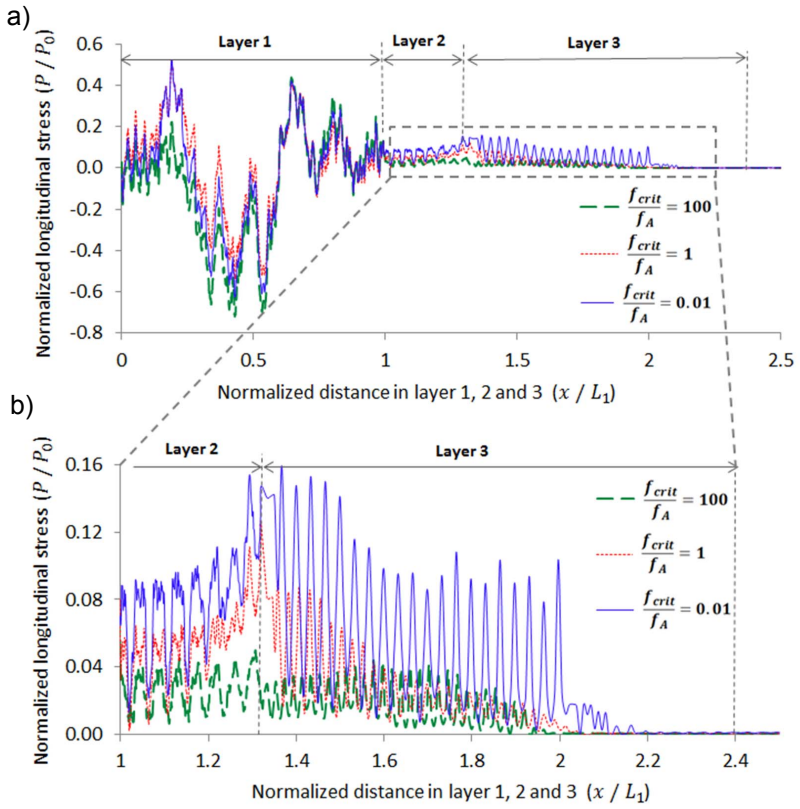

Figure 6.7: A spatial plot showing an example of how the magnitudes of the stress waves vary as a function of distance through the protective structure for a well-tuned system ($f_{crit}/f_A = 1$), and two poorly-tuned systems ($f_{crit}/f_A = 0.01$, 100). A detail of the stress waves for the first case **(a)** is shown in **(b)**. These plots were taken at a normalized time of $f_A t = 46$. The values of the other groups are given by $E_{crit}\rho_3/E_2\rho_2 = 1$, $E_r/E_u = 0.001$, $t_3/t_1 = 100$.

3. The spatial plots in Fig. 6.7 show how the magnitudes of the stress waves vary as a function of distance through the protective structure for a well-tuned system ($f_{crit}/f_A = 1$), and two poorly-tuned systems ($f_{crit}/f_A = 0.01$, 100).

6.3.4 Stress Distributions in Frequency Domain

It was noted from the results of the finite-element analyses that, in addition to f_A, two other, significantly lower, characteristic frequencies, f_B and f_C, enter the viso-elastic layer in a tuned system. These other two frequencies have periods cor-

responding to the times for the tuned wave to traverse the third and second layers, respectively. To illustrate, Figs. 6.8 and 6.9 show pressure waves (in time and frequency domains) at the beginning, middle, and end of the visco-elastic layer, in a well-tuned system (with $f_A/f_{crit} = 1$) and in a poorly-tuned system (with $f_A/f_{crit} = 0.01$), respectively. A well-tuned system dissipates all the energy carried by f_A while in a poorly-tuned system, there is no significant reduction in the impulse carried by any of these three frequencies.

To identify the contribution of f_A in carrying impulse relative to the other two lower frequencies, I applies Parseval's theorem. The interpretation of this theorem is that the total energy contained in a waveform $x(t)$ summed across all of time t is equal to the total energy of the waveform's Fourier Transform $X(f)$ summed across all of its frequency components f. The spectral analyses of the waves in the first element of the visco-elastic material indicated that, for a typical well-designed system, about 45% of the impulse is carried by f_A, about 41% is carried by f_B, and about 14% is carried by f_C and its harmonics, as shown in Fig. 6.10. Therefore, a well-tuned system dissipates the 45% of impulse carried by f_A and the remaining 55% of impulse carried by the lower frequencies gets transmitted to the supported structure. However, it should be noted that, even if the lower frequencies are not dissipated, they serve a useful purpose by transmitting some of the impulse through the protective structure at a lower velocity. As discussed in Chapter V, one strategy for blast and impact mitigation is to increase the transmission time so that the peak pressure (which can then be controlled by impedance mismatch), rather than impulse, dominates the response of the target.

Finally, in the present implementation, I have analyzed a system with only one critical frequency, so only the high-frequency, f_A, component is dissipated. In princi-

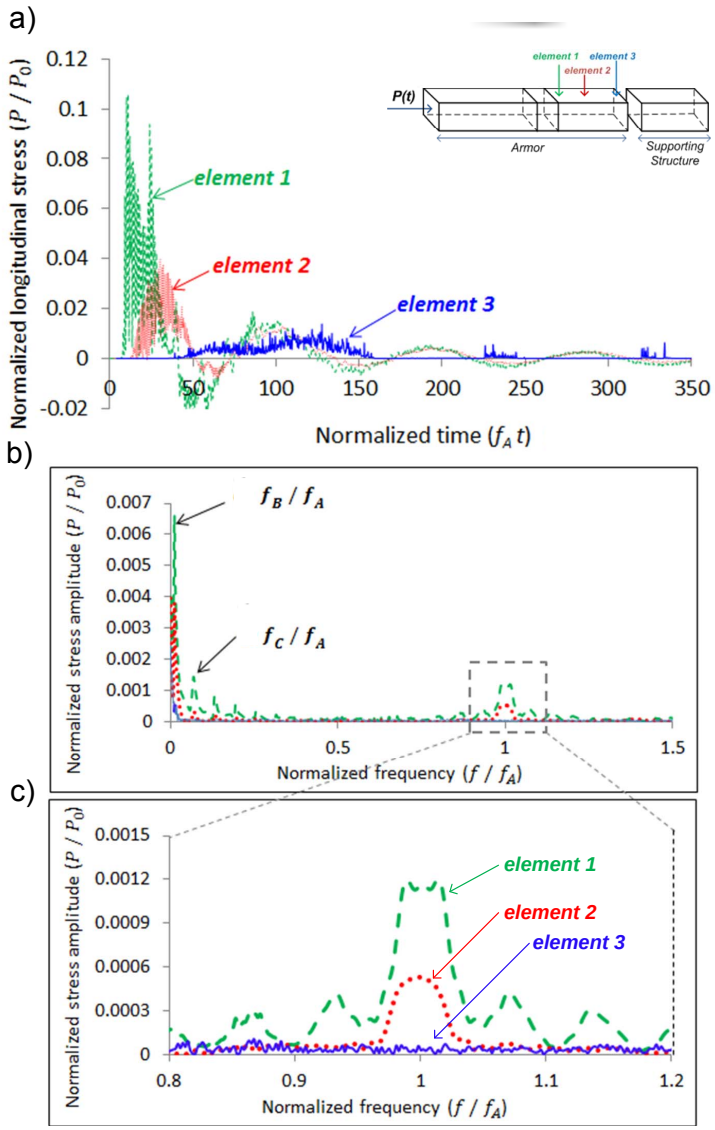

Figure 6.8: Pressure waves at the beginning, middle, and end of the visco-elastic layer, in a well-tuned system with $f_A/f_{crit} = 1$: **(a)** in time domain, **(b)** and **(c)** in frequency domain. The values of the other groups are given by $E_{crit}\rho_3/E_2\rho_2 = 1$, $E_r/E_u = 0.001$, $t_3/t_1 = 100$. There are three characteristic frequencies entering the viso-elastic layer in a tuned system: f_A, f_B and f_C. f_B and f_C are significantly lower than f_A. A well-tuned system dissipates the energy carried by f_A (in element 3, the stress amplitude at $f/f_A = 1$ merges to zero).

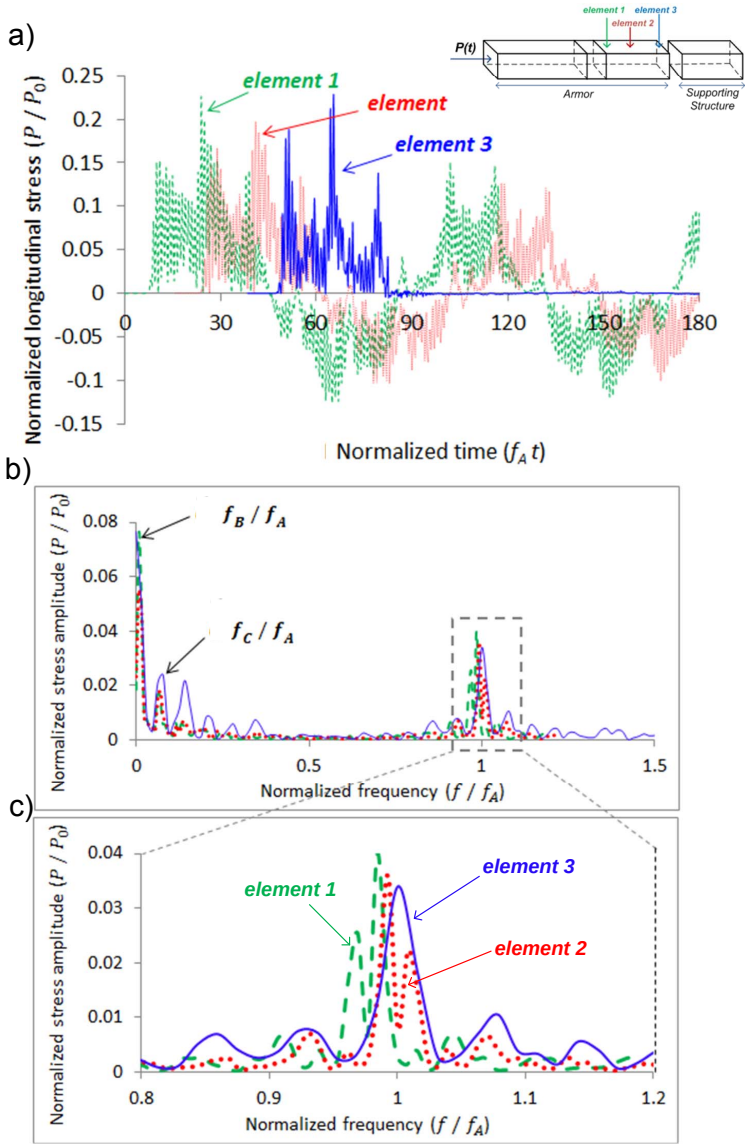

Figure 6.9: Pressure waves at the beginning, middle, and end of the visco-elastic layer, in a poorly-tuned system with $f_A/f_{crit} = 0.01$: **(a)** in time domain, **(b)** and **(c)** in frequency domain. The values of the other groups are given by $E_{crit}\rho_3/E_2\rho_2 = 1$, $E_r/E_u = 0.001$, $t_3/t_1 = 100$. There are three characteristic frequencies entering the viso-elastic layer in a tuned system: f_A, f_B and f_C. f_B and f_C are significantly lower than f_A. A poorly-tuned system cannot dissipate the energy carried by f_A (in element 3, the stress amplitude at $f/f_A = 1$ has not changed.)

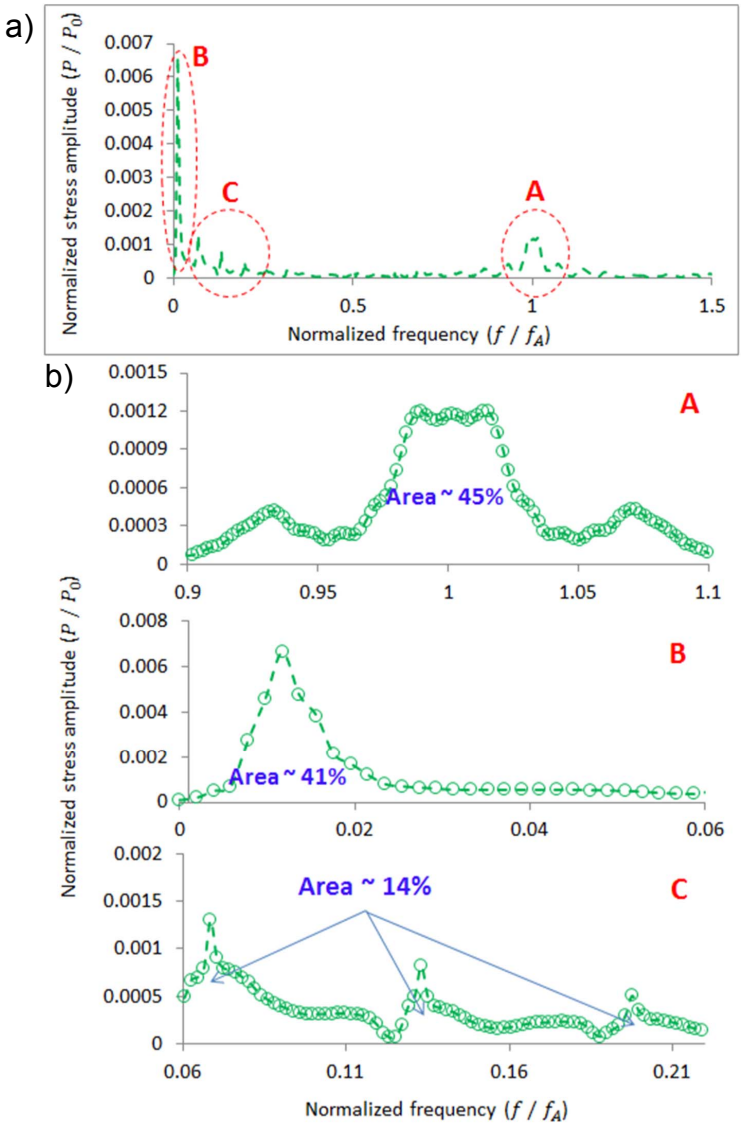

Figure 6.10: Spectral analyses of the wave in the first element of the visco-elastic material in a well-tuned system: about 45% of the impulse in carried by f_A (region A), about 41% is carried by f_B (region B), and about 14% is carried by f_C and its harmonics (region C).

ple, one might consider implementing a design with additional visco-elastic materials, or with a material having multiple relaxation times, to mitigate the other frequencies as well.

6.4 Comparison with Elastic and Plastic Designs

To highlight the enhanced performance of the blast-tuned or impact-tuned protective structure, the performance of alternative approaches relying on only elasticity or plasticity have also been analyzed, keeping equivalent parameters the same.

6.4.1 Elastic Design

The first case considered is a protective structure consisting of two linear-elastic layers. Layer 1 has a Young's modulus of E_1, a density of ρ_1, and a length of L_1. Layer 2 has a Young's modulus, of E_2, a density of ρ_2, and a length of L_2. The plate representing the supported structure has a Young's modulus of E_s, a density of ρ_s, and a mass of m_s. These dimensions and properties, plus the two characteristics of the blast/impact, P_o and t_o, make a total of eleven variables and three different units to describe the propagation of the stress wave through the protective structure. Therefore, according to the Buckingham-Π theory [111, 128, 19], the resultant pressure must be a function of eight dimensionless groups.

A series of finite-element calculations indicated that six groups could be reasonably neglected for the calculations that are presented, leaving P_t as functions of two dimensionless groups:

$$\frac{P_t}{P_o} = f\left(\frac{m_s}{\rho_1 L_1 + \rho_2 L_2}, \frac{E_1 \rho_1}{E_2 \rho_2}\right) \ . \tag{6.6}$$

The first non-dimensional group is the relative mass of the protected structure to the mass of the protective structure. I hold the masses equal to provide a valid comparison:

$$\frac{m_s}{\rho_1 L_1 + \rho_2 L_2} = 1. \tag{6.7}$$

The second non-dimensional group, $E_1\rho_1/E_2\rho_2$, is the square of the impedance mismatch between the first two layers. The transmitted pressure in an elastic system can be reduced significantly using impedance mismatch between the two layers, with $E_1\rho_1/E_2\rho_2 \gg 1$. These conditions are met with helmet designs that consist of an exterior shell made of a high-modulus glassy polymer and an interior made of a low-impedance, low-density elastic foam.

During the calculations, the remaining six non-critical groups were allowed to vary within fairly broad ranges:

$$\begin{aligned} 0.1 < t_o/t_1 < 10, \\ 0.08 < L_1/L_2 < 10, \\ 5 < E_1/E_2 < 25,000, \\ E_s/E_2 > 10,000, \\ 0.8 < \rho_s/\rho_2 < 2, \\ 10^{-5} < P_o/E_1 < 0.4. \end{aligned}$$

From a materials design perspective, the above range limits were chosen considering the elastic design made of a tough plastic polymer with a density in the range of 900 - 2000 kg/m^3 and a Young's modulus in the range of 0.1 - 5 GPa (first layer),

and a compliant elastic foam with a density in the range of 10 - 500 kg/m^3 and a Young's modulus in the range of 0.2 - 2 MPa (second layer), whereas the supporting structure is made of a hard, dense elastic material with material properties close to the ones for skull.

As shown in Fig. 6.11, with everything else being equal, the dissipation provided by a well-tuned visco-elastic system reduces the transmitted pressure more effectively than an elastic system. Furthermore, the major problem with a design that relies only on elastic materials is that there is no energy dissipation, so that any reduction in impulse depends on having a massive protective structure. However, it is noted that a low impedance for the second layer could increase the time-scale for the transmission of the impulse sufficiently to make pressure amplitude a more important design consideration. For inexpensive, low-performance armor and helmets, this is certainly a possible strategy. Whether it is an appropriate approach, or not, would depend on the application. Again, even if the design regime is within the range where pressure is important, the well-tuned visco-elastic design is still more efficient in dissipating pressure than the elastic design.

6.4.2 Plastic Design

In the design of structures that can directly accommodate a blast without loss of structural integrity (i.e. a ship's hull), it is well-recognized that a plastic layer can be used to dissipate energy [141, 26, 31, 30, 68, 98, 142, 123, 81, 25, 118, 129, 147, 7, 13]. To illustrate this, I considered the performance of a protective structure that relies on a plastic layer to dissipate energy. As has been established in the papers referenced above, the design of a plastic protective structure relies on a surface layer to convert impulse to kinetic energy which can then be dissipated by the plastic layer.

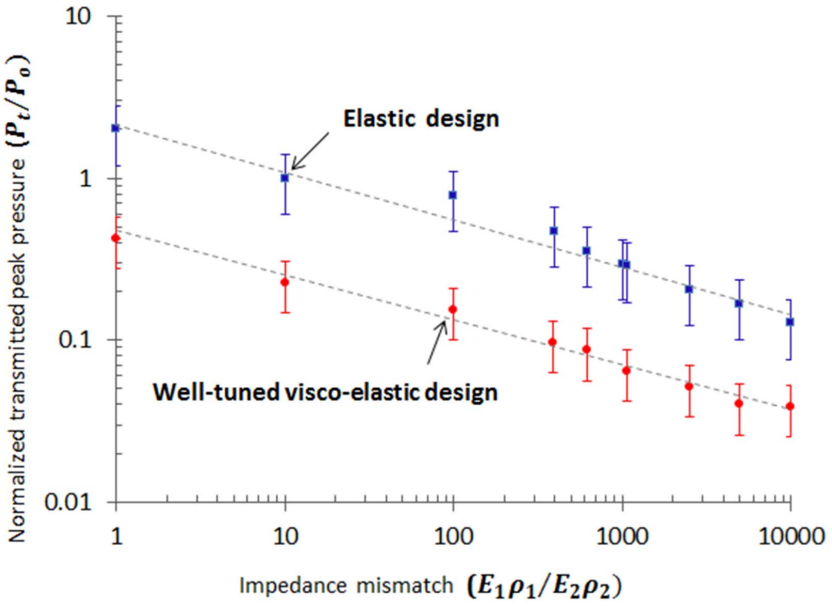

Figure 6.11: The maximum amplitude of the transmitted pressure decreases with increased impedance mismatch between the first and second layers for both the elastic and well-tuned visco-elastic designs. However, the energy dissipation associated with visco-elasticity provides a more effective reduction in the amplitude. In these calculations, the properties of the two elastic layers were identical to the first two layers of the well-tuned visco-elastic protective structure. The other parameters for the visco-elastic protective structure were set to $f_{crit}/f_A = 1$, $E_r/E_u = 0.001$, $E'_{crit}\rho_3/E_2\rho_2 = 1$ and $t_3/t_1 = 100$.

A light-weight protective structure relies on a foam (or truss) for the plastic layer, so my analysis assumes a similar form. The surface layer consists of a stiff, elastic material and the energy-dissipating layer is an elastic/perfectly-plastic foam.

Layer 1 has a Young's modulus of E_1, a density of ρ_1, and a length of L_1. Layer 2 has a Young's modulus, of E_2, a density of ρ_2, a length of L_2, a yield strength of σ_y, and a densification strain of ε_{dens}. The plate representing the supported structure has a Young's modulus of E_s, a density of ρ_s, and a mass of m_s. These dimensions and properties, plus the two characteristics of the blast/impact, P_o and t_o, make a total of twelve variables and three different units to describe the propagation of the stress wave through the protective structure. Therefore, according to the Buckingham-Π theory [111, 128, 19], the resultant pressure must be a function of nine dimensionless groups.

Finite-element calculations indicated that three non-dimensional groups were of primary importance in determining the energy dissipation while six groups could be reasonably neglected for the calculations that are presented. Therefore, I_t is a function of:

$$\frac{I_t}{I_o} = f\left(\frac{m_s}{\rho_1 L_1 + \rho_2 L_2}, \frac{\sigma_y(\sqrt{E_1\rho_1} + \sqrt{E_2\rho_2})}{2P_o\sqrt{E_2\rho_2}}, \frac{2\sigma_y L_2 \varepsilon_{dens}\rho_1 L_1}{I_o^2}\right) . \tag{6.8}$$

The first non-dimensional group is the relative mass of the protected structure to the mass of the protective structure. To provide a point of comparison between the different calculations, I set:

$$\frac{m_s}{\rho_1 L_1 + \rho_2 L_2} = 1. \tag{6.9}$$

The second group in Eqns. 6.8 is the ratio of the yield stress of the second layer

to the amplitude of the pressure wave transmitted into that layer. This ratio needs to be smaller than one, to ensure that efficient plastic deformation of the plastic layer occurs. If it is larger than one, then the foam behaves in an elastic fashion, as described in the previous section. The transmitted pressure also depends on this ratio. If the ratio is larger than one, the transmitted pressure depends on the impedance mismatch, as with the elastic protective structure. If the ratio is smaller than one, the transmitted pressure is limited to the yield strength, σ_y.

The third non-dimensional group in Eqns. 6.8 that is important in determining the energy dissipation and the transmitted impulse is what I term the "dissipative potential" of the protective structure. This is equal to the maximum plastic strain energy that can be dissipated by the second layer divided by the kinetic energy of the first layer. Fig. 6.12 shows a plot of how the transmitted impulse varies with this parameter. When the dissipative potential is small, there is no plastic deformation, and the transmitted impulse is equal to I_o. The fully-dissipative case develops when the dissipative potential is equal to one, and I_t/I_o becomes 0.5 (within numerical uncertainty).

During the calculations, the remaining six non-critical groups were allowed to vary within fairly broad ranges as shown in Eqns. 6.8.

The key point to make here is that, in contrast to the results for visco-elasticity, the results for plasticity never exhibit a regime where the impulse is transmitted to the protected structure outside an initial broad pressure wave. Therefore I_t is always at least 0.5 and a well-tuned visco-elastic design is again more efficient.

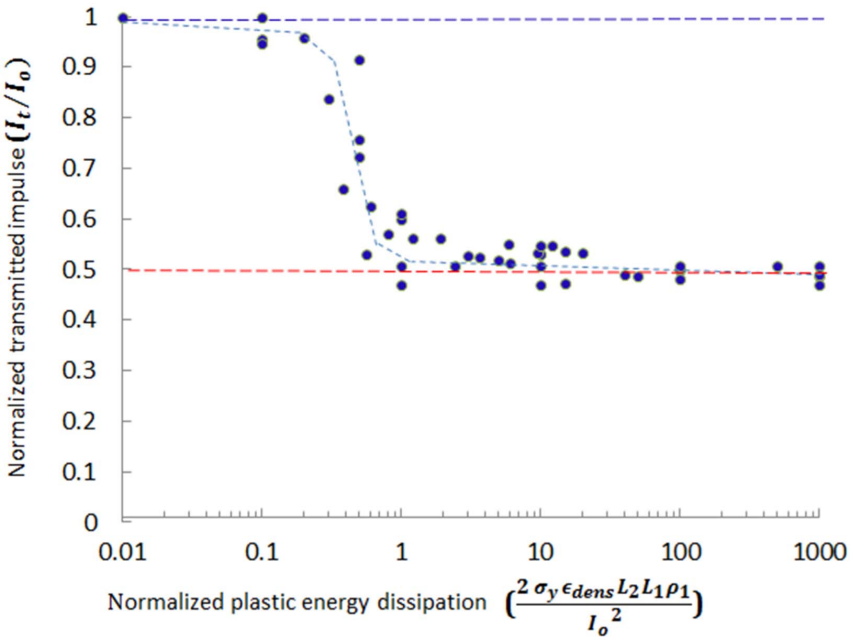

Figure 6.12: The transmitted impulse decreases as the dissipative potential of the plastic layer increases. In this calculation $\sigma_y(\sqrt{E_1\rho_1}+\sqrt{E_2\rho_2})/2P_o\sqrt{E_2\rho_2} < 0.1$. The scatter of the points indicates the magnitude of the numerical errors. When the dissipative potential is small, there is no plastic deformation, and the transmitted impulse is equal to I_o. The fully-dissipative case develops when the dissipative potential is equal to one, and I_t/I_o becomes 0.5.

6.5 Discussion

Three design strategies were investigated in this chapter:

- An elastic design which can significantly reduce the transmitted pressure using impedance mismatch. The major problem with a design that relies only on elastic materials is that there is no energy dissipation, so that any reduction in impulse depends on having a massive protective structure. This design is suitable for threats in which the duration of the original impact is relatively long (compared to the natural period of the brain) leading to move to the design regime where the amplitude of the transmitted pressure, not the impulse, is responsible for damage to the brain. Again, the natural period of the brain is not well understood and making a decision on design regimes is not easy.

- A plastic design which can dissipate the transmitted pressure and the transmitted impulse depending on the ratio of the yield stress of the second layer (foam layer) to the amplitude of the pressure wave transmitted into that layer and the dissipative potential of the protective system. The major problems with a plastic design are as follows. If the yield stress of the foam layer is larger than the amplitude of the pressure wave transmitted into that layer, no matter what the dissipative potential of the system is, the foam behaves in an elastic fashion with no impulse mitigation capabilities. If the impulse generated by the impact becomes large relative to the the dissipative potential of the system, the foam may deform beyond its densification strain where the stress-strain curve rises sharply and the transmitted pressure to the skull may elevate drastically. Therefore, the protective system may lose its pressure mitigation capabilities. Also the impulse is always transmitted over a single broad pulse, and the value of the impulse transmitted during this pulse is always in the range I_o to $0.5I_o$ (considering equal masses for the protected and protective structures), depend-

ing on the "dissipative potential" of the protective structure. Another problem with plastic design is that it is limited to a single use.

- A well-tuned visco-elastic design which can effectively minimize the transmitted pressure and the transmitted impulse repeatedly. The effective impulse transmitted by a well-tuned system in the first pulse can be less than $0.5I_o$ (considering equal masses for the protected and protective structures).

Fig. 6.13 provides representative illustrations of how the impulse transmitted to the protected structure varies with time for an elastic protective structure, a fully-dissipative plastic protective structure, a well-tuned visco-elastic protective structure and, a poorly-tuned visco-elastic protective structure. For the plastic protective structure, the impulse is always transmitted over a single broad pulse, and the value of the impulse transmitted during this pulse is always in the range I_o to $0.5I_o$, depending on the "dissipative potential" of the protective structure. For the visco-elastic protective structure, if the impulse transmitted in the initial pulse is greater than $0.5I_o$, then there is no further transmission at a later time. However, the effective impulse transmitted in this first pulse by a well-tuned system can be less than $0.5I_o$. With the freely-moving protected structure assumed in the calculations, contact can be momentarily lost between the protective structure and the protected structure even with partial transmission of the impulse, and not re-established over a time scale of relevance.

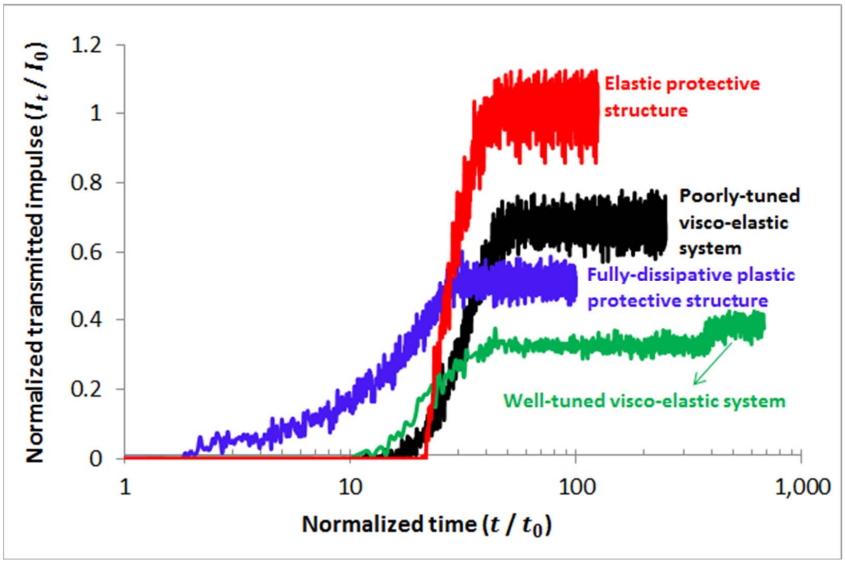

Figure 6.13: The total impulse transmitted to the protected structure, as a function of time. The curves show the results from finite-element calculations with an elastic protective structure, a fully-dissipative plastic protective structure, a well-tuned visco-elastic protective structure, and a poorly-tuned visco-elastic protective structure.

CHAPTER VII

Application: Protection Design Strategies for Impact-Born Threats

7.1 Impact-Born Threats

There are several impact-born threats causing brain injuries despite the use of safety helmets. These threats include motorcycle crashes, typical falls/collisions in football, hockey, baseball, soccer, biking, skateboarding, skiing, and lacrosse, and accidents for fire fighters and construction workers. For all of these threats, wearing a helmet can reduce the risk of a severe head injury. However, no helmet design has been proven to effectively prevent brain injuries. Therefore, there is an urgent need to battle concussion and in general brain injuries in these threats by proposing more efficient helmet designs with superior impact mitigation capabilities. To do so, as explained throughout this thesis, the first step is to study the mechanics of impact in these threats to identify and calculate the characteristics of impact. Here I am investigating this step for some selected impact-born threats. Then I proceed to inquire into the mechanics of damage to the brain as a result of such impacts and to briefly highlight the mitigation issues in current helmet designs.

7.2 Impact Characteristics

In Chapter III, I investigated the mechanics of impact for spherical shells with varying shell thickness to shell outer radius ratios (in the range of 0.005 to 1) and Poisson's ratio of 0.3 loaded by a rigid flat plate to derive contact load-deflection relationships and accordingly, the generalized parametric equations for the characteristics of impact. I assumed that the isotropic, elastic spherical shell has a Young's modulus of E_1, a Poisson's ratio of ν_1, an outer radius of R_1, a thickness of h_1, and a mass of m_1 while the flat plate is rigid. P_o (Eqn. 3.30), t_o (Eqn. 3.34), I_o (Eqn. 3.38) and F_{max} (Eqn. 3.27) are the characteristics of the impact in generalized form. As illustrated in theses equations, the impact characteristics are functions of the relative velocity (V_o) and the material and geometrical parameters of the spherical shell (E_1, ν_1, R_1, h_1, and m_1). C, n, D, and m also depend on the ratio of the shell thickness to shell outer radius, h_1/R_1, as reported in Tables 3.1 and 3.2 .

Eqns. 3.30, 3.34, 3.38, and 3.27 can be applied to compute the impact characteristics for impact-born threats involving

- a collision of a spherical shell-like geometry (eg. helmet, head, ...) to a rigid flat plate (eg. ground, wall, vehicle windshield, cement barriers, ...), and
- a collision of two identical spherical shell-like geometries (eg. helmet-to-helmet collision in football).

In the following, the impact load-time history and the impact pressure-time history for two threats will be plotted to compare the characteristics of impact in these threats.

7.2.1 Helmet-to-Helmet Collision in Professional Football

Concussion, or mild Traumatic Brain Injury (mTBI) is the signature injury in professional football. According to the National Football League (NFL) mTBI committee [131, 134], a direct helmet-to-helmet impact in head-down tackles may induce concussion in football players. A typical football helmet is composed of an outer shell and a foam liner (eg. vinyl nitrile, polyurethane, ...). A football helmet can be approximated as a spherical half shell with a shell thickness ($\approx$ 4 mm) to outer radius ($\approx$ 140 mm) ratio of $\approx$ 0.03. The typical shell is made of polycarbonate (PC) or acrylonitrile butadiene styrene (ABS) plastic with typical mechanical properties reported in Table 7.1. In head-down tackles, the striking player lines up his head, neck, and torso and delivers his force and momentum to the struck player whose body is aligned more or less perpendicularly to that of the striking player, such that the struck player's head or neck receives the full force of the impact. In head-down tackles in professional football, the mass of the struck player is reported as $\approx$ 8.5 kg including the head (4.38 kg), neck (1.06 kg), helmet and face mask (1.92 kg), and a portion of the torso mass (1.04 kg) and the mass of the striking player is $\approx$ 14.5 kg including the head, neck, helmet and face mask, and torso (7 kg). The relative velocity at which the helmets collide is in the range of 9 - 11 m/s [131].

Table 7.1: Mechanical properties of some typical materials used in the structure of helmets [2].

Material	Density (kg/m^3)	Poisson's Ratio	Young's Modulus (GPa)	Yield Strength (MPa)
Polycarbonate (PC)	1140 - 1210	0.3	2.0 - 2.4	59 - 70
ABS	1010 - 1210	0.3	1.1 - 2.9	19 - 51
Expanded Polyethylene (EPE)	55	0.1	0.02	0.6

For youth players, a football helmet has a shell thickness ($\approx$ 4 mm) to outer radius ($\approx$ 110 mm) ratio of $\approx$ 0.04. The maximum relative velocity at which two players

collide is considered to be $\approx$ 7 m/s [131, 133, 134] and the masses of the striking player and the struck player are assumed to be 20% lower than the ones in professional football. The assumption is based on the fact that the radius of the head is roughly following this ratio and therefore, the mass of the head has the same ratio.

Fig. 7.1 and Table 7.2 report the results of calculations for the characteristics of helmet-to-helmet impact in football (adult and youth).

Table 7.2: The characteristics of helmet-to-helmet impact in football (adult and youth). The parameters used for adult football: $m_1 = 8.5$ kg, $h_1 = 4$ mm, $R_1 = 140$ mm, $E_1 = 2.2$ GPa, $\nu_1 = 0.3$, $V_o = 11$ m/s, $C = 2.39$, $n = 1.05$, $D = 0.23$ and $m = 0.32$. The parameters used for youth football: $m_1 = 6.5$ kg, $h_1 = 4$ mm, $R_1 = 110$ mm, $E_1 = 2.2$ GPa, $\nu_1 = 0.3$, $V_o = 7$ m/s, $C = 2.43$, $n = 1.07$, $D = 0.24$ and $m = 0.32$.

	F_{max} (kN)	P_o (MPa)	t_o (msec)	I_o (N.sec)
Adult Football	27.9	4.3 - 18.1	13.4	234
Youth Football	17.7	6.4 - 24.0	10.3	113

As shown in Fig. 7.1, in football helmet-to-helmet collisions, adult players are exposed to larger impulses, I_o, relative to youth players due to the fact that I_o is linearly proportional to m_1 and V_o which are both smaller in youth players. Therefore, impulse mitigation is more effective in adult players. For impulse mitigation, energy dissipation is required in the helmet. As discussed in Section 5.1.2, one possible approach for a football helmet for adult players can be a plastic design. In a plastic design, the plastic deformation is irreversible and limited to single use. Once an element of material has plastically deformed, it is unavailable to absorb energy from subsequent stress waves of the same magnitude. A more efficient design strategy for a football helmet for adult players is a well-tuned visco-elastic system that can reduce the transmitted impulse very effectively and is not limited to single use. Another limitation with a plastic design in a football helmet is that the yield strength

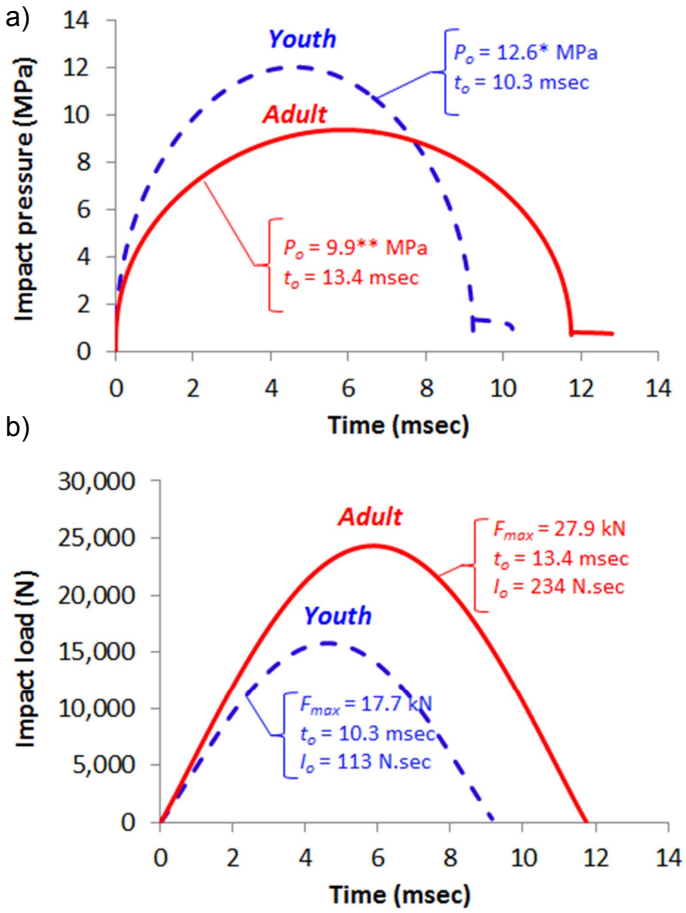

Figure 7.1: a) Impact pressure vs. time, and b) impact load vs. time for helmet-to-helmet collision in head-down tackles in football (adult versus youth). The parameters used for adult football: $m_1 = 8.5$ kg, $h_1 = 4$ mm, $R_1 = 140$ mm, $E_1 = 2.2$ GPa, $\nu_1 = 0.3$, $V_o = 11$ m/s, $C = 2.39$, $n = 1.05$, $D = 0.23$ and $m = 0.32$. The parameters used for youth football: $m_1 = 6.5$ kg, $h_1 = 4$ mm, $R_1 = 110$ mm, $E_1 = 2.2$ GPa, $\nu_1 = 0.3$, $V_o = 7$ m/s, $C = 2.43$, $n = 1.07$, $D = 0.24$ and $m = 0.32$. * P_o in youth football can be in the range of 6 - 24 MPa. ** P_o in adult football can be in the range of 4 - 17 MPa.

of the foam liner may be larger than the amplitude of the pressure wave transmitted into that layer. Therefore, no matter what the dissipative potential of the foam liner is, the foam would behave in an elastic fashion with no energy dissipation capabilities.

Youth players and adult players experience almost the same overpressure which has a significant magnitude. Therefore, football helmet has to be effective in mitigating pressure as well. As discussed in Section 6.4.2, one possible design strategy for an inexpensive, low performance football helmet can be an elastic design involving a large impedance mismatch. Elastic design has no energy dissipation to dissipate impulse. However, a low impedance for the second layer could increase the time-scale for the transmission of the impulse sufficiently to make pressure amplitude a more important design consideration. Again, a more efficient design strategy for a football helmet with superior pressure mitigation capabilities is a well-tuned visco-elastic system which can reduce the transmitted pressure even more effectively than an elastic system. A well-tuned visco-elastic design can also dissipate impulse efficiently.

7.2.2 Typical Collisions in Bicycling

While football tends to dominate the discussion of sports-related head injuries, research shows that bicycling accidents account for far more traumatic brain injuries each year [89] considering both helmeted and non-helmeted riders (the data does not separate out the two situations). Bicyclists are at high risk of colliding with motor vehicles resulting in impacts between helmeted heads and vehicle windshields (or the ground or cement barriers). A typical bicycle helmet is composed of a thick foam liner covered by a very thin polycarbonate coating. The foam of a bicycle helmet can be approximated as a spherical shell with a shell thickness ($\approx$ 24 mm) to outer radius ($\approx$ 130 mm) ratio of $\approx$ 0.18 for adults and with a shell thickness ($\approx$ 24 mm)

to outer radius ($\approx$ 100 mm) ratio of $\approx$ 0.24 for children. The typical foam is made of expanded polyethylene (EPE) with material and mechanical properties reported in Table 7.1. The mass involved in bicycle accidents can be the mass of the helmet and head only or the mass of the helmet and the whole (or part of the) body. Therefore, three values of 5 kg, 25 kg, and 50 kg have been considered for m_1 in this study. 5 kg, 25 kg, and 50 kg are assumed to be the mass of head and helmet only, the mass of head, helmet and a part of the body, and the mass of head, helmet and the whole body, respectively. The relative velocity at which the helmet collides with a hard object also depends on the nature of the accident. Thus three different values of 5 m/s, 15 m/s and 25 m/s have been assigned for V_o. 5 m/s is assumed to be related to a bike rider who rides at the speed of 5 m/s and falls on the ground head first. 15 m/s is assumed to be related to a bike rider who rides at the speed of 5 m/s and collides with the windshield of a moving vehicle with the speed of 10 m/s. 25 m/s is assumed to be related to a bike rider who rides at the speed of 5 m/s and collides with the windshield of a moving vehicle with the speed of 20 m/s.

In the following, the sensitivity of the characteristics of impact (impact over-pressure, P_o, impact duration, t_o, impact impulse, I_o and maximum impact load, F_{max}) in bicycling accidents with respect to varying V_o (5 m/s vs. 15 m/s vs. 25 m/s), varying m_1 (5 kg vs. 25 kg vs. 50 kg), and varying R_1 (100 mm vs. 130 mm) are examined and the conclusions can be generalized to any other type of impacts in impact-born threats. Then, biking accidents in kids and adults will be compared in particular.

Figs. 7.2, 7.3, and 7.4 show the results of calculations for the characteristics of helmet-to-rigid flat object impacts in bicycle accidents:

- Fig. 7.2 demonstrates the effect of varying relative velocity, V_o, on the pressure-

time history profile and the load-time history profile of bicycle helmet impacts. As the relative velocity increases from 5 m/s to 25 m/s, both impact pressure, P_o, and impulse, I_o, increase by 100% and 400%, respectively. Here the other parameters have been fixed as $m_1 = 5$ kg, $h_1 = 24$ mm, $R_1 = 130$ mm, $E_1 = 20$ MPa, $\nu_1 = 0.1$, $C = 2.92$, $n = 1.23$, $D = 0.42$ and $m = 0.37$.

- Fig. 7.3 reveals the sensitivity of impact characteristics in bicycle accidents to the mass, m_1. As the mass involved in the impact elevates from 5 kg to 50 kg, all three major impact characteristics including pressure, P_o, duration, t_o, and impulse, I_o, increase by 66%, 180% and 900%, respectively. Here the other parameters have been fixed as $V_o = 5$ m/s, $h_1 = 24$ mm, $R_1 = 130$ mm, $E_1 = 20$ MPa, $\nu_1 = 0.1$, $C = 2.92$, $n = 1.23$, $D = 0.42$ and $m = 0.37$.

- Fig. 7.4 shows how the pressure-time history profile and the load-time history profile of bicycle helmet impacts are affected by changing shell outer radius, R_1. As the shell outer radius decreases from 130 mm to 100 mm, impact pressure, P_o, increases by 25% while impulse, I_o remains unchanged. Here the other parameters have been fixed as $m_1 = 5$ kg, $h_1 = 24$ mm, $V_o = 5$ m/s, $E_1 = 20$ MPa, $\nu_1 = 0.1$.

The results above can be generalized for any kind of impacts in impact-born threats.

The impact characteristics in bicycle accidents for adults versus youths are investigated considering two different scenarios: an adult bicycle rider wearing a helmet ($h_1 = 24$ mm, $E_1 = 20$ MPa, $\nu_1 = 0.1$, $R_1 = 130$ mm, $C = 2.92$, $n = 1.23$, $D = 0.42$ and $m = 0.37$) involved in a car accident hits the windshield with a relative velocity of $V_o = 25$ with his total mass of $m_1 = 50$ kg; whereas a youth bicycle rider wearing a helmet ($h_1 = 24$ mm, $E_1 = 20$ MPa, $\nu_1 = 0.1$, $R_1 = 100$ mm, $C = 2.95$, n

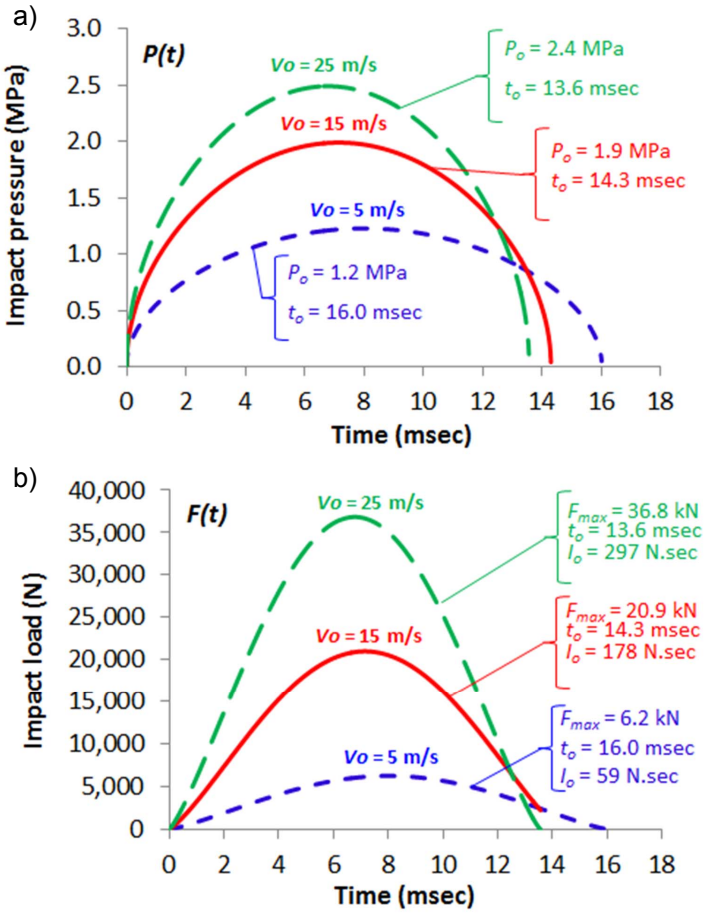

Figure 7.2: a) Impact pressure vs. time, and b) impact load vs. time for helmet-to-rigid flat plate (windshield, ground, or cement barrier) impacts in bicycle accidents for three different values of V_o. The other parameters have been fixed as: $m_1 = 5$ kg, $h_1 = 24$ mm, $R_1 = 130$ mm, $E_1 = 20$ MPa, $\nu_1 = 0.1$, $C = 2.92$, $n = 1.23$, $D = 0.42$ and $m = 0.37$..

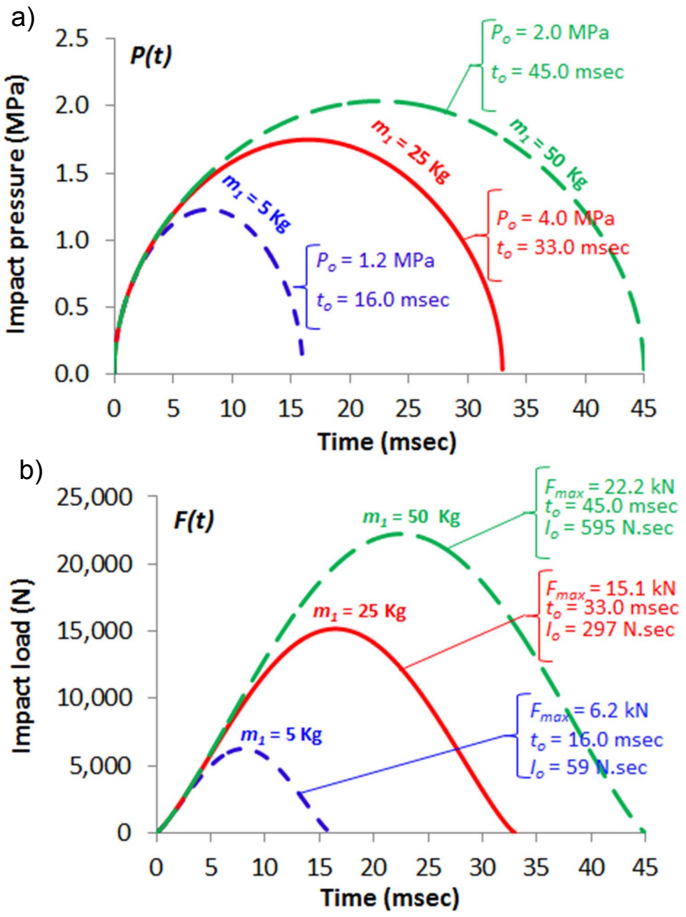

Figure 7.3: a) Impact pressure vs. time, and b) impact load vs. time for helmet-to-rigid flat plate (windshield, ground, or cement barrier) impacts in bicycle accidents for three different values of m_1. The other parameters have been fixed as: $V_o = 5$ m/s, $h_1 = 24$ mm, $R_1 = 130$ mm, $E_1 = 20$ MPa, $\nu_1 = 0.1$, $C = 2.92$, $n = 1.23$, $D = 0.42$ and $m = 0.37$.

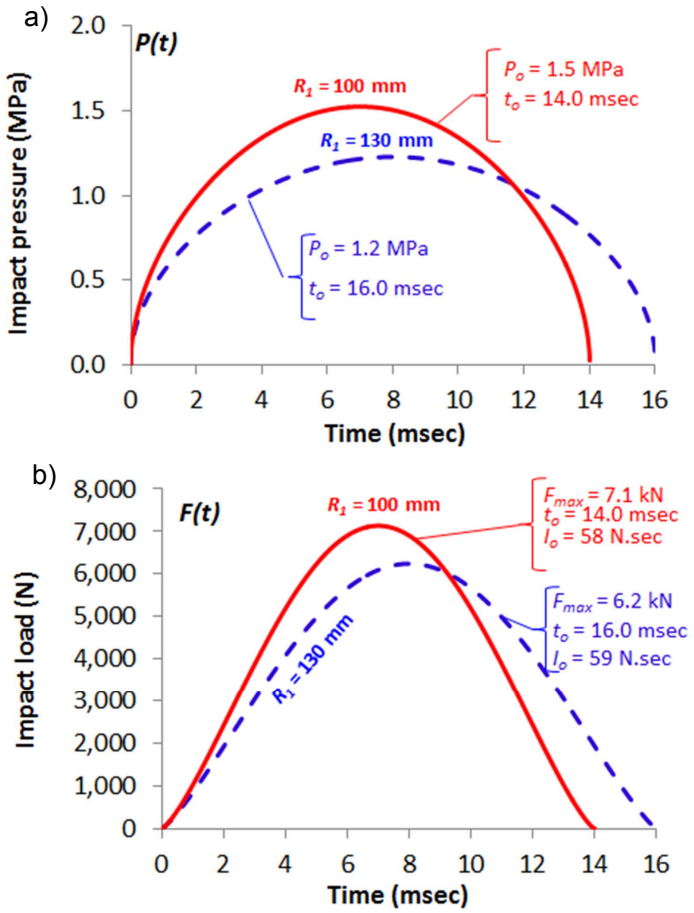

Figure 7.4: a) Impact pressure vs. time, and b) impact load vs. time for helmet-to-rigid flat plate (windshield, ground, or cement barrier) impacts in bicycle accidents for two different values of R_1. $R_1 = 130$mm and $R_1 = 100$mm correspond to an adult bicycle helmet and a youth bicycle helmet, respectively. The parameters used for the adult bicycle helmet: $m_1 = 5$ kg, $h_1 = 24$ mm, $V_o = 5$ m/s, $E_1 = 20$ MPa, $\nu_1 = 0.1$, $C = 2.92$, $n = 1.23$, $D = 0.42$ and $m = 0.37$. The parameters used for the youth bicycle helmet: $m_1 = 5$ kg, $h_1 = 24$ mm, $V_o = 5$ m/s, $E_1 = 20$ MPa, $\nu_1 = 0.1$, $C = 2.95$, $n = 1.30$, $D = 0.51$ and $m = 0.39$.

= 1.30, $D = 0.51$ and $m = 0.39$) involved in a car accident hits the windshield with a relative velocity of $V_o = 15$ with his total mass of $m_1 = 25$ kg. Table 7.3 reports the results of calculations for the characteristics of helmet-to-windshield impacts in bicycle accidens (adult versus kid).

Table 7.3: The characteristics of helmet-to-windshield impact in bicycle accidents (adult and youth). The parameters used for an adult bicycle rider: $m_1 = 50$ kg, $V_o = 25$ m/s, $h_1 = 24$ mm, $E_1 = 20$ MPa, $\nu_1 = 0.1$, $R_1 = 130$ mm, $C = 2.92$, $n = 1.23$, $D = 0.42$ and $m = 0.37$. The parameters used for a youth bicycle rider: $m_1 = 25$ kg, $V_o = 15$ m/s, $h_1 = 24$ mm, $E_1 = 20$ MPa, $\nu_1 = 0.1$, $R_1 = 100$ mm, $C = 2.95$, $n = 1.30$, $D = 0.51$ and $m = 0.39$.

	F_{max} (kN)	P_o (MPa)	t_o (msec)	I_o (N.sec)
Adult Bicycle Rider	131.2	3.1 - 5.2	38.1	2,980
Youth Bicycle Rider	61.3	2.9 - 4.5	24.4	877

Adult bicycle riders are exposed to larger impulses, I_o, relative to youth bicycle riders which is due to larger mass and velocity associated with adult bicycle riders.

In helmet-to-windshield collisions in bicycle accidents, the impulse, I_o, is large relative to that calculated for helmet-to-helmet collisions in head-down tackles in professional football. Overpressure, P_o, is relatively lower, still holding a significant value. Again, an elastic design is one possible design strategy for a bicycle helmet to mitigate pressure. The major problem with an elastic design is that it involves no energy dissipation to dissipate impulse. Similarly, a plastic design is another possible design strategy for a bicycle helmet to mitigate pressure and impulse. The major problem with a plastic design is that plastic deformation is irreversible and limited to single use. Moreover, in bicycle accidents with small relative velocities and/or small masses involved, there is a possibility that the impact overpressure becomes smaller than the yield strength of the foam liner in the helmet and therefore, the foam remains in the elastic region, experiencing no plastic deformation, no energy

dissipation and consequently, no impulse mitigation. On the other hand, in bicycle accidents with large relative velocities and/or large masses involved, there is a possibility that mitigating impulse necessitates either a thick layer of foam (which violates the design thickness requirements for bicycle helmets), or excessive foam deformation beyond the densification strain (where the stress-strain curve rises sharply and the transmitted pressure to the skull may elevate significantly).

CHAPTER VIII

Conclusions and Future Directions

8.1 Summaries

The research presented in this work has focused on proposing a systematic and effective design for blast-resistant and impact-resistant protective structure by considering three mechanics: the mechanics of blast/impact, the mechanics of damage to the protected structures due to blast/impact, and the mechanics of how to mitigate effectively the damaging features of blast/impact through the design of protective structure. Some of the key findings of this research are summarized below:

- The impact behavior of elastic spherical shells with varying shell thickness to shell outer radius ratios (0.005 - 1) and Poisson ratio of 0.3 was investigated computationally using a 2D axisymmetric finite element model for spherical shells subjected to axial compression from a rigid flat plate. Two dimensionless material and geometrical parameters controlling the contact load-interference relationship were identified. It was shown how the exponent in the contact load-interference relationship increases from unity to 1.5 as the shell thickness to shell outer radius ratio increases from 0.005 to 1.

- The impact response of spherical shells with varying shell thickness to shell outer radius ratios subjected to a rigid flat plate was investigated in this research and the generalized parametric formulations for impact characterization including overpressure, duration, and impulse were developed in terms of material and geometrical parameters of the spherical shells and the relative impact velocities. These formulations are very important in the sense that they provide useful tools for design optimization and show the sensitivity of each impact characteristic with respect to material and geometrical parameters of protective structures. Moreover, they make costly computational and experimental analysis of impact events unnecessary. Finally, they may suggest the proper design strategies/regimes.

- The stress induced within a target that is part of a dynamical system, such as the brain within a skull, is determined either by the directly transmitted pressure, or by the transmitted impulse. The relative importance of the two depends on the duration of the pressure wave impinging upon the protected structure compared to the characteristic time of the dynamic response of the system. The design of any armor used as protection from blast in military applications, or by impact in sporting or industrial applications, needs to consider both of these time scales. Armor can mitigate both the pressure and the impulse. It can also change the time scale over which a pressure wave is transmitted, so as to move the design away from one in which impulse needs to be mitigated, to one in which the pressure needs to be limited. Impedance mismatch can control the transmitted pressure. Energy dissipation mechanisms can mitigate the transmitted impulse. Dispersion can increase the interaction time between the supported structure and the threat, so as to change the damage regime from one controlled by impulse to one controlled by pressure.

- Visco-elastic polymers can be used for protection over multiple events. However, for this concept to be realized, it is necessary for the stress waves traveling through the armor do so at frequencies corresponding to appropriate dissipative molecular transitions in the polymers. Typically, the energy of the stress waves induced by blast or impact is broadly distributed over multiple frequencies. Therefore, this energy must be tuned to a narrow spectrum before it can be optimally dissipated by the polymer. Here, it is proposed to do this through a multi-layer design in which the outer layers tune the stress waves to match the critical damping frequency of the inner visco-elastic layer. As a high frequency stress wave travels through this visco-elastic layer, it undergoes multiple loading-unloading cycles which can result in significant energy dissipation over a short duration. A finite-element analysis of this concept has illustrated several important constraints on the design. The outer layer needs to have a high acoustic impedance compared to its neighbor, so that the wave can be tuned by multiple reflections at the interface between the two layers. The impedance mismatch must not be so high that the stress waves are transmitted inefficiently through successive layers. The numerical simulations suggest that an impedance mismatch of about 70 is optimal. Typically, one would expect to use an outer layer with a relatively high modulus; but it is recognized that the outer layer may also have to serve other functional purposes, such as resistance to ballistic penetration. It is also recognized that in sports applications involving impact, more compliant helmets may increase the characteristic time for transmission of an impulse, and move the design space to a regime where dissipation of energy is less critical.

- There are two significant constraints on the material properties of the visco-elastic layer used for energy dissipation. First, it needs to have a very low ratio

of the relaxed modulus to the unrelaxed modulus. This will result in a high value of $\tan\delta$ at a critical frequency that matches the tuned frequency from the first layer. Second, for realistic thicknesses of the outer layer, the critical frequency of the polymer will need to be quite high. For example, if the modulus of the outer layer is of the order of 1-10 GPa, its density is 1000 kg/m^3, and its thickness is 5 mm, the critical frequency that needs to be damped will be about 100-300 kHz. This leads to some experimental challenges in identifying and designing suitable polymers, for it is far above the range of frequencies at which polymers are typically investigated. However, ultrasonic methods [5] and dielectric analyses [54] have been used to measure $\tan\delta$ and the storage and loss moduli in the MHz range.

- The glass transition is a possible energy-loss peak to explore for these purposes [102, 15], and it is instructive to consider what value of glass-transition temperature, T_g, measured in the 1 Hz range, might correspond to a glass transition in the 200 kHz range at an operating temperature of T_o. This can be estimated from the WLF equation [138], for a shift factor of 2×10^5:

$$\log(2 \times 10^5) = \frac{17.5(T_o - T_g)}{52 + T_o - T_g} \tag{8.1}$$

This expression results in a glass transition temperature measured at 1 Hz which is about 23 °C below the operating temperature. For example, if the inside of a helmet is maintained at body temperature, the required glass-transition temperature would be about 14 °C. However, there will obviously be a range of operating temperatures, depending on the external environment. Fortunately, the analysis shows that the efficacy of the proposed design is relatively insensitive to f_{crit}, provided that $f_{crit}/f_A > 1$ and E_r/E_u is very small. In practice,

this puts an upper bound on T_g of about 20-30 °C below the lowest temperature that the armor will experience in service. Higher temperatures, within a reasonable range, will result in the system being within the plateau where the response is not very sensitive to f_{crit}/f_A. In conclusion, this result would seem to indicate that there is plenty of flexibility to use even higher tuning frequencies than 200kHz, since the required value of T_g is not particularly low.

8.2 Conclusions

The effective design strategies for impact-resistant protective structures depend on the relative values for the duration of the impact, the natural period of the target, and the relaxation times of the target. If the duration of the impact is long relative to the natural period of the target, then it is the amplitude of the transmitted pressure that has to be reduced. If the duration of the impact is short relative to the natural period of the target, then depending on the relative values for the natural period of the target and the relaxation times of the target, it is either the transmitted impulse or the amplitude of the transmitted pressure that has to be minimized.

There is a potential efficiency of protective designs that stiffen the "neck". By immobilizing (stiffening) the supporting structure (i.e. neck) in a protected structure (i.e. head), both the damaging features of the blast/impact (including pressure and impulse) transmitted to the delicate target (i.e. brain) reduce.

The maximum force on the skull does not always correlate with the maximum force on the brain. The skull and brain accelerations are uncorrelated if the blast/impact duration is shorter than the natural period of the brain. A practical implication of this is that a simple measurement of maximum acceleration of a skull gives no in-

dication of the force that a brain may experience. The instrumented studies of the helmet-to-helmet impacts in professional football reveal that such impact events give the impact duration of $\approx$ 15 ms whereas the characteristic relaxation times in the brain are in the range of $30 - 1000\ ms$. Assuming the natural period of the brain in the same range as its characteristic relaxation times, the current football helmet designs fall in the region where the skull and brain accelerations are uncorrelated. This may help to explain why measurements of peak accelerations at the skull fail to correlate with brain injury.

In football helmet-to-helmet collisions, adult players are exposed to larger impulses relative to youth players. Therefore, impulse mitigation is more effective in adult players. For impulse mitigation, energy dissipation is required in the helmet. One possible approach for an inexpensive, low performance football helmet for adult players can be a plastic design. In a plastic design, the plastic deformation is irreversible and limited to single use. Another limitation with a plastic design in a football helmet is that the yield strength of the foam liner may be larger than the amplitude of the pressure wave transmitted into that layer. Therefore, no matter what the dissipative potential of the foam liner is, the foam would behave in an elastic fashion with no energy dissipation capabilities. A more efficient design strategy for a football helmet for adult players is a well-tuned visco-elastic system that can reduce the transmitted impulse very effectively.

In football helmet-to-helmet collisions, youth players and adult players experience almost the same overpressure which has a significant magnitude. Therefore, football helmet has to be effective in mitigating pressure as well. One possible design strategy for an inexpensive, low performance football helmet can be an elastic design involving a large impedance mismatch. Elastic design has no energy dissipation to dissipate

impulse. However, a low impedance for the second layer could increase the time-scale for the transmission of the impulse sufficiently to make pressure amplitude a more important design consideration. Again, a more efficient design strategy for a football helmet with superior pressure mitigation capabilities is a well-tuned visco-elastic system which can reduce the transmitted pressure even more effectively than an elastic system.

In helmet-to-windshield collisions in bicycle accidents, impulse is large relative to the one calculated for helmet-to-helmet collisions in head-down tackles in professional football. In a bike helmet, a plastic design that actually plastically deforms is a practical design. In bicycle accidents with large relative velocities and/or large masses involved, there is a possibility that mitigating impulse necessitates either a thick layer of foam (which violates the design thickness requirements for bicycle helmets), or excessive foam deformation beyond the densification strain (where the stress-strain curve rises sharply and the transmitted pressure to the skull may elevate significantly).

8.3 Future Work

The novel design concept introduced in Chapter VI involved a three-layered protective structure in which the first and second layers tune the stress waves to three characteristics frequencies: f_A, f_B, and f_C, among which f_A carries the largest percentage of energy associated with blast/impact. The third layer is a visco-elastic polymer having a critical damping frequency matching f_A to optimally dissipate the energy carried by f_A. Future investigation can be focused on adding more visco-elastic layers having critical damping frequencies matching f_B and f_C in order to dissipate more energy of blast/impact.

The finite element analysis of the head and the football helmet (current design versus proposed well-tuned design) can be performed first considering the 2D cross-sectional area of head/helmet and then considering 3D finite element modelling of head/helmet. 2D FE computational approach is valid for comparison-basis and not prohibitively costly. However, 3D finite element modelling of head/helmet involves more accurate masses and geometries resulting in more precise absolute values for translational and rotational accelerations of the brain. Therefore, future investigation can be focused on performing 2D and 3D finite element modelling of head/helmet in helmet-to-helmet impacts in professional football.

Experimental investigations can also be performed involving a simple 2D experimental mock-up of a skull/brain system equipped with 2D helmets (the existing design versus the proposed well-tuned design) to measure shear deformation, translational velocity, and translational acceleration of the brain. Moreover, future investigation can rely on building 3D helmet prototypes (the existing design versus the proposed well-tuned design) and performing impact tests using hybrid III dummy heads and a drop weight apparatus to measure translational and rotational accelerations in the dummy head. Additional improvement can be achieved by mounting pressure sensors in addition to accelerameters in the hybrid III dummy head to record the impact pressure-time history profile on the surface of the dummy head. This pressure profile holds valuable information on how much pressure and impulse have been transmitted through the helmet (the existing design versus the proposed well-tuned design).

APPENDICES

APPENDIX A

SIMULINK Analysis I

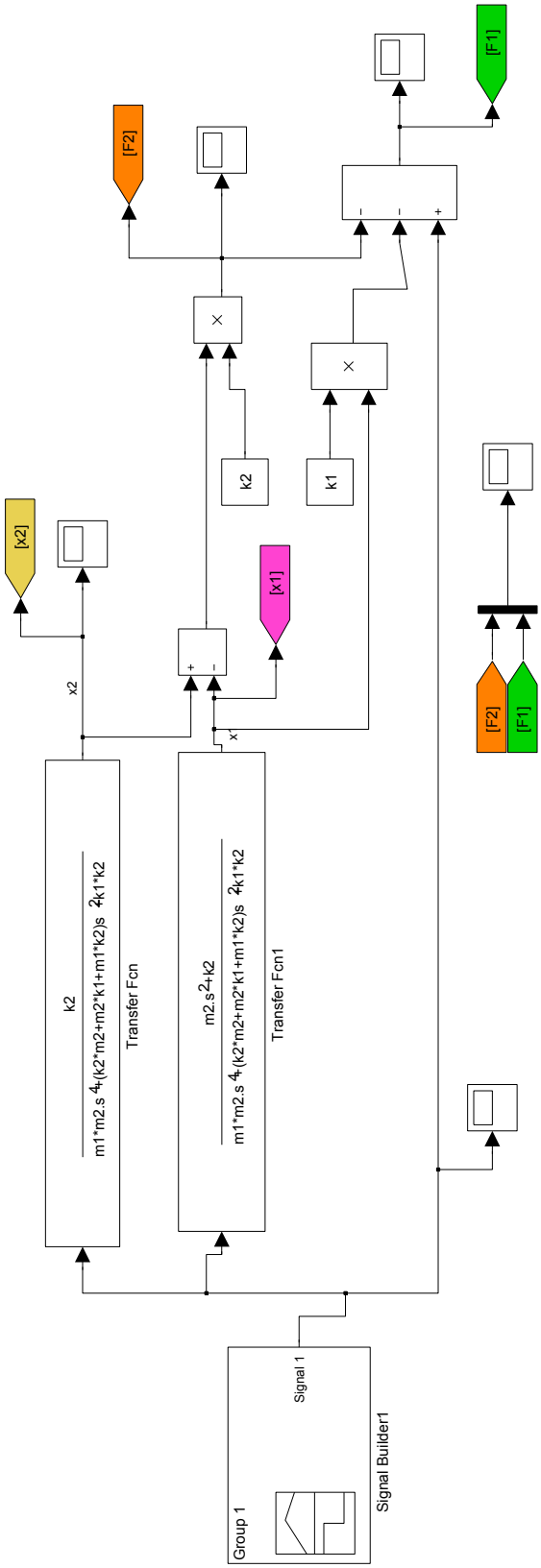
[F1]
[F2]
[x2]
[x1]
k2
k1
x2
x1
k2
m1*m2.s4+(k2*m2+m2*k1+m1*k2)s2+k1*k2
Transfer Fcn
m2.s2+k2
m1*m2.s4+(k2*m2+m2*k1+m1*k2)s2+k1*k2
Transfer Fcn1
Signal 1
Group 1
Signal Builder1

APPENDIX B

SIMULINK Analysis II

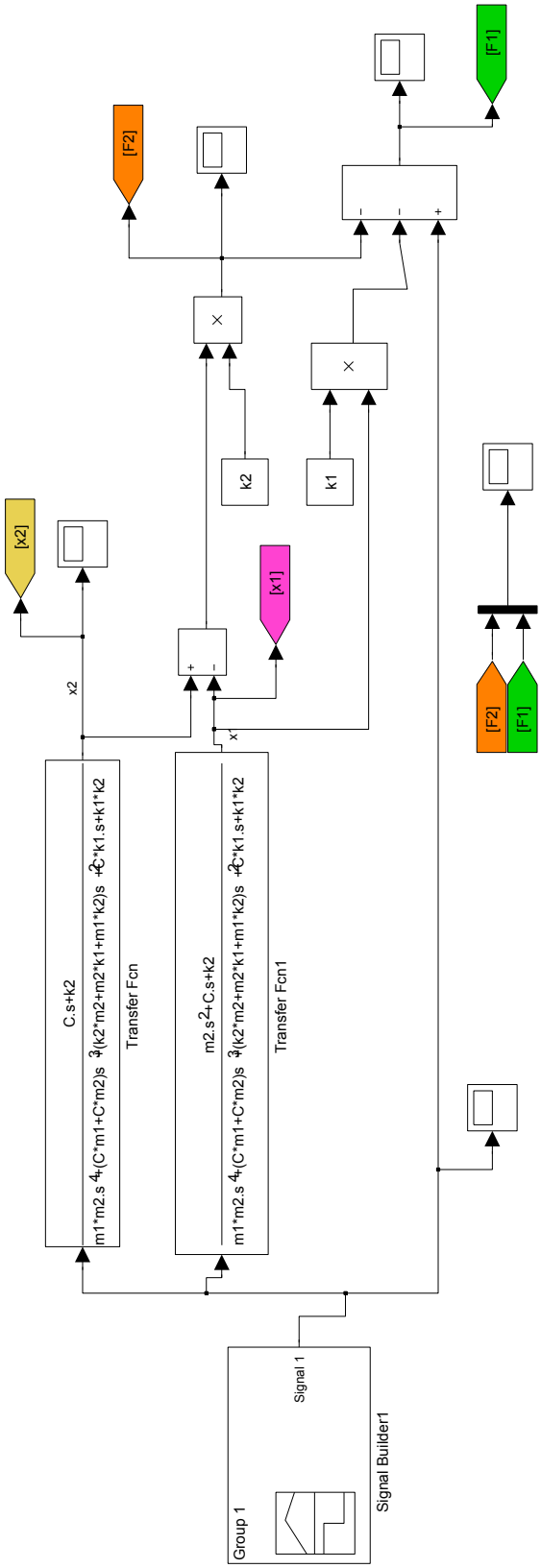
[F1]
[F2]
[x2]
[x1]
k2
k1
x2
x1
C.s+k2
m1*m2.s^4+(C*m1+C*m2)s^3+(k2*m2+m2*k1+m1*k2)s^2+C*k1.s+k1*k2
Transfer Fcn
m2.s^2+C.s+k2
m1*m2.s^4+(C*m1+C*m2)s^3+(k2*m2+m2*k1+m1*k2)s^2+C*k1.s+k1*k2
Transfer Fcn1
Signal 1
Group 1
Signal Builder1

BIBLIOGRAPHY

BIBLIOGRAPHY

[1] (2008), ABAQUS version 6.8-1, User Documentation, Dassault Systems.

[2] (2009), CES EduPack release 4, Research Version, User Documentation, Granta Design Limited.

[3] (2011), MATLAB SIMULINK R2011a, MathWorks.

[4] (2012), Standard performance specification for newly manufactured football helmet, NOCSAE DOC (ND)002-11m12.

[5] Alig, I., F. Stieber, and S. Wartewig (1991), Ultrasonic examination of the dynamic glass transition in amorphous polymers, *Journal of Non-Crystalline Solids*, *131-133*, 808–811.

[6] Allen, R. M., D. J. Kirkpatrick, A. W. Longbottom, A. M. Milne, and N. K. Bourne (2004), Experimental and numerical study of free-field blast mitigation, *AIP Conference Proceedings*, *706*(1), 823–826.

[7] Amini, M. R., A. V. Amirkhizi, and S. Nemat-Nasser (2010), Numerical modeling of response of monolithic and bilayer plates to impulsive loads, *International Journal of Impact Engineering*, *37*(1), 90–102.

[8] Amini, M. R., J. Isaacs, and S. Nemat-Nasser (2010), Investigation of effect of polyurea on response of steel plates to impulsive loads in direct pressure-pulse experiments, *Mechanics of Materials*, *42*(6), 628–639.

[9] Amini, M. R., J. Isaacs, and S. Nemat-Nasser (2010), Experimental investigation of response of monolithic and bilayer plates to impulsive loads, *International Journal of Impact Engineering*, *37*(1), 82–89.

[10] Amirkhizi, A. V., J. Isaacs, J. McGee, and S. Nemat-Nasser (2006), An experimentally-based viscoelastic constitutive model for polyurea, including pressure and temperature effects, *Philosophical Magazine*, *86*(36), 5847–5866.

[11] Ashby, M. F., A. G. Evans, N. A. Fleck, L. J. Gibson, J. W. Hutchinson, and H. N. G. Wadley (2000), *Metal Foams: A Design Guide*, Butterworth Heinemann, Woburn, MA, USA.

[12] Bahei-El-Din, Y. A., and G. J. Dvorak (2007), Wave propagation and dispersion in sandwich plates subjected to blast loads, *Mechanics of Advanced Materials and Structures*, *14*(6), 465–475.

[13] Bahei-El-Din, Y. A., G. J. Dvorak, and O. J. Fredricksen (2006), A blast-tolerant sandwich plate design with a polyurea interlayer, *International Journal of Solids and Structures*, *43*(25-26), 7644–7658.

[14] Bhattacharjee, Y. (2008), Shell shock revisited: solving the puzzle of blast trauma, *Science*, *319*, 406408.

[15] Bogoslovov, R., C. Rowland, and R. Gamache (2007), Impact-induced glass transition in elastomeric coatings, *Applied Physics Letters*, *90*(221910), 1–3.

[16] Brode, H. L. (1955), Numerical solution of spherical blast waves, *Journal of Applied Physics, American Institute of Physics, Ney York*.

[17] Broglio, S. P., B. Schnebel, J. J. Sosnoff, S. Shin, X. Fend, X. He, and J. Zimmerman (2010), Biomechanical properties of concussions in high school football., *Medicine and science in sports and exercise*, *42*(11), 2064–2071.

[18] Broglio, S. P., J. T. Eckner, T. Surma, and J. S. Kutcher (2011), Post-concussion cognitive declines and symptomatology are not related to concussion biomechanics in high school football players., *Journal of neurotrauma*, *28*(10), 1–8.

[19] Buckingham, E. (1914), On physically similar systems: illustrations of the use of dimensional equations, *Physical Reviews*, *4*(4), 345–376.

[20] Daneshvar, D. H., C. M. Baugh, C. J. Nowinski, A. C. McKee, R. A. Stern, and R. C. Cantu (2011), Helmets and mouth guards: the role of personal equipment in preventing sport-related concussions., *Clinics in sports medicine*, *30*(1), 145–163.

[21] Daniel, R. W., S. Rowson, and S. M. Duma (2014), Head impact exposure in youth football: middle school ages 12 to 14 years., *Journal of Biomechanical Engineering*, *136*(094501), 1–6.

[22] Daraio, C., V. F. Nesterenko, E. Herbold, and S. Jin (2006), Energy trapping and shock disintegration in a composite granular medium, *Physical Review Letters*, *96*(5), 1–4.

[23] Denny-Brown, D., and W. R. Russell (1941), Experimental cerebral concussion, *Brain*, *64*(2-3), 93–164.

[24] Deresiewicz, H. (1968), A note on Hertz Theory of Impact, *Acta Mechanica*, *6*, 110–112.

[25] Deshpande, V. S., and N. A. Fleck (2000), High strain rate compressive behaviour of aluminium alloy foams, *International Journal of Impact Engineering*, *24*(3), 277–298.

[26] Deshpande, V. S., A. Heaver, and N. A. Fleck (2006), An underwater shock simulator, *Proceedings of the Royal Society A*, *462*(2067), 1021–1041.

[27] Dvorak, G. J., and A. P. Suvorov (2005), Protection of sandwich plates from low-velocity impact, *Journal of Composite Materials*, *40*(15), 1317–1331.

[28] Engin, A. E. (1969), The axisymmetric response of a fluid-filled spherical shell to a local radial impulse A model for head injury, *Journal of Biomechanics*, *2*(3), 325–341.

[29] Essenberg, F. (1962), On surface constraint in plate problems, *Transaction of ASME, Journal of Appllied Mechanics*, *29*(1), 340344.

[30] Ferri, E., E. Antinucci, M. Y. He, J. W. Hutchinson, F. W. Zok, and A. G. Evans (2006), Dynamic buckling of impulsively loaded prismatic cores, *Journal of Mechanics of Materials and Structures*, *1*(8), 1345–1365.

[31] Fleck, N. A., and V. S. Deshpande (2004), The resistance of clamped sandwich beams to shock loading, *Journal of Applied Mechanics*, *71*(3), 1–16.

[32] Florence, A. L. (1966), Clamped circular rigid-plastic plates under central blast loading, *International Journal of Solids Structures*, *2*, 319–335.

[33] Ganpule, S. G., L. Gu, A. L. Alai, and N. Chandra (2012), Role of helmet in the mechanics of shock wave propagation under blast loading conditions, *Computer Methods in Biomechanics and Biomedical Engineering*, *15*(11), 1233–1244.

[34] Gardner, N., E. Wang, P. Kumar, and A. Shukla (2011), Blast mitigation in a sandwich composite using graded core and polyurea interlayer, *Experimental Mechanics*, *52*(2), 119–133.

[35] Gelfand, B. E., M. V. Silnikov, A. I. Mikhailin, and A. V. Orlov (2001), Attenuation of blast overpressures from liquid in an elastic shell, *Combustion, Explosion and Shock Waves*, *37*(5), 607–612.

[36] Gilchrist, A., and N. J. Mills (1994), Modelling of the impact response of motorcycle helmets, *International Journal of Impact Engineering*, *15*(3), 201–218.

[37] Goldstein, L. E., A. M. Fisher, C. A. Tagge, and X. L. Zhang (2012), Chronic traumatic encephalopathy in blast-exposed military veterans and a blast neurotrauma mouse model., *Science translational medicine*, *4*(134), 1–14.

[38] Greenwald, R. M., J. T. Gwin, J. J. Chu, and J. J. Crisco (2008), Head impact severity measures for evaluating mild Traumatic Brain Injury risk explosure, *Neurosurgery*, *62*(4), 789–798.

[39] Grujicic, M., G. Arakere, and H. T. (2010), Material-modeling and structural-mechanics aspects of the traumatic brain injury problem, *Multidiscipline Modelling in Materials and structures*, *6*, 335–363.

[40] Grujicic, M., W. C. Bell, B. Pandurangan, and T. He (2010), Blast-wave impact-mitigation capability of polyurea when used as helmet suspension-pad material, *Materials & Design*, *31*(9), 4050–4065.

[41] Gupta, P. K., and N. K. Gupta (2006), An experimental and computational study of the crushing of metallic hemispherical shells between two rigid flat platens, *The Journal of Strain Analysis for Engineering Design*, *41*(6), 453–466.

[42] Gupta, P. K., and N. K. Gupta (2009), A study of axial compression of metallic hemispherical domes, *Journal of Materials Processing Technology*, *209*, 2175–2179.

[43] Gurdjian, E. S., and H. R. Lissner (1944), Mechanisms of head injury as studied by the cathode ray oscilloscope: preliminary report., *Journal of Neurol. Neurosurg. Psychiatry*, *1*, 393–399.

[44] Gurdjian, E. S., H. R. Lissner, F. R. Latimerr, B. F. haddad, and J. E. Webster (1953), Quantitative determination of acceleration and intercranial pressure in experimental head injury, *Neurology*, *3*, 417–423.

[45] Gurdjian, E. S., V. L. Roberts, and L. M. Thomas (1966), Tolerance curves of acceleration and intracranial pressure protective index in experimental head injury, *J Trauma*, *6*(5), 600–604.

[46] Guskiewicz, K. M., J. P. Mihalik, V. Shankar, S. W. Marshall, D. H. Crowell, S. M. Oliaro, M. F. Ciocca, and D. N. Hooker (2007), Measurement of head impacts in collegiate football players: relationship between head impact biomechanics and acute clinical outcome after concussion., *J Trauma*, *61*(6), 1244–1252.

[47] Hardy, W. N., T. B. Khalil, and A. I. King (1994), Litrature review of head injury biomechanics, *International Journal of Impact Engineering*, *15*(4), 561–586.

[48] Hartman, W. F., B. A. Boughton, and M. E. Larsen (2006), Blast mitigation capabilities of aqueous foam, *Tech. Rep. SAND2006-0533*, Sandia National Laboratories, Albuquerque, NM 87185, USA.

[49] Hassan, M. Z., Z. W. Guan, W. J. Cantwell, G. S. Langdon, and G. N. Nurick (2012), The influence of core density on the blast resistance of foam-based sandwich structures, *International Journal of Impact Engineering*, *50*, 9–16.

[50] Henn, H. W. (1998), Crash tests and head injury criteria, *Teaching Mathematics and its Applications*, *17*(4), 162–170.

[51] Hertz, H. (1882), On the contact of elastic solids, *J. reine und angewandte Mathematik*, *92*, 156–171.

[52] Hibbeler, R. C. (1989), *Engineering Mechanics: Statics and Dynamics*, 5th ed., Macmillan Publishing Company, New York, NY, USA.

[53] Holbourn, A. H. S. (1943), Mechanics of head injuries, *Lancet*, *242*, 438–441.

[54] Hsieh, A. J., T. L. Chantawansri, W. Hu, K. E. Strawhecker, and D. T. Casem (2014), New insight into microstrcuture-mediated segmental dynamics in select model poly(urethane urea) elastomers, *Polymer*, *55*, 1883–1892.

[55] Johnson, K. L. (2004), Contact Mechanics, Cambridge University Press, Cambridge, UK.

[56] Johnson, V. E., W. Stewart, and S. D. H. (2013), Axonal pathology in traumatic brain injury, *Experimental Neurology*, *246*, 35–43.

[57] Jones, N. (1971), A theoretical study of the dynamic plastic behaviour of beams and plates with finite-deflections, *International Journal of Solids and Structures*, *7*(8), 1007–1029.

[58] Jones, N. (1989), *Structural Impact*, 2nd ed., Cambridge University Press, Cambridge, UK.

[59] Kambouchev, N., L. Noels, and R. Radovitzky (2006), Nonlinear compressibility effects in fluid-structure interaction and their implications on the air-blast loading of structures, *Journal of Applied Physics*, *100*(063519), 1–12.

[60] Kambouchev, N., L. Noels, and R. Radovitzky (2007), Numerical simulation of the fluid-structure interaction between air blast waves and free-standing plates, *Computers & Structures*, *85*(11-14), 923–931.

[61] Kambouchev, N., R. Radovitzky, and L. Noels (2007), Fluid-structure interaction effects in the dynamic response of free-standing plates to uniform shock loading, *Journal of Applied Mechanics*, *74*(5), 1042–1045.

[62] Kenner, V. H., and W. Goldsmith (1972), Dynamic loading of a fluid-filled spherical shell, *International Journal of Mechanical Sciences*, *14*(1), 557–568.

[63] Kimpara, H., and M. Iwamoto (2012), Mild traumatic brain injury predictors based on angular accelerations during impacts, *Annals of Biomedical Engineering*, *40*(1), 114–126.

[64] Kitching, R., R. Houlston, and W. Johnson (1975), A theoretical and experimental study of hemispherical shells subjected to axial loads between flat plates, *International Journal of Mechanical Sciences*, *17*(11-12), 693–694.

[65] Koller, M. G., and M. Busenhart (1986), Elastic impact of spheres on thin shallow spherical shells, *Journal of Impact Engineeering*, *4*(1), 11–21.

[66] Kolsky, H. (2012), *Stress Waves in Solids*, 2nd ed., Dover Publications, New York, NY, USA.

[67] Kunukkasseril, V. X., and R. Palaninathan (1975), Impact experiments on shallow spherical shells, *Journal of Sound Vibration*, *40*(5), 101–117.

[68] Lee, S., F. Barthelat, J. W. Hutchinson, and H. D. Espinosa (2006), Dynamic failure of metallic pyramidal truss core materials: Experiments and modeling, *International Journal of Plasticity*, *22*(11), 2118–2145.

[69] Lei, X. Y., M. K. Huang, and X. Wang (1994), Analysis of the explicit fundamental solution of a shallow spherical shell involving shear deformation, *Appllied Mathematical Modelling*, *19*(3), 656–662.

[70] Leonard, A., and C. Daraio (2012), Stress wave anisotropy in centered square highly nonlinear granular systems, *Physical Review Letters*, *108*(21), 1–4.

[71] Levy, M. L., B. M. Ozgur, and C. Berry (2004), Birth and evolution of the football helmet, *Neurosurgery*, *55*(3), 656–662.

[72] Li, L., I. Etsion, A. Ovcharenko, and F. E. Talke (2011), The onset of plastic yielding in a spherical shell compressed by a rigid flat, *Journal of Appllied Mechanics*, *78*(1), 011,016.

[73] Liepins, A. A. (1969), Two-dimensional finite-difference equations for shallow spherical shells, *AIAA Journal*, *7*(4), 737–739.

[74] Love, A. E. H. (1920), A Treatise on the Mathematical Theory of Elasticity, 1863-1940, 3th edition, articles 138, 139, 140, Cambridge University Press.

[75] Lowenhielm, P. (1975), Mathematical simulation of gliding contusions., *Journal of biomechanics*, *8*(6), 351–356.

[76] Lubock, P., and W. Goldsmith (1980), Experimental cavitation studies in a model head-neck system, *Journal of biomechanics*, *13*, 1041–1052.

[77] Mansoorbaghaei, S., and A. M. Sadegh (2011), Elastic spherical shell impacted with an elastic barrier: A closed form solution, *International Journal of Solids and Structures*, *48*, 3257–3266.

[78] Margulies, S. S., and L. E. Thibault (1992), A proposed tolerance criterion for diffuse axonal injury in man., *Journal of biomechanics*, *25*(8), 917–923.

[79] McCrory, P., W. Meeuwisse, K. Johnston, J. Dvorak, M. Aubry, M. Molloy, and R. Cantu (2009), Consensus statement on concussion in sport - the 3rd International Conference on Concussion in Sport held in Zurich, November 2008., *SAJSM*, *21*(2), 36–46.

[80] McCrory, P., W. H. Meeuwisse, M. Aubry, and B. Cantu (2013), Consensus statement on concussion in sport: the 4th International Conference on Concussion in Sport held in Zurich, November 2012., *British journal of sports medicine*, *47*, 250–258.

[81] McShane, G. J., S. M. Pingle, V. S. Deshpande, and N. A. Fleck (2012), Dynamic buckling of an inclined structure, *International Journal of Solids and Structures*, *49*(19-20), 2830–2838.

[82] Meythaler, J. M., J. D. Peduzzi, E. Eleftheriou, and T. A. Novack (2001), Current concepts: Diffuse axonal injuryassociated traumatic brain injury, *Archives of Physical Medicine and Rehabilitation*, *82*(10), 1461–1471.

[83] Mills, C. A. (1987), The design of concrete structure to resist explosions and weapon effects, *Proceedings of the 1st Int. Conference on concrete for hazard protections, Edinburgh, UK*, pp. 61–73.

[84] Mills, N. J., and A. Gilchrist (1991), The effectiveness of foams in bicycle and motorcycle helmets., *Accident; analysis and prevention*, *23*(2/3), 153–163.

[85] Morgan, G. (1971), US Patent 3609764 - Energy absoring and sizing means for helmets.

[86] Nesterenko, V. F. (2001), *Dynamics of Heterogeneous Materials*, Springer-Verlag, New York, NY, USA.

[87] Nesterenko, V. F. (2002), Shock (blast) mitigation by "soft" condensed matter, in *Materials Research Society Symposium Proceedings*, vol. PROC-759-MM4.3.

[88] Nevin, N. C. (1967), Neuropathological changes in the white matter following head injury, *Journal of Neuropathology and Experimental Neurology*, *26*, 77–84.

[89] O'Connor, A. (2013), Really? cycling is the top sport for head injuries, the new york times, 2013-06-03.

[90] Ogata, K. (2004), *System Dynamics, International Edition,*, 5th ed., Pearson Prentice Hall, Pearson Eduacation Inc., New York, NY, USA.

[91] Ommaya, A. K., A. E. Hirsch, P. Yarnell, and E. H. Harris (1967), Scaling of experimental data on cerebral concussion in sub-human primates to concussion threshold for man, *the 11th Stapp Car Crash Conference, Anaheim, CA*.

[92] Palaninathan, R., and V. X. Kunukkasserili (1973), Axisymmetric impulsive loading of shallow spherical shells, *AIAA Journal*, *11*(12), 225–233.

[93] Pauchard, L., and S. Rica (1998), Contact and compression of elastic spherical shells: the physics of a ping pong ball, *Philosophical Magazine B*, *78*(2), 225–233.

[94] Pellman, E. J., D. C. Viano, C. Withnall, N. Shewchenko, C. A. Bir, and P. D. Halstead (2003), Concussion in professional football: Reconstructionlong of game impacts and injuries, *Neurosurgery*, *35*(4), 799–814.

[95] Pellman, E. J., D. C. Viano, C. Withnall, N. Shewchenko, C. A. Bir, and P. D. Halstead (2006), Concussion in professional football: Helmet testing to assess impact performance – Part 11, *Neurosurgery*, *58*(1), 78–96.

[96] Ponomarev, V., and I. Ponomaryova (2006), US Patent 7017705 - Blast compression wave absorbing device.

[97] Post, A., and T. B. Hoshizaki (2015), Rotational acceleration, brain tissue strain, and the relationship to concussion, *Journal of Biomechanical Engineering*, *137*(3), 030,801–1–8.

[98] Radford, D. D., G. J. McShane, V. S. Deshpande, and N. A. Fleck (2007), Dynamic compressive response of stainless-steel square honeycombs, *Journal of Applied Mechanics*, *74*(4), 658–667.

[99] Rahimzadeh, T., E. M. Arruda, and M. D. Thouless (2015), Design of armor for protection against blast and impact, *Journal of the Mechanics and Physics of Solids*, *85*, 98–111.

[100] Reissner, E. (1947), Stresses and small displacements of shallow spherical shells, Part II, *Journal of Mathematics and Physics*, *25*(3), 279–300.

[101] Rosanova, M., A. Casali, V. Bellina, F. Resta, M. Mariotti, and M. Massimini (2009), Natural frequencies of human corticothalamic circuits, *Journal of Neuroscience*, *29*(24), 7679–7675.

[102] Rowland, C. M., and R. Casalini (2007), Effect of hydrostatic pressure on the viscoelastic response of polyurea, *Polymer*, *48*, 5747–5752.

[103] Rowson, S., and S. M. Duma (2011), Development of the STAR evaluation system for football helmets: integrating player head impact exposure and risk of concussion, *Annals of Biomedical Engineering*, *39*(8), 2130–2140.

[104] Ruan, J. S., and P. Prasad (1995), Coupling of a finite element human head model with a lumped parameter hybrid III dummey model: Preliminary results, *Journal of Neurotrauma*, *12*(4), 725–734.

[105] Schimizze, B. R., S. F. Son, R. Goel, A. P. Vechart, and L. R. Young (2013), An experimental and numerical study of blast induced shock wave mitigation in sandwich structures, *Applied Acoustics*, *74*(1), 1–9.

[106] Schneider, R. C. (1987), Football head and neck injury, *Surgery Neurology*, *27*, 507–508.

[107] Schwartz, N. J., R. S. Mackay, and J. L. Sackman (1966), A theoretical and experimental study of the mechanical behavior of the cornea with application to the measurement of intraocular pressure, *The Bulletin of Mathematical Biophysics*, *28*(4), 585–643.

[108] Shuaeib, F. M., A. M. S. Hamouda, M. M. Hamdan, and R. S. Umar (2002), Motorcycle helmet Part II: Materials and design issues, *Journl of Materials Processing Technology*, *123*, 422–431.

[109] Smith, G. D. (1985), *Numerical solution of Partial Differential Equations - Finite Difference Method - third edition*, Clarendon Press, Oxford, Burlington, MA, USA.

[110] Smith, P. D., and J. G. Hetherington (1994), *Blast and Ballistic Loading of Structures*, Butterworth Heinemann, Burlington, MA, USA.

[111] Srutt, J. W. (1892), On the equation of the stability of the flow of liquids, *Philosophical Magazine*, *34*, 59–70.

[112] Stern, R. A., D. O. Riley, and D. H. Daneshvar (2011), Long-term consequences of repetitive brain trauma: chronic traumatic encephalopathy., *PM & R : the journal of injury, function, and rehabilitation*, *3*(10), 460–467.

[113] Stewart, D., L. R. Young, R. Goel, G. Christou, and M. D. Gilchrist (2010), Evaluating the performance of helmet linings incorporating fluid channels, *Journal of ASME International*, *7*(10).

[114] Stritch, S. J. (1961), Shearing of nerve fibres as a cause of brain damage due to head injury: A pathological study of twenty cases, *Lancet*, *278*, 443–448.

[115] Stuhmiller, J. H. (2008), Quantitative physiology: problems and concepts in military operational medicine. Textbook of Military Medicine, Dept. of the Army, (USA).

[116] Swisdak, M. M. (1978), Explosion effects and properties: Part II - Explosion effects in water, *Tech. Rep. NSWCIWOL TR 76-116*, Naval Surface Weapons Center, White Oak, Silver Spring, MD 20910, USA.

[117] Symonds, P. S., and T. Wierzbicki (1979), Membrane mode solutions for impulsively loaded circular plates, *Journal of Applied Mechanics*, *46*(1), 58–64.

[118] Tan, P. J., S. R. Reid, J. J. Harrigan, Z. Zou, and S. Li (2005), Dynamic compressive strength properties of aluminium foams. Part I: Experimental data and observations, *Journal of the Mechanics and Physics of Solids*, *53*(10), 2174–2205.

[119] Tarlakovskii, D. V., and G. V. Fedotenkov (2014), Two dimensional nonstationary contact of elastic cylindrical or spherical shells, *Journal of Machinery Manufacture and Reliability*, *43*(2), 145–152.

[120] Taylor, G. I. (1963), Pressure and impulse of submarine explosion waves on plates, in *The Scientific Papers of Sir Geoffrey Ingram Taylor, Volume III: Aerodynamics and the Mechanics of Projectiles and Explosions*, edited by G. Batchelor, pp. 287–303, Cambridge University Press, Cambridge, UK.

[121] Tekalur, S. A., A. Shukla, and K. Shivakumar (2008), Blast resistance of polyurea based layered composite materials, *Composite Structures*, *84*(3), 271–281.

[122] Thouless, M. D., T. Rahimzadeh, E. M. Arruda, and W. A. M. (2014), Patent Application Filed Nov 14, 2014; US14/65658 - Blast/impact frequency tuning and mitigation.

[123] Tilbrook, M. T., D. D. Radford, V. S. Deshpande, and N. A. Fleck (2007), Dynamic crushing of sandwich panels with prismatic lattice cores, *International Journal of Solids and Structures*, *44*(18-19), 6101–6123.

[124] Updike, D. P. (1972), On the large deformation of a rigid-plastic spherical shell compressed by a rigid plate, *Transaction of ASME, Journal of Manufacturing Science Engineering*, *94*(3), 949–955.

[125] Updike, D. P., and A. Kalnins (1970), Axisymmetric behavior of an elastic spherical shell compressed between rigid plates, *Transaction of ASME, Journal of Appllied Mechanics*, *37*(3), 635–640.

[126] Updike, D. P., and A. Kalnins (1972), Contact pressure between an elastic spherical shell and a rigid flat, *Transaction of ASME, Journal of Appllied Mechanics*, *39*(4), 1110–1114.

[127] Updike, D. P., and A. Kalnins (1972), Axisymmetric postbuckling and nonsymmetric buckling of a spherical shell compressed between rigid plates, *Transaction of ASME, Journal of Appllied Mechanics*, *39*(1), 172–178.

[128] Vaschy, A. (1892), Sur les lois de similitude en physique, *Annales Telegraphiques*, *19*, 25–28.

[129] Vaziri, A., and J. W. Hutchinson (2007), Metal sandwich plates subject to intense air shocks, *International Journal of Solids and Structures*, *44*(6), 2021–2035.

[130] Vaziri, A., Z. Xue, and J. W. Hutchinson (2007), Performance and failure of metal sandwich plates subjected to shock loading, *Journal of Mechanics of Materials and Structures*, *2*(10), 1947–1963.

[131] Viano, D. C., and E. J. Pellman (2005), Concussion in professional football: Biomechanics of the striking player – Part 8, *Neurosurgery*, *56*(2), 266–280.

[132] Viano, D. C., I. R. Casson, E. J. Pellman, L. Zhang, A. I. King, and K. H. Yang (2005), Concussion in professional football: Brain responses by finite element analysis – Part 9, *Neurosurgery*, *57*(5), 891–916.

[133] Viano, D. C., E. J. Pellman, C. Withnall, and N. Shewchenko (2006), Concussion in professional football: Performance of newer helmets in reconstructed game impacts – Part 13, *Neurosurgery*, *59*(3), 591–606.

[134] Viano, D. C., I. R. Casson, and E. J. Pellman (2007), Concussion in professional football: Biomechanics of the struck player – Part 14, *Neurosurgery*, *61*(2), 313–328.

[135] Wadley, H. N. G., K. P. Dharmasena, M. Y. He, R. M. McMeeking, A. G. Evans, T. Bui-Thanh, and R. Radovitzky (2010), An active concept for limiting injuries caused by air blasts, *International Journal of Impact Engineering*, *37*(3), 317–323.

[136] Wan, F. Y. M. (1967), Membrane and bending stresses in shallow spherical shells, *International Journal of Solids Structures*, *3*, 353–366.

[137] Wang, A. J., and H. G. Hopkins (1954), On the plastic deformation of built-in circular plates under impulsive load, *Journal of the Mechanics and Physics of Solids*, *8*, 22–87.

[138] Williams, M. L., R. F. Landel, and L. D. Ferry (1955), The temperature dependence of relaxation mechanisms in amorphous polymers and other glass-forming liquids, *Journal of the American Chemical Society*, *77*(14), 3701–3707.

[139] Wineman, A. S., and K. R. Rajagopal (2000), *Mechanical Response of Polymers: An Introduction*, Cambridge University Press, Cambridge, UK.

[140] Xue, Z., and J. W. Hutchinson (2003), Preliminary assessment of sandwich plates subject to blast loads, *International Journal of Mechanical Sciences*, *45*(4), 687–705.

[141] Xue, Z., and J. W. Hutchinson (2004), A comparative study of impulse-resistant metal sandwich plates, *International Journal of Impact Engineering*, *30*(10), 1283–1305.

[142] Xue, Z., and J. W. Hutchinson (2006), Crush dynamics of square honeycomb sandwich cores, *International Journal for Numerical Methods in Engineering*, *65*(13), 2221–2245.

[143] Yehia, A., Y. A. Bahei-El-Din, and G. J. Dvorak (2008), Enhancement of blast resistance of sandwich plates, *Composites B*, *39*(1), 120–127.

[144] Young, P. (2003), An analytical model to predict the response of fluid-filled shells to impacta model for blunt head impacts, *Journal of Sound and Vibration*, *267*, 1107–1126.

[145] Zhang, L., K. H. Yang, and A. I. King (2004), A proposed injury threshold for mild traumatic brain injury, *Journal of Biomechanical Engineering*, *126*(2), 226.

[146] Zhang, L., R. Makwana, and S. Sharma (2013), Brain response to primary blast wave using validated finite element models of human head and advanced combat helmet., *Frontiers in neurology*, *4*(88), 1–12.

[147] Zhu, F., Z. Wang, G. Lu, and G. Nurick (2010), Some theoretical considerations on the dynamic response of sandwich structures under impulsive loading, *International Journal of Impact Engineering*, *37*(6), 625–637.

[148] Zhuang, S., G. Ravichandran, and D. E. Grady (2003), An experimental investigation of shock wave propagation in periodically layered composites, *Journal of the Mechanics and Physics of Solids*, *51*(2), 245–265.